ROBUST CONTROL OF A MISSILE SYSTEM

BİR FÜZE SİSTEMİNİN GÜRBÜZ KONTROLÜ

HANDAN GÜRSOY DEMİR

PROF. DR. MEHMET ÖNDER EFE
Supervisor

Submitted to
Graduate School of Science and Engineering of Hacettepe University
as a Partial Fulfillment to the Requirements
for the Award of the Degree of Doctor of Philosophy
in Computer Engineering

2022

ABSTRACT

ROBUST CONTROL OF A MISSILE SYSTEM

Handan GÜRSOY DEMİR

Doctor of Philosophy, Computer Engineering

Supervisor: Prof. Dr. Mehmet Önder EFE

May 2022, 206 pages

Missiles, known for their high agility and fast speed, are becoming increasingly important for defense purposes and they are frequently encountered, especially in air defense scenarios. In an air defense scenario, the missile is guided towards the target with the goal of intersecting the target's trajectory as quickly as possible or minimizing the deviation that will occur at the intersection point. Since these trajectories are produced in the missile guidance unit, this unit is vital to achieving the expected results from the missile. For years, intensive studies on this unit have been carried out by using different control methods, intelligent approaches as well as classical guidance laws.

Within this thesis, novel alternative structures are developed based on robust control methodologies with the purpose of designing the guidance laws that demand more than enough high accuracy in a short, finite amount of time. The first structure is based on two conventional control methods, which are the proportional-integral-derivative (PID) and the sliding mode control (SMC), while two traditional guidance controls, the Proportional Navigation (PN) guidance law and the Augmented Proportional Navigation (APN) guidance law, are designed for comparison of results. In the second structure, a novel composite 3D guidance law based on an adaptive integral sliding mode (AISM) control method utilizing an

nonlinear disturbance observer technique is proposed for missiles. Firstly, the integral sliding mode control is proposed to get rid of the reaching phase of traditional SMC, as well as the adaptive law is used to design without the upper bound of the target information. Moreover, the NDOB is designed to estimate the target acceleration by handling as the disturbance to minimize the chattering phenomenon. The third proposed new guidance law includes a high-order sliding mode control technique that utilizes an adaptive algorithm and fuzzy gain scheduling to obtain its parameters online. In this guidance law, the super-twisting sliding mode guidance law, which is a high-order sliding mode control technique, is designed to overcome the chattering phenomenon, and also an adaptive law and fuzzy control are used to determine the controller parameters and gains. Stability analyzes of the proposed guidance laws are performed using the Lyapunov method. In the last structure, a new law based on the APN guidance law utilizing an NDOB technique is proposed. Thus, a different approach has been brought to classical guidance law. Here, an NDOB technique is used to obtain the target acceleration, and so when designing the APN guidance law, it can be designed without the need for target acceleration information.

Through numerical simulations, all designed and proposed guidance laws are evaluated and compared with different guidance laws according to several cases of the target. In addition, all guidance laws are evaluated in terms of the miss distance and interception time, and the results are presented. Throughout this thesis, it was clearly observed that the proposed guidance laws outperform the other schemes regarding the miss distance and interception time.

Keywords: Robust Control, Sliding Mode Control, Integral Sliding Mode Control, High-Order Sliding Mode Control, Missile, Guidance

ÖZET

BİR FÜZE SİSTEMİNİN GÜRBÜZ KONTROLÜ

Handan GÜRSOY DEMİR

Doktora, Bilgisayar Mühendisliği

Danışman: Prof. Dr. Mehmet Önder EFE

Mayıs 2022, 206 sayfa

Çeviklikleri ve yüksek hızları ile bilinen füzelerin, savunma amaçlı kullanımı her geçen gün artmakta ve özellikle hava savunma senaryolarında sıklıkla karşılaşılmaktadır. Bir hava savunma senaryosunda, hedefin yörüngesini olabildiğince hızlı bir şekilde kesmek veya kesişme noktasında oluşacak sapmayı en aza indirmek amacıyla füze hedefe doğru yönlendirilir. Bu yörüngeler füze güdüm ünitesinde üretildiği için bu birim oldukça önemlidir. Klasik güdüm kanunlarının yanı sıra farklı denetim yöntemleri, akıllı yaklaşımlar kullanılarak bu ünite üzerinde yıllardır yoğun çalışmalar yapılmaktadır.

Bu tez kapsamında, kısa ve sonlu bir zaman diliminde fazlasıyla yüksek doğruluk gerektiren güdüm kanunlarını tasarlamak amacıyla gürbüz denetim metodolojilerine dayalı yeni alternatif yapılar geliştirilmiştir. İlk yapıda, güdüm kanununu tasarlamak için geleneksel denetim yöntemlerinden en çok tercih edilen oransal-integral-türevsel ve kayan kipli denetim yöntemleri tasarlanmıştır. Sonuçların karşılaştırılması için geleneksel güdüm kanunlarından Orantılı Navigasyon ve Artırılmış Orantılı Navigasyon güdüm kanunları seçilmiştir. İkinci yapıda, füzeler için bir doğrusal olmayan bozucu gözlemci (NDOB) tekniğini kullanan uyarlanabilir bir integral kayan kipli denetim yöntemini temel alan yeni bir güdüm kanunu önerilmiştir. İlk olarak, geleneksel kayan kipli denetimin dezavantajı olarak görülen ulaşma

aşamasından kurtulmak için integral kayan kipli denetim önerilmiş, ayrıca uyarlamalı yasa, hedef bilginin üst sınırı olmadan tasarlamak için kullanılmıştır. Tüm bunlara ek olarak, NDOB yapısı, bozucu olarak ele aldığı hedef ivmeyi tahmin etmek üzere tasarlanmıştır. Bu yapıyla, kayan kipli denetimin diğer bir dezavantajı olarak görülen çatırdama problemini en aza indirgemek amaçlanmıştır. Önerilen üçüncü yeni güdüm kanunu, parametrelerini çevrimiçi olarak elde etmek için uyarlanabilir bir algoritma ve bulanık kazanç planlaması kullanan daha yüksek dereceli bir kayan kipli denetim tekniği içerir. Bu yeni yaklaşımda, çatırdama probleminin üstesinden gelmek için yüksek dereceli kayan kipli denetim methodu olan süper büküm kayan kipli denetim ile güdüm kanunu tasarlanırken, denetleyici parametrelerinin ve kazançlarının belirlenmesi için bir uyarlamalı yasa ve bulanık kontrol kullanılır. Ek olarak, önerilen güdüm kanunlarının kararlılık analizleri Lyapunov yöntemi kullanılarak gerçekleştirilir. Son yapıda, bir NDOB tekniği ile desteklenen yeni bir APN güdüm kanunu önerilmiştir. Böylece klasik güdüm kanununa farklı bir yaklaşım getirilmiştir. Burada, hedef ivmeyi elde etmek için NDOB tekniği kullanılır ve böylece APN güdüm kanunu tasarlanırken, hedef ivme bilgisine ihtiyaç duymadan tasarlanabilir.

Tasarlanan ve önerilen tüm güdüm kanunları, tatmin edici sonuçlar veren sayısal simülasyonlar aracılığıyla değerlendirilir ve çeşitli hedef durumlarına göre farklı güdüm kanunlarıyla karşılaştırılarak sonuçlar sunulur. Ayrıca, tüm güdüm kanunları, ıskalama mesafesi ve durdurma süresi açısından değerlendirilmektedir. Bu tez boyunca elde edilen sonuçlardan, tasarlanan yeni güdüm kanunlarının, ıskalama mesafesi ve durdurma süresi parametreleri değerlendirildiğinde diğer kanunlardan daha iyi performans gösterdiği açıkça görülmüştür.

Keywords: Gürbüz Denetim, Kayan Kipli Denetim, İntegral Kayan Kipli Denetim, Yüksek Dereceli Kayan Kipli Denetim, Füze, Güdüm

To my family who showed me the way I was following;
Zeynep, Cebrail, Hakan

To my lover who accompanied and supported me on this way;
Mehmet

And to my dear daughter, who is my luck on this way.
Defne

ACKNOWLEDGEMENTS

First and foremost, I would like to thank to my supervisor, Prof. Dr. Mehmet Önder Efe for his valuable advice and guidance. He supported me with his knowledge and experience during the emergence, maturation, and completion of my Ph.D. research studies. It was an honour for me to start my academic life as his student.

I am also very thankful to my doctoral committee members, Prof. Dr. Coşku Kasnakoğlu, Assoc. Prof. Dr. Murat Aydos , Prof. Dr. Ali Bozbey and Asst. Prof. Dr. Burak Kürkçü for sparing their precious time to evaluate the progress of my work.

A special thanks to Abdurrahman Bayrak for supporting me with his knowledge and experience not only in this doctoral research but also in all my academic studies. I would like to thank Aysun Koçak Özcan, whose knowledge and friendship I found the strength to progress at every point I am bored in this process. I would also like to thank to my colleagues in Hacettepe University and Iskenderun Technical University Computer Eng. Dept. for their kind help during my academic work.

My deepest gratitude goes to to my parents, Zeynep Gürsoy and Cebrail Gürsoy, for the continuous love and support showered on me throughout. The opportunities that they have given me and their unlimited sacrifices are the reasons for my being where I am and what I have accomplished so far. I especially thank my brother, Hakan Gürsoy, for giving me strength with his presence in all areas of life. I am grateful to him for always being my best friend, understanding and trusting me. I would like to express my deepest gratitude to my precious lover, Dr. Mehmet Demir, not only in my thesis research but in every minute of my life, who does not spare his love and understanding, who illuminates my way with the light in his eyes. Defne, my dear daughter, you have added different meanings to our lives with your arrival and made every day special. My biggest thanks to you for being our daughter.

In my PhD study, I was supported by TÜBITAK BIDEB for their 2211-C program. I would like to thank because it benefits on my Ph. D. education with monetary support.

CONTENTS

Page

ABSTRACT i

ÖZET iii

ACKNOWLEDGEMENTS vi

CONTENTS vii

TABLES x

FIGURES xi

ABBREVIATIONS xv

1. INTRODUCTION 1

1.1. Overview of control system 6

1.2. Thesis Motivations and Aims 9

1.3. Contributions 11

1.4. Organization 12

2. RELATED WORK 14

3. BACKGROUND OVERVIEW 23

3.1. Mathematical Modeling for Missile 23

3.1.1. Coordinate Systems 23

3.1.2. Coordinates Transformation and Matrices of Transformation 26

3.1.3. Equations of Motion 30

3.1.3.1. Dynamical Equations of Motion 31

3.1.3.2. Kinematical Equations of Motion 36

3.1.4. Aerodynamic Forces and Moments 37

3.1.5. Flight Parameters 39

3.1.6. Deflection Angles of Control Surfaces 50

3.1.7. Control Actuation System 52

3.2. Guidance Law Methods 52

3.2.1. Classical Guidance Laws 53

3.2.1.1. Proportional Navigation Guidance 53

3.2.1.2. Pursuit Guidance 56
3.2.1.3. Line of Sight Guidance 57
3.2.2. Guidance Methods based on Classical Control Techniques 58
3.2.3. Guidance Methods based on Robust Control Techniques 60
3.2.4. Guidance Methods with Applications of Artificial Intelligence Techniques 64
3.2.5. Guidance Methods based on Optimal Control Theory 67
3.3. Missile Autopilot Methods 69
4. GUIDANCE LAW BASED ON CONTROL METHODS 72
4.1. Missile-Target Engagement Geometry 72
4.2. Design of the Guidance Law 74
4.2.1. PID Guidance Law 74
4.2.2. Sliding Mode Guidance Law 75
4.3. Results of the Numerical Simulations 78
4.3.1. Simulation Scenarios Setting 79
4.3.2. Simulation Results 80
4.4. Summary 90
5. ADAPTIVE INTEGRAL SLIDING MODE GUIDANCE LAW WITH A NONLINEAR DISTURBANCE OBSERVER 91
5.1. Design the Guidance Law 91
5.1.1. Mathematical Preliminaries 91
5.1.2. Integral Sliding Mode Approach for Guidance Law Design 93
5.1.3. Adaptive Integral Sliding Mode Approach for Guidance Law Design 97
5.2. Composite Guidance Law Design 102
5.2.1. Design of Nonlinear Disturbance Observer 102
5.2.2. Composite Guidance Law Based on Nonlinear Disturbance Observer 105
5.3. Results of the Numerical Simulations 108
5.3.1. Simulation Scenarios Setting and Initial Conditions 109
5.3.2. Simulation Results 110
5.4. Summary 123

6. ADAPTIVE HIGH-ORDER SLIDING MODE GUIDANCE LAW WITH FUZZY LOGIC SYSTEM 125
6.1. Design the Guidance Law 125
6.1.1. Mathematical Preliminaries 125
6.1.2. Super-Twisting Sliding Mode Guidance Law Design 126
6.1.3. Design of the Adaptive Super-Twisting Sliding Mode Guidance Law 127
6.2. Adaptive Super-Twisting Sliding Mode Guidance Law Design with Fuzzy Logic System 134
6.3. Results of the Numerical Simulations 137
6.3.1. Simulation Scenarios Setting 137
6.3.2. Simulation Results 139
6.4. Summary 148
7. INVESTIGATION OF THE EFFECT OF THE OBSERVER ON AUGMENTED PROPORTIONAL NAVIGATION GUIDANCE 149
7.1. Design the Guidance Law 149
7.1.1. Augmented Proportional Navigation Guidance Law 149
7.1.2. Nonlinear Disturbance Observer 149
7.1.3. Augmented Proportional Navigation Guidance Law with Nonlinear Disturbance Observer 150
7.2. Results of the Numerical Simulations 151
7.2.1. Simulation Scenarios Setting and Initial Conditions 151
7.2.2. Simulation Results 152
7.3. Summary 158
8. CONCLUSION 160

TABLES

Page

Table 3.1 General features of frames [1] 23

Table 3.2 Axis Definition [2] 31

Table 3.3 Moment Designation [2] 32

Table 3.4 Some Variables Affecting Aerodynamic Force 38

Table 4.1 The overall effects of each controller parameter (K_p, K_d, K_i) on a system 74

Table 4.2 Accelerations setting of target in interception scenarios 79

Table 4.3 Miss distance and Interception time for non-maneuvering target 85

Table 4.4 Miss distance and Interception time for maneuvering target 85

Table 5.1 Accelerations setting of target in interception scenarios 109

Table 5.2 Miss distance and Interception time for all cases 123

Table 6.1 Two Dimensional Fuzzy Rule Bases 136

Table 6.2 Two Dimensional Fuzzy Rule Bases 137

Table 6.3 Accelerations setting of target in interception scenarios 139

Table 6.4 Miss distance and Interception time for Case 1 139

Table 6.5 Miss distance and Interception time for Case 2 144

Table 7.1 Accelerations setting of target in interception scenarios 151

Table 7.2 Miss distance and Interception time for Case 1 152

Table 7.3 Miss distance and Interception time for Case 2 155

FIGURES

Page

Figure 1.1 Air-to-Air Missile 2
Figure 1.2 Surface-to-Air Missile 2
Figure 1.3 Surface-to-Surface Missile 2
Figure 1.4 Air-to-Surface Missile 3
Figure 1.5 The structure of missile 5
Figure 1.6 Three phases of guidance 6
Figure 3.1 Sun-centered (heliocentric) frame 24
Figure 3.2 Earth frame 25
Figure 3.3 Missile frame 26
Figure 3.4 Inertial frame 27
Figure 3.5 The rotation z axis and ϕ (yaw angle) 28
Figure 3.6 The rotation y axis and θ (pitch angle) 28
Figure 3.7 The rotation of x axis and ψ (roll angle) 29
Figure 3.8 The missile and the body-fixed coordinate-system illustrated 31
Figure 3.9 (a) Drag coefficient with $\delta_r = -20^\circ$ bias (b) Lift coefficient with $\delta_r = -20^\circ$ δ_r bias (c) Moment coefficient with $\delta_r = -20^\circ$ δ_r bias ... 40
Figure 3.10 (a) Drag coefficient with $\delta_r = -15^\circ$ bias (b) Lift coefficient with $\delta_r = -15^\circ$ bias (c) Moment coefficient with $\delta_r = -15^\circ$ bias 41
Figure 3.11 (a) Drag coefficient with $\delta_r = -10^\circ$ bias (b) Lift coefficient with $\delta_r = -10^\circ$ bias (c) Moment coefficient with $\delta_r = -10^\circ$ bias 42
Figure 3.12 (a) Drag coefficient with $\delta_r = -5^\circ$ bias (b) Lift coefficient with $\delta_r = -5^\circ$ bias (c) Moment coefficient with $\delta_r = -5^\circ$ bias 43
Figure 3.13 (a) Drag coefficient with $\delta_r = 0^\circ$ bias (b) Lift coefficient with $\delta_r = 0^\circ$ bias (c) Moment coefficient with $\delta_r = 0^\circ$ bias 44
Figure 3.14 (a) Drag coefficient with $\delta_r = 5^\circ$ bias (b) Lift coefficient with $\delta_r = 5^\circ$ bias (c) Moment coefficient with $\delta_r = 5^\circ$ bias 45

Figure 3.15 (a) Drag coefficient with $\delta_r = 10\,^\circ$ bias (b) Lift coefficient with $\delta_r = 10\,^\circ$ bias (c) Moment coefficient with $\delta_r = 10\,^\circ$ bias 46
Figure 3.16 (a) Drag coefficient with $\delta_r = 15\,^\circ$ bias (b) Lift coefficient with $\delta_r = 15\,^\circ$ bias (c) Moment coefficient with $\delta_r = 15\,^\circ$ bias 47
Figure 3.17 (a) Drag coefficient with $\delta_r = 20\,^\circ$ bias (b) Lift coefficient with $\delta_r = 20\,^\circ$ bias (c) Moment coefficient with $\delta_r = 20\,^\circ$ bias 48
Figure 3.18 Angle of Attack 50
Figure 3.19 X configuration 51
Figure 3.20 Pure proportional navigation guidance geometry 55
Figure 3.21 True proportional navigation guidance geometry 55
Figure 3.22 Pursuit guidance geometry 57
Figure 3.23 Line of sight guidance geometrical rule 57
Figure 3.24 Classical control system block diagram 59
Figure 3.25 The block diagram of PID controller 60
Figure 3.26 General scheme of H_∞ control design 61
Figure 3.27 Graphical representation of SMC 62
Figure 3.28 The structure of neural network for a neuron 65
Figure 3.29 General architecture of fuzzy logic 66
Figure 3.30 General scheme of LQR control design 67
Figure 4.1 Missile-Target engagement geometry 73
Figure 4.2 Sliding surface and the chattering phenomenon 76
Figure 4.3 Results of Case 1: Relative range 81
Figure 4.4 Results of Case 1: LOS angles 81
Figure 4.5 Results of Case 1: LOS angular rates 82
Figure 4.6 Results of Case 1: Phase space behavior 82
Figure 4.7 Results of Case 1: Missile and target trajectories 83
Figure 4.8 Results of Case 1: Missile and target trajectories 83
Figure 4.9 Results of Case 1: Mach number 84
Figure 4.10 Results of Case 1: Closing velocity 84
Figure 4.11 Results of Case 2: Relative range 86

Figure 4.12 Results of Case 2: LOS angles 86
Figure 4.13 Results of Case 2: LOS angular rates 87
Figure 4.14 Results of Case 2: Phase space behavior 87
Figure 4.15 Results of Case 2: Missile and target trajectories 88
Figure 4.16 Results of Case 2: Missile and target trajectories 88
Figure 4.17 Results of Case 2: Mach Number 89
Figure 4.18 Results of Case 2: Closing velocity 89
Figure 5.1 Results of Case 1: Target acceleration estimation errors 111
Figure 5.2 Results of Case 1: Missile and target trajectories 111
Figure 5.3 Results of Case 1: LOS angular rates 112
Figure 5.4 Results of Case 1: Phase space behavior 112
Figure 5.5 Results of Case 1: Target acceleration estimation errors 113
Figure 5.6 Results of Case 1: Missile and target trajectories 113
Figure 5.7 Results of Case 2: Relative range 115
Figure 5.8 Results of Case 2: LOS angles 115
Figure 5.9 Results of Case 2: LOS angular rates 116
Figure 5.10 Results of Case 2: Phase space behavior 116
Figure 5.11 Results of Case 2: Target acceleration estimation errors 117
Figure 5.12 Results of Case 2: Missile and target trajectories 117
Figure 5.13 Results of Case 3: Relative range 119
Figure 5.14 Results of Case 3: LOS angles 119
Figure 5.15 Results of Case 3: LOS angular rates 120
Figure 5.16 Results of Case 3: Phase space behavior 120
Figure 5.17 Results of Case 3: Target acceleration estimation errors 121
Figure 5.18 Results of Case 3: Missile and target trajectories 121
Figure 6.1 The block diagram of the ASTWSM with Fuzzy Logic System guidance law 135
Figure 6.2 General fuzzy logic system structure with input/output quantities $(\phi, \dot{\phi}) \rightarrow k_1$ and $(\theta, \dot{\theta}) \rightarrow k_2$. 136
Figure 6.3 Membership function of linguistic variables for the outputs k_1, k_2 138

Figure 6.4 Results of Case 1: Relative range 141
Figure 6.5 Results of Case 1: LOS angles 141
Figure 6.6 Results of Case 1: Phase space behavior of the elevation angle 142
Figure 6.7 Results of Case 1: Phase space behavior of the azimuth angle 142
Figure 6.8 Results of Case 1: Missile and Target trajectories 143
Figure 6.9 Results of Case 1: Missile and Target trajectories 143
Figure 6.10 Results of Case 2: Relative range 145
Figure 6.11 Results of Case 2: LOS angles 145
Figure 6.12 Results of Case 2: Phase space behavior of the elevation angle 146
Figure 6.13 Results of Case 2: Phase space behavior of the azimuth angle 146
Figure 6.14 Results of Case 2: Missile and Target trajectories 147
Figure 6.15 Results of Case 2: Missile and Target trajectories 147
Figure 7.1 Results of Case 2: Relative range 153
Figure 7.2 Results of Case 2: LOS angular rates 153
Figure 7.3 Results of Case 2: The actual and the estimated target accelerations .. 154
Figure 7.4 Results of Case 2: The actual and the estimated target accelerations .. 154
Figure 7.5 Results of Case 2: Missile and Target trajectories 155
Figure 7.6 Results of Case 2: Relative range 156
Figure 7.7 Results of Case 2: LOS angular rates 156
Figure 7.8 Results of Case 2: The actual and the estimated target accelerations .. 157
Figure 7.9 Results of Case 2: The actual and the estimated target accelerations .. 157
Figure 7.10 Results of Case 2: Missile and Target trajectories 158

ABBREVIATIONS

AAM	:	**A**ir-to-**A**ir **M**issiles
AAM	:	**A**ir-to-**S**urface **M**issiles
AISM	:	**A**daptive **I**ntegral **S**liding **M**ode
ASTWSM	:	**A**daptive **S**uper **T**wisting **S**liding **M**ode
AOA	:	**A**ngle-**o**f-**A**ttack
APN	:	**A**ugmented **P**roportional **N**avigation
CG	:	**C**enter of **G**ravity
CAS	:	**C**ontrol **A**ctuation **S**ystem
DCM	:	**D**irection **C**osine **M**atrix
DO	:	**D**isturbance **O**bserver
FOV	:	**F**ield **o**f **V**iew
FPA	:	**F**light **P**ath **A**ngle
HG	:	**H**oming **G**uidance
ISMC	:	**I**ntegral **S**liding **M**ode **C**ontrol
LHG	:	**L**inear **H**oming **G**uidance
LOS	:	**L**ine-**o**f-**S**ight
PI	:	**P**roportional **I**ntegral
PID	:	**P**roportional plus **I**ntegral **D**erivative
PNG	:	**P**roportional **N**avigation **G**uidance
PPNG	:	**P**ure **P**roportional **N**avigation **G**uidance
SOSM	:	**S**econd **O**rder **S**liding **M**ode
SM	:	**S**liding **M**ode
SMC	:	**S**liding **M**ode **C**ontrol
SMG	:	**S**liding **M**ode **G**uidance
SAM	:	**S**urface-to-**A**ir **M**issiles
SSM	:	**S**urface-to-**S**urface **M**issiles

STWSM	:	**S**uper **T**wisting **S**liding **M**ode
TPNG	:	**T**rue **P**roportional **N**avigation **G**uidance
VSC	:	**V**ariable **S**tructure **C**ontrol
3D	:	**T**hree **D**imensional
2D	:	**T**wo **D**imensional

1. INTRODUCTION

A missile is an aerospace vehicle that is self-propelled through space with variable guidance capabilities with the goal of hitting a specific target. Although the first unguided missile was invented in China in 1044 AD, it was first used practically in 1232 AD in China against the Mongols. Although it had several uses in the following years, its main emergence was during the First World War, when a missile was first fired from the aircraft that tried to bring down the balloon filled with hydrogen gas [2]. With the Second World War, the development of missiles was accelerated and improvements were increased. After that time period, the guidance system has also started to attract attention. While the German V-1 was a missile with a simple guidance structure, it was guided to its target by a pilot on a suicide mission. Radio guidance was used in the German V-2, American GB-1, and American VB-1 missiles, and the missiles were manually guided from the ground. The American VB-6 missile had a heat-seeking guidance system and was able to self-guide. Following the Second World War, missile development expanded to include not only guided missiles, but also studies and improvements on body shape, engine, explosives, navigation systems, guidance systems, sensors, and actuators [2].

Missiles that are guided are categorized according to launch environment, speed, size, mission, and vehicle type [2]. These categories will be briefly described and listed below.

- **Launch environment**

  The environment in which missiles are launched might be classified as ground, underground, underwater or air. Generally, the initials are used when naming these environments; A denotes the air, S denotes the surface, L denotes the underground, and U denotes the underwater.

  1. Air-to-Air Missiles (AAM): These missiles, with their small size, short range, high launch speed, and high maneuverability, are launched from the aircraft against another flying target and try to neutralize it.

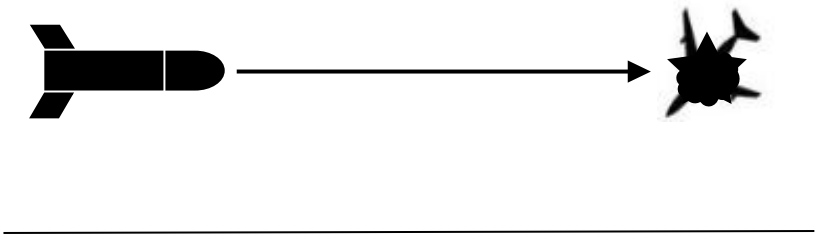

Figure 1.1 Air-to-Air Missile

2. Surface-to-Air Missiles (SAM): These missiles, with their short-to-medium range, medium launching speed, high manoeuvrability, and small-to-medium size, are designed for defence against another flying targets to attack and try to neutralize it.

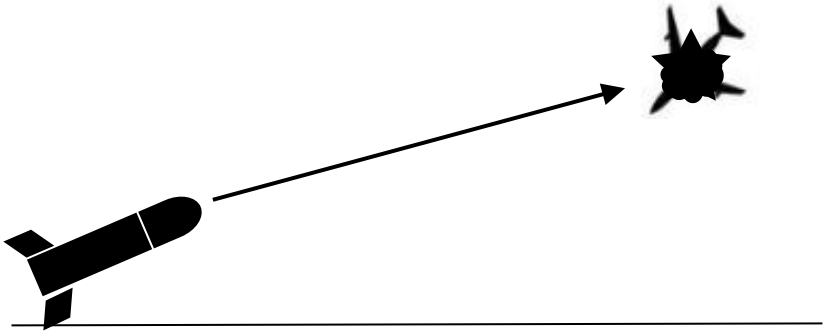

Figure 1.2 Surface-to-Air Missile

3. Surface-to-Surface Missiles (SSM): These missiles are meant to knock out a larger range of adversary surface targets because to their varied range and size, high-to-medium launching speed and limited agility, and small-to-medium size.

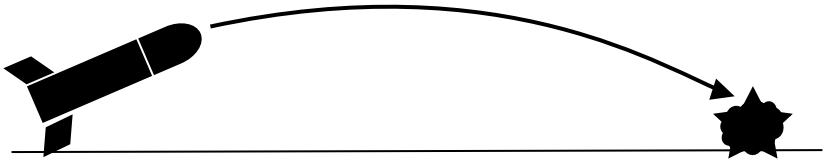

Figure 1.3 Surface-to-Surface Missile

4. Air-to-Surface Missiles (ASM): These missiles are meant to knock out enemy surface targets such as gun emplacements or tanks or airfields with their

short-range, high launching speed, low manoeuvrability and small-to-medium size.

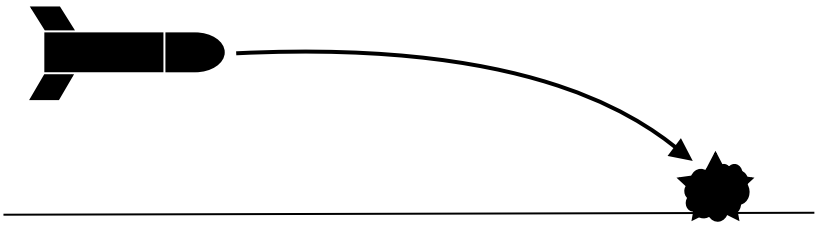

Figure 1.4 Air-to-Surface Missile

- **Speed**

  Missiles are also categorized according to their speed capabilities, which is indicated by using Mach numbers. The ratio of the speed of the object to the speed of sound in a given medium is called the Mach number. The sonic speed is expressed at about Mach 1.0, taking into account standard atmospheric conditions. It is generally divided into four categories, which will be briefly given below.

  1. Subsonic: Missiles with a speed of up to Mach 0.8 are called subsonic missiles.
  2. Transonic: The speed of transonic missiles must be between Mach 0.8 and Mach 1.2.
  3. Supersonic: Missiles with a speed of between Mach 1.2 and Mach 5.0 are called subsonic missiles.
  4. Hypersonic: The speed of hypersonic missiles must be above Mach 5.0.

- **Size**

  The missile size is expressed in terms of the range supported. For example, some types of missiles are referred to as short-range, medium-range, long-range, intermediate-range, and intercontinental missiles, and according to these, missile sizes vary.

- **Engine type**

  Missiles are powered by different types of engines, and these engines are divided into two basic classes.

  1. Rocket engines
     - Solid
     - Liquid
     - Hybrid
  2. Jet engines
     - Turbojet
     - Pulsejet
     - Ramjet
     - Scramjet

  A missile can have more than one engine stage, and it is possible for these engines to be of the same or different types.

- **Target detection**

  1. Passive: Passive defense is a necessary precautionary arrangement created to minimize force losses, to minimize the effects of nuclear, biological, or chemical attacks, and to enable friendly forces exposed to such attacks to be ready for action again.
  2. Semi-Active: The system, which is preferred the most prevalent form for longer-range AAM and SAM systems, utilizes an external, controlled source of radiation, that it reflects off the target.
  3. Active: Active defense is an architecture created for the destruction and neutralization of tactical ballistic missiles during flight, which threatens air defense systems.

The guided missiles generally consist of three basic parts. These are the guidance control, warhead, and propulsion sections. Its general structure is shown in Figure 1. However, the layout of these structures varies depending on the missile types. Guidance is the part of a missile with which it is guided toward a target and is called the missile's brain. The propulsion part provides the force that propels the missile, while the warhead section, if present, carries the missile's explosive charge as well as the firing system that explodes the charge. The features of the this two parts, warhead and propulsion, vary depending on the guidance requirements, the existing threat, and the missile's hull characteristics.

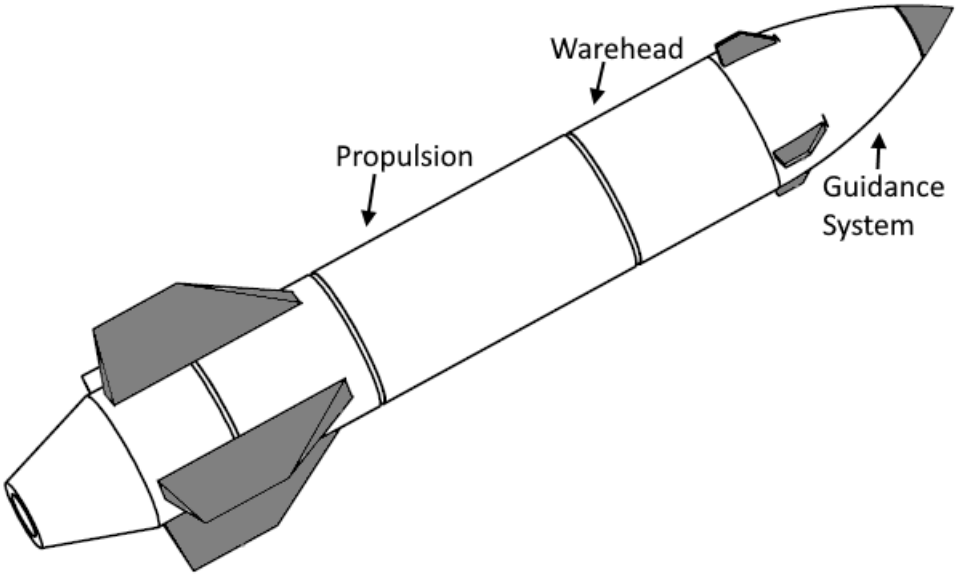

Figure 1.5 The structure of missile

A guidance system is a generic term to reach the desired position from its starting point in two or three-dimensional space a missile, satellite, rocket, aircraft, helicopter, ship, or similar vehicle. Basically, the goal of the guidance system is to ensure the guidance necessary to direct the missile towards the target [3].

guidance is divided into three fundamental phases: the boost phase, the midcourse phase, and the terminal phase, which are depicted in Figure

In general, the boost phase, the midcourse phase, and the terminal phase are the three basic phases of the guidance, as depicted in Figure.1.6.

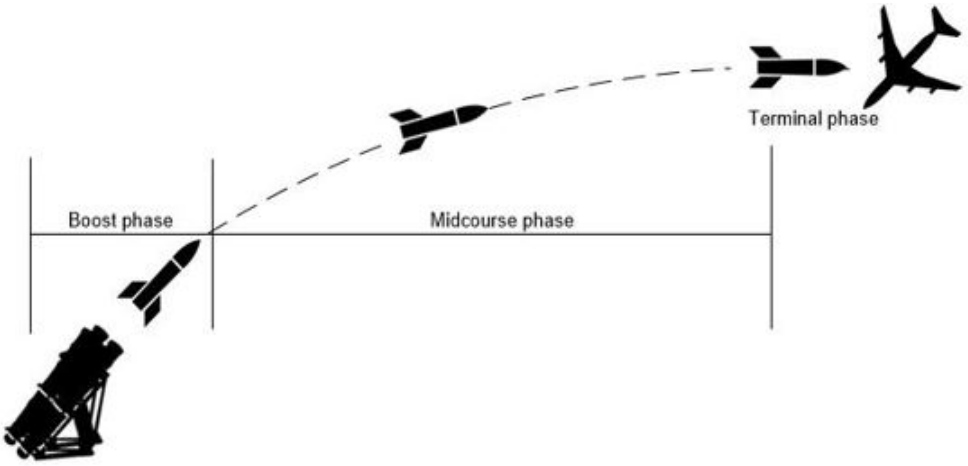

Figure 1.6 Three phases of guidance

- **The Boost Phase:**

  The boost phase is called the initial phase, and the missile gets into a position where it can lock on the target or take the external guidance signals in this part.

- **The Midcourse Phase:**

  The midcourse phase is the longest phase in terms of time and distance. This phase is where the missile tries to get near the target and is processed to the terminal phase afterward. The missile attempts to approach the target during this phase, following which it routes to the terminal phase.

- **The Terminal Phase:**

  Because high precision and fast response are necessary to hit the target, the performance of the missile is most critical in the terminal phase.

1.1. Overview of control system

Throughout the thesis, robust controllers that are robust against uncertainties and disturbances and allow us to better achieve the results expected from the traditional laws of guidance have been developed by using the standard controllers based on the

above-mentioned guidance law. A general review will be conducted of the control approaches to be studied in the thesis.

The Proportional-Integral-Derivative (PID) control technique is the most well-known classical control system, and it is preferred due to its simplicity and ease of application in all areas. The first idea of this PID controller, which has been studied for years and continues to be studied intensively, emerged in 1769 with James Watt's development of a steam engine. In 1911, the PID controller structure was fully developed for the US Navy. With the development of Zieglers and Nichols tuning methods in 1942, PID came to the fore and has been widely applied in the industry since the 1950s. Since then, it has undergone various developments and changes and has been proposed in new structures such as adaptive PID, intelligent PID, fractional-order PID, optimal PID, auto-tuning of PID, etc. Thus, the performance of the controller has been increased and has continued to be applied in every field [4–9].

Sliding mode control (SMC) that is originated from Russia in the early 1960s is an effective and robust nonlinear control method because of the ability to eliminate matched external disturbances and parameter uncertainties [10]. The first studies that made this theorem popular were the book published in 1976 by Itkis and the research paper written by Utkin in 1977 [10]. Up to now, this method has been used for a wide range of scientific and industrial problems, such as robotics [11], electro-mechanical systems [12, 13], stochastic Markovian jumping systems [14], etc. Despite its prominent features, there are two major problems when using SMC. These problems are the chattering phenomenon, and the emergence of reaching phase, which causes unnecessarily large control signals. Researchers have proposed various SMC strategies to overcome these deficiencies and to improve the performance of the control. Moreover, several researchers have used traditional SMCs together with other control algorithms. Some of these methods are high-order SMC, terminal SMC, integral SMC, fuzzy SMC [15–17].

The chattering phenomenon is a major disadvantage in the use of the SMC and its proposed variants. This problem, referred to as high-frequency oscillations in the control signal, results

in unnecessary wear and tear on the actuator [18, 19]. To alleviate the disadvantages of discontinuity in the control law, a solution could be to use a saturation function or add a boundary layer around the sliding subspace. Another solution is the use of a high-order SMC approach, which has been studied extensively in recent years [20–22]. While new methods continue to be proposed to reduce or eliminate the chattering, super-twisting sliding mode control has been put forward. The super-twisting SMC method is one of the second-order SMC methods and it is known for its robustness and ability to eliminate chattering [22–25].

In order to overcome the chattering phenomenon, a new scheme called disturbance observer based control has been designed because the previous methods (the saturation function, the boundary layer, the high order SMC, etc.) need the upper bound of the disturbance as well. The disturbance observer (DOB) is an efficient technique to observe parameter uncertainties and external disturbances in the system, [26]. Although this technique appears with different names and prospects in terms of design, all of them have the same idea: they estimate the disturbance or uncertainties of the system and then compensate by making use of the estimate. This technique has been applied in many different fields in the literature since it was designed by K. Ohnishi [27].

Another disadvantage of SMC is the reaching phase. The system states are moved from their initial state to a manifold called the sliding surface, and the time it takes to reach this is called the reaching phase. In this phase, the system is precision to noise and uncertainties and can be affected by them. As a solution to this problem, an integral sliding mode (ISMC) is presented by Utkin and Shi [28]. The ISMC method is one of the sophisticated SMC methods, and its literature that addresses both linear and nonlinear systems in a variety of control fields has been growing rapidly [29, 30]. This method intends to eliminate the reaching phase in order to ensure the invariance of the SMC from the initial instant of time, according to the traditional SMC method. Thus, the system can guarantee robustness throughout the entire response. However, there is a significant shortcoming concerning the ISMC method. Determining the switching gain is always a troublesome process, such that the upper bound of the external disturbance needs to be known and this gain must be chosen bigger than this upper bound. Most of the research outcomes for the ISMC method are

based on assumptions about the upper bound disturbance knowledge. However, this is not always possible in practical applications. To overcome the abovementioned problem, the adaptive law has been proposed in previous studies, and this has enabled the development of an adaptive integral sliding mode control [31, 32].

For many years, numerous studies in which fuzzy logic has been used together with the SMC method have been reported in the literature. Fuzzy logic theory, proposed by Zadeh in 1965, was developed to represent uncertainties, replacing the concept of net sets. Fuzzy logic and fuzzy sets come into play if the information is uncertain and has subjective uncertainties [33, 34]. In the past few years, researchers have begun to use fuzzy logic and various control methods together, and numerous studies in which fuzzy logic has been used together with the SMC method have been reported in the literature [35–38]. One of the benefits of using control methods and fuzzy logic methods together is that, since the fuzzy logic control method is a rule-based algorithm, determining different gains for different parts of the input space is a solution to the very large and small gain selection problem [39–41].

1.2. Thesis Motivations and Aims

Motivated by the above sections considerations, the fact that the guidance systems are still being investigated intensely in the realms of research and industry has been a light for us, and the basic purpose of the thesis has been decided to be to design a robust control scheme for missile guidance systems.

This thesis mainly focuses on developing a robust control structure to cope with disturbances, uncertainties for the missile guidance system. Therefore, more efficient and robust composite structures have been obtained by combining different control methods and other supportive approaches such as nonlinear observer, intelligent methods, and adaptive algorithms. The approaches proposed in the thesis, as well as their goals, will be discussed briefly below.

In the first approach, two guidance laws based on traditional control techniques, the PID and the SMC, are developed and compared with the results of the classical two guidance laws, which are the Proportional Navigation (PN) guidance law and the Augmented

Proportional Navigation (APN) guidance law. Firstly, the missile and target are modelled in three-dimensional (3D) engagement geometry. Secondly, all guidance laws are developed for non-maneuvering as well as maneuvering targets considering external disturbances. Furthermore, the saturation function is used in order to eliminate the chattering phenomenon, which is the most important disadvantage of the present SM-based guidance laws.

In the second approach, a novel composite 3D guidance law based on an adaptive integral sliding mode (AISM) control technique utilizing an NDOB method is designed for interception scenarios missile-target. Firstly, an integral sliding mode (ISM) control method is selected to design the guidance law to get rid of the reaching phase of traditional SMC. The upper bound of the target's unknown accelerations is estimated by designing an adaptive algorithm, and prior information of the upper bound is not needed. Secondly, the NDOB technique is designed to estimate and compensate for the accelerations of the target that are considered as the disturbance. Thus, the NDOB technique and the AISM guidance law are combined into a novel composite guidance law to improve guidance performance and reduce the chattering phenomenon. According to the results, the proposed composite guidance law guarantees convergence of the line-of-sight (LOS) angular rate to zero in finite-time. Moreover, in terms of miss distance and interception time, the proposed guidance law outperforms the other schemes.

The third approach is propose the design of a 3D missile guidance law based on a second-order SMC technique employing an adaptive tuning law and fuzzy gain scheduling. At the outset, the super-twisting sliding mode guidance law is obtained to overcome the chattering problem. Then, without knowledge about the bounds of disturbances, an adaptive law is used to determine the control gains. The results are enhanced using a fuzzy module that provides the controller parameters according to a set of linguistic rules. To validate the proposed guidance law's performance and effectiveness, we compared it to the SM guidance law, the traditional super-twisting SM (STWSM) guidance law, the adaptive super-twisting SM (ASTWSM) guidance law, and the adaptive fuzzy super-twisting SM (AFSTWSM) guidance law. The simulation scenarios consider fundamental target movements. The results

demonstrate that the presented adaptive guidance laws display better performance in terms of intercept time and miss distance compared to the alternatives considered in this study.

In the last approach, a new guidance approach utilizing the APN guidance law with an NDOB technique is proposed, considering different target models. The APN guidance law is designed by considering the acceleration information of the target. For this purpose, an NDOB technique is utilized to obtain the target acceleration. Thus, when designing the APN guidance law, it can be designed without the need for target acceleration information. Moreover, when the results obtained are examined, it can be seen that this newly presented design is more successful than the classical APN guidance law.

1.3. Contributions

In this thesis, the main contributions can be summarized as follows:

- Development of the guidance law based on the traditional control methods such as PID and SMC
- Investigation of these control methods that satisfy missile-target interception geometry in 3D for different target accelerations
- Development a novel composite guidance approach that consists of the integral sliding mode control method, adaptive algorithm, and nonlinear disturbance observer technique
- Investigation of this composite method that satisfies missile-target interception geometry in 3D for different target accelerations
- Proposing a novel guidance law that consists of the higher-order sliding mode control method, adaptive algorithm, and fuzzy gain scheduling
- Investigation of this new guidance law that satisfies missile-target interception geometry in 3D for different target accelerations

- Development of a new guidance law that consists of augmented proportional navigation, one of the traditional guidance laws, and nonlinear disturbance observer
- Investigation of this new guidance law that satisfies missile-target interception geometry in 3D for different target accelerations

Among the studies mentioned in the above section, the first and last techniques were presented as two separate international conference papers, whilst the second and third approaches were edited as journal articles. The International Journal of General Systems has accepted one, while the Proceedings of the Institution of Mechanical Engineers, Part G: Journal of Aerospace Engineering is still reviewing the other.

1.4. Organization

The organization of the thesis is given as below:

- Chapter 1 introduces the overview of control system, thesis motivations and aims, contributions and the scope of the thesis.
- Chapter 2 presents a brief overview of the previous published work on the missile guidance system based on the control methods.
- Chapter 3 gives a general overview of the missile system. This chapter is separated into two subsections. The first subsection introduces a detailed description of the mathematical model of the missile. The second subsection gives the classical guidance law methods.
- Chapter 4 introduces the guidance law based on traditional control methods. Firstly, the PID control technique is utilized to design the guidance law. Then, the SMC method is handled in the designed guidance law. Moreover, this chapter gives the results of numerical simulations, comparative analysis, and discussion.

- Chapter 5 describes the novel guidance law in detailed. Then, we show the results of numerical simulations of this proposed method. In addition, this chapter presents the results of numerical simulations, comparative analysis, and discussion.
- Chapter 6 describes the other novel guidance law in detailed. Then, we demonstrate the simulation results of this method. In addition, this chapter presents comparative analysis and discussion.
- Chapter 7 expresses the effect of the nonlinear disturbance observer on the augmented proportional law that one of the classical guidance laws. In addition, this chapter presents the results of numerical simulations, comparative analysis, and discussion.
- Chapter 8 states the summary of the thesis and possible future directions.

2. RELATED WORK

The PID control method is the most well-known classical control method and is preferred thanks to its nature of being simple and easy to apply in every area. This law depends not only on the LOS rate but also on the LOS angle in order to overcome disturbances and miss distance problems [42–52].

Golestani et al. [42] proposed a state-of-the-art guidance algorithm, which was developed by using PID guidance law. In that paper, the stability analysis was made by utilizing a circle criterion. According to the results, it significantly improved performance the guidance based on the classical PN guidance law for a maneuvering target.

In 2018, Xie and Su [43] presented a guidance law with PID and fuzzy logic. The fuzzy logic algorithm was employed to improve the controller parameters in the system online that were utilized for guiding the missile. The results were evaluated according to different scenarios.

The research in [44] focused on designing the PID control method with a fuzzy set-point weighting in a 2D differential geometric for guidance and control systems. The model was supposed to be exposed to track the commanded angle of attack efficiently. In the results, it was stated that the proposed system responded quickly and performed as a stable system.

In 1995, Gonsalves et al. [45] reported the conventional PID approach based on fuzzy logic terminal guidance for a surface-to-surface missile. Simulations conducted against two different targets, and they stated that it differed from conventional guidance methods with advantages such as robustness to sensor noise and failure accommodation.

Li and Jing [46] designed a guidance law by utilizing the PID control technique for the guidance problem of the missile. They compared the results of the simulation with PN, which is one of the classical guidance laws, and stated that the guidance law they offered was effective and a fast-response system.

In [47], Lin et al. presented the importance of choosing the appropriate navigation constant and guidance law using the PID method, PPN, and APN guidance laws, and the performance results of the system in terms of miss distance were also demonstrated.

The research in [48] proposed a new guidance law by using the fractional order PID control method and dynamic inversion based autopilot against maneuvering targets for hit-to-kill interceptors. In that paper, the stability analysis was made by utilizing a circle criterion. Numerical simulations were performed to demonstrate the performance of the proposed guidance law and its effectiveness was verified.

In 2017, Yaghi and Efe [49] designed the new guidance system using many intelligent tuning techniques and the fractional order PID system. The used intelligent methods were the particle swarm optimization, genetic algorithms, and neural tuning techniques. According to the results presented, it was seen that the proposed guidance systems had fewer miss distance values and thus were more accurate in hitting the target. It had also been shown to perform well in terms of increased stability at the angle of attack.

Nobahari and Pourtakdoust [50] proposed a novel method for line-of-sight guidance law. In the paper, the new guidance approach was handled as two phases: a proportional derivative (PD) fuzzy sliding mode controller has been developed for the first phase, and a new hybrid fuzzy PID has been developed for the second phase. Moreover, the presented guidance law parameters for the phases were optimized utilizing ant colony optimisation. The results were evaluated according to different scenarios.

Evcimen et al. [51] developed an adaptive, optimal guidance law based on the PID control method to increase efficiency against fast maneuvering targets. The PID parameters were determined as adaptive by using linear optimal control theory.

The research in [52] presented the optimal fuzzy reasoning and a fuzzy-PID controller. In that study, a controller based on optimal fuzzy reasoning method was proposed for the attitude control system of missile terminal guidance and a stable fuzzy-PID structure was obtained.

The SMC is a robust and nonlinear control technique in the presence of uncertainty of the system parameters as well as external disturbances and it also has been used as control method in many studies for many years. Up to now, sliding mode control has been compared against several guidance laws by many researchers for designing missile guidance systems. SMC has provided better results compared to the others due to having many advantages such as robustness against uncertainties, parameter variations as well as disturbances [53–65].

Moon et al. [53] demonstrated a guidance law using variable structure control by taking the target acceleration bound during maneuvering into account. Numerical simulations were performed to demonstrate the performance of the proposed guidance law and its effectiveness was verified.

Shtessel et al. [54] proposed the novel guidance law by utilizing smooth second-order sliding mode (SOSM) against the evasive maneuvers of target. The results of the method suggested in the comparison were produced against a maneuvering ballistic missile and compared with the results of APN guidance law.

In 2010, Lee et al. [55] conducted research on guidance law by using the SMC method for two different movements of the target, such as a slowly moving or a stationary. In the results of that paper, it was emphasized that the sliding surface and lateral miss distance converged to zero at terminal time.

In [56] two guidance laws in two-dimensional engagement were introduced using the fast SM guidance law and the variable dynamic SM guidance law. The results of that paper stated that fast SM guidance law was better than variable dynamic SM guidance law in terms of convergence time and at eliminating the chattering phenomenon.

In [57], Lee and Kim proposed a guidance law with a sliding mode by using dual sliding surfaces considering terminal impact angle constraints. The guidance law was designed in 3D engagement geometry and 6-DOF numerical simulations were conducted for missile-target engagement scenarios. The results demonstrated an up-and-coming performance along with efficiency by using the proposed guidance law.

In 2016, Sun et al. [58] developed a novel fast terminal SMC with an extended state observer in order to satisfy a more optimized trajectory for guidance law. Moreover, the missile interception was modelled, taking impact angle constraints into account. The efficiency of the presented law was supported and demonstrated by taking stationary targets, constant velocity targets, and maneuvering targets into account by numerical simulation.

Wang and He [59] reported a guidance law with LOS angle constraints for intercepting targets that are maneuvering. They used an optimal SM guidance law and developed the equivalent control part of the SMC method using model predictive control to satisfy the terminal angle constraint in that paper. Moreover, both the missile and the target were assumed to have a point mass, and this law was designed for planar missile–target engagement.

The research in [60] proposed a finite-time convergent sliding mode guidance law by taking the terminal impact angle constraint into account. The results showed that the LOS angular rate converged to zero in a finite time. The simulation outcomes verified the capabilities of the presented guidance law for intercepting the target.

Utilizing the SMC algorithm, Shin et al. [61] presented a new 3D guidance law for the interception of maneuvering targets. The performance of the developed law was examined in two different ways according to the presence of disturbance, and the validity of the introduced law was proven with respect to the simulation results.

In [62], the authors introduced the SMC based on PN guidance law. Furthermore, they did not require data of the target acceleration bounds and used inertial delay control for the estimation of the target's information. The results of simulation proved the efficiency of the introduced law.

In 2012, Zhu et al. [63] examined the SMC with finite-time convergence to design guidance laws. To alleviate the effect of the chattering phenomenon, they designed the extended state observer, which obtains the estimation of the target acceleration. The outcomes showed that it was obtained as a better law than the other simulated guidance laws.

The research introduced by [64], contains two guidance laws that were designed by using adaptive algorithm and non-singular terminal SMC in the presence of an impact angle constraint. In that paper, the engagement geometry was handled as 2D geometry. Moreover, it had an online adaptive algorithm to guess the upper bound of the target accelerations. The capabilities of these newly introduced guidance laws were verified by testing the system against different models of target maneuvering.

Guo et al. [65] proposed the new observer-based continuous adaptive sliding mode guidance in the 2D geometry. To estimate the target acceleration, a renewed nonlinear extended state observer was introduced. The results of simulation proved the efficiency of the proposed guidance law.

On the other hand, it is well known that the SMC framework suffers from the chattering problem arising due to the discontinuous switching term. To alleviate the disadvantages of the discontinuity in the control law, the ISMC has been proposed as one remedy. When a literature review is carried out, this method is encountered in most areas and shows great potential in the area of missile guidance systems [31, 32, 66–72].

In [31], an adaptive ISM guidance law was presented for planar engagement geometry with respect to impact angle constraint considering autopilot lag. A sliding surface, which was acceleration, the LOS angular rate and tracking error of LOS angle were considered together, was designed in that paper.

Junhong and Shenmin [32] proposed the guidance law in three-dimensional space by using the ISMC. Then, an adaptive guidance law based on ISMC was improved to forecast the target acceleration's upper bound. The performance of the presented guidance law was examined for the missiles air-intercepting the maneuvering targets at constant and time-varying speeds. The simulations were run against the ISMC guidance law, and the results demonstrated the proposed guidance law's accuracy. The numerical simulations were conducted comparatively, and the outcomes showed that it was obtained as a better law than the other simulated guidance laws.

Golestani et al. [66] proposed a finite-time integral sliding mode scheme for the guidance system of a missile regarding the geometry of planar interception. The capabilities of these newly introduced guidance laws were verified by testing the system against different models of target maneuvering.

In the article published by Zhang et al. [67], impact angle control over guidance based on the ISM manifold with finite-time control was proposed, and also the second-order extended state observer (ESO) was used. Besides, the missile and target were designed with a point mass model.

In [68], the authors proposed a new composite law for the guidance system of a missile intercepting maneuvering targets in planar interception geometry using an ISM method and NDOB technique. Moreover, the guidance law was designed considering the constrained impact angle as well as a first-order-lag autopilot. The efficiency of the conducted guidance law was verified and shown by numerical simulation.

Liang et al. [69] investigated a robust guidance law by utilizing an ISM scheme, and both the missile and the target were taken to be point-mass models. The simulation results were achieved according to four different situations in that study, and the findings demonstrated the effectiveness of the presented guidance.

Meng and Zhou [70] presented a new guidance law by using a super-twisting algorithm with nonlinear ISM by considering missile autopilot dynamics for planar missile-target engagement. Furthermore, the disturbance observer was used in this case to handle the disturbances caused by the target's acceleration.

Zhang et al. [71] designed the terminal guidance law by using both the linear and nonlinear ISM control methods and the NDOB technique, considering impact angle constraints. In addition, a point-mass model was used in the missile and target design in that paper. It was emphasized in the study that the switching gains should be selected greater than the target acceleration to achieve a high level of performance in the design made with the ISM

guidance law. However, this situation led to the chattering phenomenon. Therefore, they used the NDOB technique for target acceleration estimation.

In 2020, the authors [72] proposed the ISM guidance law to address the maneuvering target considering impact angle constraints and also the dynamic specifications of the autopilot. The stability analysis was conducted with the Lyapunov method. Numerical simulations were applied to two cases: the nominal case and the real missile model case, and the results were compared with the trajectory shaping guidance law and the general impact angle constrained SM guidance law to prove that the proposed guidance system was effective. Moreover, the results demonstrated that the introduced method was able to accomplish the interception at the intended impact angle.

The second remedy is the use of a high-order SMC approach, which has been studied extensively in recent years, and a widely used variant of it is called super-twisting SMC [20–24]. A large and growing body of literature has investigated the super-twisting SMC method to design the guidance law for missiles [21, 73–81].

In [21], the authors proposed an adaptive smooth second-order sliding mode (SOSM) law, which was employed as a homing guidance law. The performance of the employed guidance scheme was examined considering uncertainty of parametric and disturbances with no information of bounds, and also the accurate ability of the presented guidance law was evaluated via numerical simulations.

In [73], a nonsingular adaptive super-twisting guidance was proposed for missile-target planar engagement geometry subject to impact angle constraint. The efficiency of the presented guidance law was validated and shown by utilizing numerical simulations.

In [74], a nonsingular fast terminal SM guidance law was developed for the targets. The approach considered the maneuvering motion and impact angle constraints and addressed the singularity problem of the terminal SMC scheme. Moreover, that work proposed a fast terminal SM dynamics with an adaptive smooth super-twisting algorithm.

The research in [75] introduced a newly robust guidance law by using SOSM and a back-stepping design method against maneuvering targets, and also a proposed guidance law was designed considering autopilot dynamics in 3D geometry. Moreover, an adaptive SOSM observer was used to estimate the knowledge about the target acceleration.

Xu et al. [76] presented a novel guidance law based on the composite nonsingular fast terminal SM and adaptive super-twisting algorithm. However, that research considered the missile's and target's motion in the pitch plane.

Using the SMC method and a fuzzy logic system, Li et al. [77] presented a new scheme for guidance law under various terminal constraints, which were impact angle, miss distance, and acceleration for the interception scenarios between the missile and the target. The efficiency of the conducted guidance law was verified and shown by using numerical simulations.

Another remarkable application of the fuzzy SMC method was reported by Elhalwagy et al. [78], where a guidance law for the trajectory control of a command guidance system was considered.

In 2019, Zhao and Zhou [79] presented a fixed-time SOSM guidance law considering constraints of impact angle in the planar engagement geometry. In that study, the zero placement principle of a close-loop system was used to make various adjustments and improve the performance. The proposed guidance law was tested on rigid spacecraft, hypersonic missiles, and a variety of real-world systems.

The research in [80] presented the SM guidance law for a passive ranging based missile system in 3D engagement space. The stability of the newly introduced guidance law was guaranteed by using the stability analysis of Lyapunov. By comparing the results of the SM guidance law to the outcomes of the introduced guidance law, the efficacy and feasibility of the new system were validated.

In [81], Zhang et al. presented a new approach to design guidance law by using a stochastic fast smooth SOSM control method in planar geometry. In that study, the guidance law was designed to consider the track imprecision occurring in the presence of inertial lag, model

uncertainties, as well as stochastic noises. Moreover, the designed system added a high-order sliding mode observer. The results were shown in comparison with three methods: APN, SM, and nonsingular terminal SM guidance law. Finally, the feasibility of that proposed guidance approach was validated by using simulations of the guidance law against targets performing evasive maneuvers.

3. BACKGROUND OVERVIEW

In this section, preliminary concepts are presented briefly relevant to missile's mathematical modeling, guidance laws and control systems.

3.1. Mathematical Modeling for Missile

The missile system consists of a number of subsystems that interact with each other to obtain different dynamics and behaviors. In general, these subsystems will be mentioned, and the equations of motion will be explained mathematically.

3.1.1. Coordinate Systems

One of the most important pieces of information to know before modeling the missile system is the coordinate frames [2]. Among these axes, the most important sets of axes that should be known are the sun-centered (heliocentric) frame, the earth frame, the inertial frame, and the body frame. These frames will be briefly explained below, and their key features are briefly tabulated in Table 3.1.

Frame	**Base point**	**First direction**	**Third direction**	**Base vectors**
Heliocentric	H center of sun	h_1 Aries	h_3 normal of ecliptic	h_1, h_2, h_3
Inertial	I center of Earth	i_1 vernal equinox	i_3 Earth's spin axis	i_1, i_2, i_3
Earth	E center of Earth	e_1 Greenwich	e_3 Earth's spin axis	e_1, e_2, e_3
Body	B center of mass	b_1 nose	b_3 down	b_1, b_2, b_3

Table 3.1 General features of frames [1]

Sun-centered (heliocentric) frame:

A sun-centered (heliocentric) coordinate system with the Z-axis normal to and northward from the ecliptic plane is known as the Heliocentric frame [1]. Furthermore, the x-axis

is determined towards the first point of the Vernal Equinox, the y-axis is determined with respect to the standard right-hand rule. This frame is shown in Figure 3.1 [1].

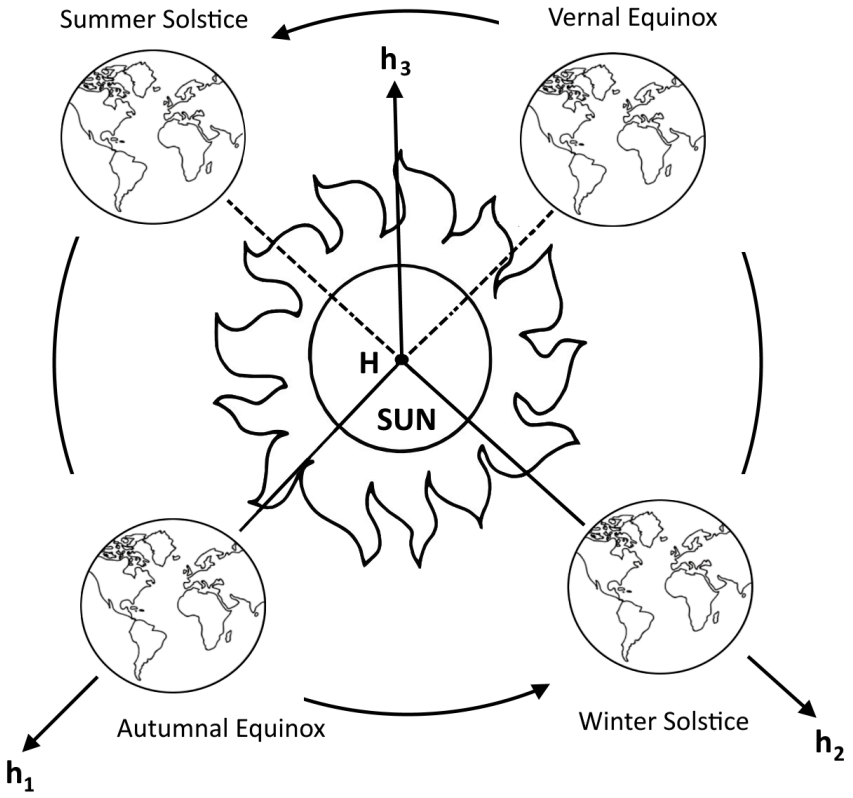

Figure 3.1 Sun-centered (heliocentric) frame

Earth frame:

Its center coincides with the world center. The z-axis of this set of axes passes through the north pole region, while the x-axis passes through the intersection of the Greenwich meridian and the equator line. Additionally, the Y-axis is determined with respect to the standard right-hand rule. In Figure 3.2, the Earth frame is demonstrated [1].

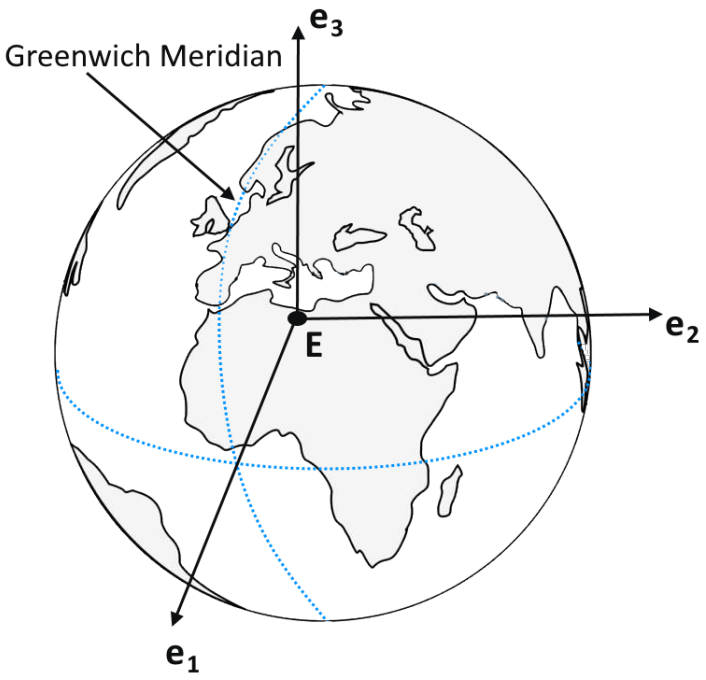

Figure 3.2 Earth frame

Missile frame:

The center of this axis coincides with the center of gravity of the missile. Thus, the x-axis is determined towards the nose of the missile, the y-axis is determined towards the right, and the z-axis is determined with respect to the standard right-hand rule and this frame is given in Figure 3.3.

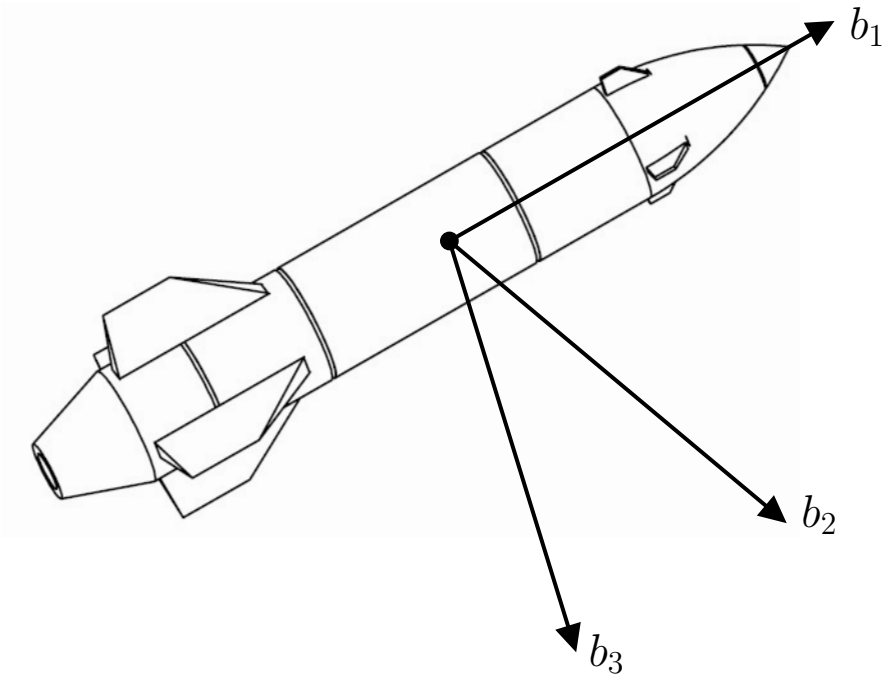

Figure 3.3 Missile frame

Inertial frame:

An inertial coordinate system is a reference frame that is not undergoing acceleration. The center of the inertial axes is determined as the world center. However, it is assumed that this axis does not rotate and accelerate with respect to the stars. In this set of axes, the z-axis is selected in the earth plane, and the x and y-axes are selected in the equatorial plane [2]. This frame is displayed in Figure 3.4 [1].

3.1.2. Coordinates Transformation and Matrices of Transformation

The yaw angle, the direction of in the z-axis, the roll angle, the direction of in the x-axis, and the pitch angle, the direction of in the y-axis are used to calculate the transformation between the Earth axis set and the missile axis set. In the literature, yaw, pitch, and roll angles are generally referred to as ”Euler angles” [1].

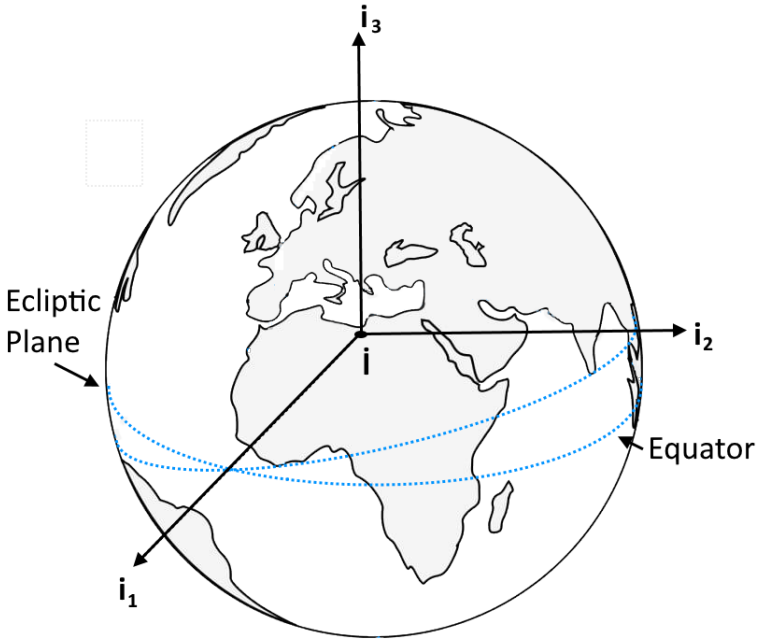

Figure 3.4 Inertial frame

Firstly, Equation 1 and Figure 3.5 show how to calculate the transformation matrix using ϕ (yaw angle) around the z_e access.

$$\begin{bmatrix} x_b \\ y_b \\ z_b \end{bmatrix} = C_\psi \begin{bmatrix} x_e \\ y_e \\ z_e \end{bmatrix} = \begin{bmatrix} \cos\psi & \sin\psi & 0 \\ -\sin\psi & \cos\psi & 0 \\ 0 & 0 & 1 \end{bmatrix} \begin{bmatrix} x_e \\ y_e \\ z_e \end{bmatrix} \tag{1}$$

Secondly, Equation 2 and Figure 3.6 are given considering one rotation θ (pitch angle) around the y_e access to calculate the transformation matrix.

$$\begin{bmatrix} x_b \\ y_b \\ z_b \end{bmatrix} = C_\theta \begin{bmatrix} x_e \\ y_e \\ z_e \end{bmatrix} = \begin{bmatrix} \cos\theta & 0 & -\sin\theta \\ 0 & 1 & 0 \\ \sin\theta & 0 & *cos\theta \end{bmatrix} \begin{bmatrix} x_e \\ y_e \\ z_e \end{bmatrix} \tag{2}$$

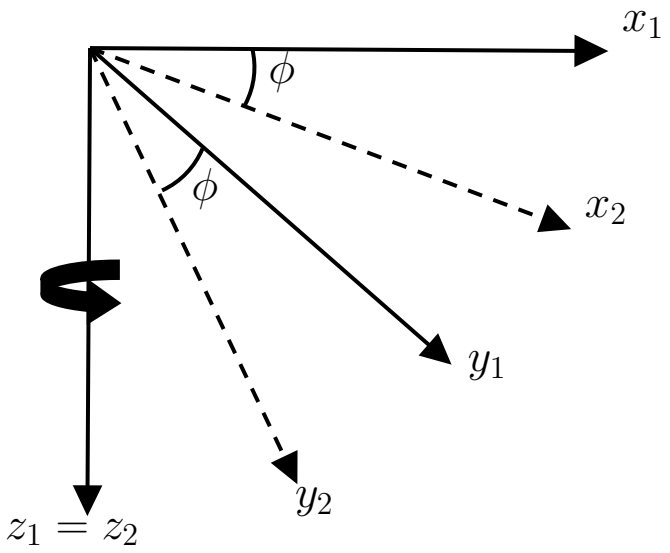

Figure 3.5 The rotation z axis and ϕ (yaw angle)

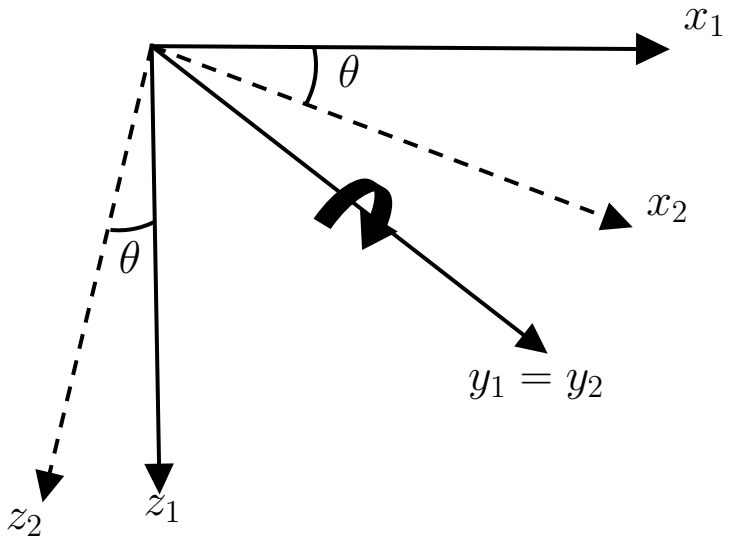

Figure 3.6 The rotation y axis and θ (pitch angle)

Finally, Equation 3 and Figure 3.7 show how to calculate the transformation matrix using one rotation of ψ (roll angle) around the z_e access.

$$\begin{bmatrix} x_b \\ y_b \\ z_b \end{bmatrix} = C_\phi \begin{bmatrix} x_e \\ y_e \\ z_e \end{bmatrix} = \begin{bmatrix} 1 & 0 & 0 \\ 0 & \cos\phi & \sin\phi \\ 0 & -\sin\phi & \cos\phi \end{bmatrix} \begin{bmatrix} x_e \\ y_e \\ z_e \end{bmatrix} \tag{3}$$

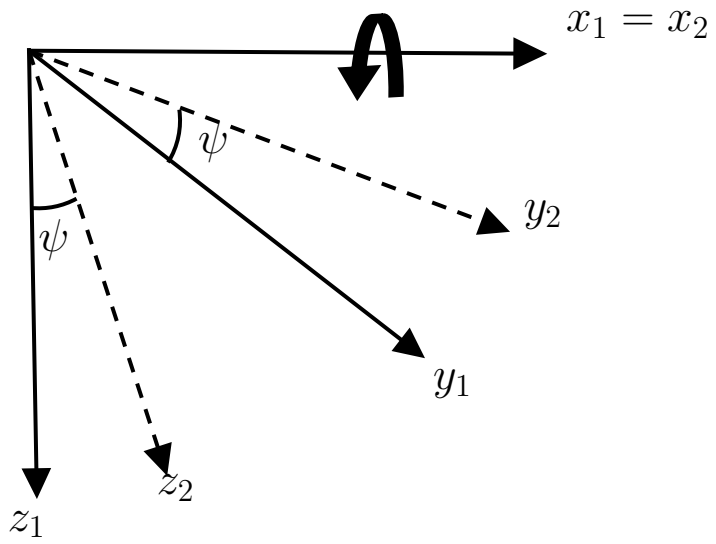

Figure 3.7 The rotation of x axis and ψ (roll angle)

The matrices of transformation are obtained by multiplying the rotation matrices, and the order of the axis is important during this multiplication. These transformation matrices are also known as the Direction Cosine Matrix (DCM). In the equations below, the transformation is performed in the order of the z, y, x axes.

$$\begin{bmatrix} x_b \\ y_b \\ z_b \end{bmatrix} = C_\phi C_\theta C_\psi \begin{bmatrix} x_e \\ y_e \\ z_e \end{bmatrix} \tag{4}$$

Substituting (1), (2) and (3) into (4) yields the following the equation.

$$\begin{bmatrix} x_b \\ y_b \\ z_b \end{bmatrix} = \begin{bmatrix} 1 & 0 & 0 \\ 0 & \cos\phi & \sin\phi \\ 0 & -\sin\phi & \cos\phi \end{bmatrix} \begin{bmatrix} \cos\theta & 0 & -\sin\theta \\ 0 & 1 & 0 \\ \sin\theta & 0 & \cos\theta \end{bmatrix} \begin{bmatrix} \cos\psi & \sin\psi & 0 \\ -\sin\psi & \cos\psi & 0 \\ 0 & 0 & 1 \end{bmatrix} \begin{bmatrix} x_e \\ y_e \\ z_e \end{bmatrix} \tag{5}$$

Accordingly, the following equation is obtained.

$$\begin{bmatrix} x_b \\ y_b \\ z_b \end{bmatrix} = \begin{bmatrix} \cos\theta\cos\psi & \cos\theta\sin\psi & -\sin\theta \\ \cos\phi\sin\psi + \sin\phi\sin\theta\cos\psi & \cos\phi\cos\psi + \sin\phi\sin\theta\sin\psi & -\sin\phi\cos\theta \\ \sin\phi\sin\psi + \cos\phi\sin\theta\cos\psi & -\sin\phi\cos\psi + \cos\phi\sin\theta\sin\psi & \cos\phi\cos\theta \end{bmatrix} \begin{bmatrix} x_e \\ y_e \\ z_e \end{bmatrix} \tag{6}$$

Equation (6) cab be rewritten as below.

$$\begin{bmatrix} x_b \\ y_b \\ z_b \end{bmatrix} = C^{(b,e)} \begin{bmatrix} x_e \\ y_e \\ z_e \end{bmatrix} \tag{7}$$

Transformation matrices can be made using the Quaternion angle model as well as Euler angles. Although it is preferred because there are no trigonometric expressions in the Quaternion angle model, its use is avoided because it requires normalization after each calculation. In addition, it is possible to convert each Quaternion and Euler angle to each other.

3.1.3. Equations of Motion

First of all, a dynamic model of the missile will be created to obtain the missile's equations of motion [82]. For this reason, this section will be examined under the sub-headings of dynamic equations and kinematic equations. The axis and motion variables of the missile

are given in Figure 6, and the definitions of these variables are explained in Table 3.2 and 3.3.

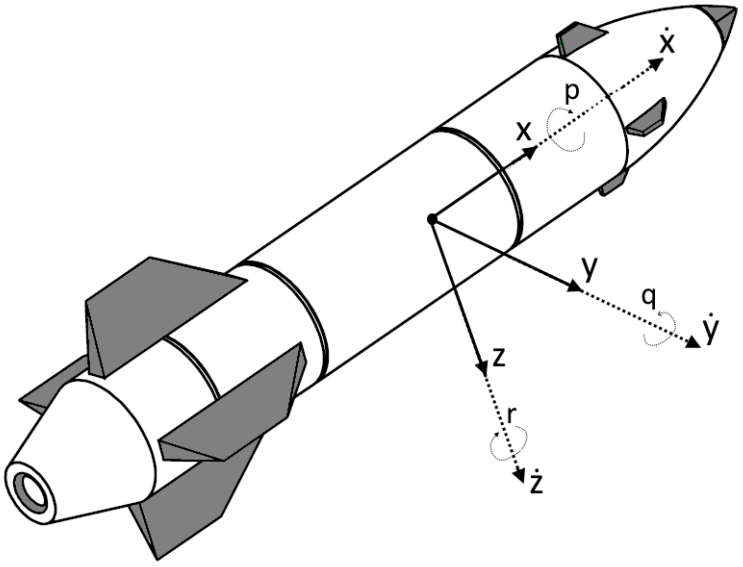

Figure 3.8 The missile and the body-fixed coordinate-system illustrated

In general, the kinematic and dynamic equations, which are necessary to define the missile model, are discussed separately as rotational and translational below.

Axis	**Name**	**Linear Velocity**	**Angular Displacement**	**Angular Rates**
OX	Roll	u	ϕ	P
OY	Pitch	v	θ	Q
OZ	Yaw	w	ψ	R

Table 3.2 Axis Definition [2]

3.1.3.1. Dynamical Equations of Motion In order to derive the dynamic model of the missile, first of all, the force equations are obtained taking Newton's Second Law into account.

Axis	Force	Moment	Moment of Inertia	Product of Inertia
OX	F_x	L	I_x	$I_{xy} = 0$
OY	F_y	M	I_y	$I_{yx} = 0$
OZ	F_z	N	I_z	$I_{zx} \neq 0$

Table 3.3 Moment Designation [2]

$$\overrightarrow{F} = \frac{d}{dt}(m\overrightarrow{V})|_E \tag{8}$$

Equation given in (8) is rewritten as below.

$$\overrightarrow{F} = m\frac{d}{dt}(\overrightarrow{V})|_E \tag{9}$$

which m represents the mass of the missile and V represents the total speed of the missile.

Also, the expression $|_E$ next to (9) means that that parameter is expressed in the earth axes. If we re-express (9) according to the body axes,

$$\overrightarrow{F} = m\left\{\frac{d}{dt}(\overrightarrow{V})|_B\right\} + \overrightarrow{\omega}_{ang} \times \overrightarrow{V} \tag{10}$$

which $\overrightarrow{F}$, $\overrightarrow{V}$, and $\overrightarrow{\omega}_{ang}$ are defined as the following equations. $\overrightarrow{F}$ is shown by the following column vectors.

$$\overrightarrow{F} = \begin{bmatrix} F_x \\ F_y \\ F_z \end{bmatrix} \tag{11}$$

where F_X, F_Y, F_Z denote aerodynamic drag, aerodynamic lift, and aerodynamic lateral force, respectively.

In 10, $\overrightarrow{V}$ denotes the velocity of the missile and is written as below.

$$\overrightarrow{V} = \begin{bmatrix} u \\ v \\ w \end{bmatrix} \tag{12}$$

in which u, v, w represent the components of linear velocity.

In 10, $\overrightarrow{\omega}_{ang}$ denotes the angular velocity of the missile and is written as below.

$$\overrightarrow{\omega}_{ang} = \begin{bmatrix} p \\ q \\ r \end{bmatrix} \tag{13}$$

where p, q, r denote the angular velocity components.

Substituting (11),(12) and (13) into (10)

$$\begin{bmatrix} F_x \\ F_y \\ F_z \end{bmatrix} = m \left\{ \begin{bmatrix} \dot{u} \\ \dot{v} \\ \dot{w} \end{bmatrix} + \begin{bmatrix} p \\ q \\ r \end{bmatrix} \times \begin{bmatrix} u \\ v \\ w \end{bmatrix} \right\} \tag{14}$$

If the necessary manipulations are made in the equation given above,

$$\begin{bmatrix} \dot{u} \\ \dot{v} \\ \dot{w} \end{bmatrix} = \begin{bmatrix} \frac{F_x}{m} \\ \frac{F_y}{m} \\ \frac{F_z}{m} \end{bmatrix} - \begin{bmatrix} p \\ q \\ r \end{bmatrix} \times \begin{bmatrix} u \\ v \\ w \end{bmatrix} \tag{15}$$

Translational dynamics can be described through equations such as the following:

$$\dot{u} = \frac{F_x}{m} - qw + rw \tag{16}$$

$$\dot{v} = \frac{F_y}{m} - ru + pw \tag{17}$$

$$\dot{w} = \frac{F_z}{m} - pv + qu \tag{18}$$

Rotational dynamic equations are obtained as follows. In missile motion, angular movement is also important along with axial movement. Euler's equations are used to express this.

$$\overrightarrow{M} = \frac{d}{dt}(\overrightarrow{H})|_E \tag{19}$$

in which $\overrightarrow{M}$ is the total of the applied torques, and $\overrightarrow{H}$ denotes the angular momentum. The angular momentum expression can be written as follows.

$$\overrightarrow{H} = \hat{J}\overrightarrow{\omega}_{ang} \tag{20}$$

which $\hat{J}$ denotes is the inertia dyadic. Substituting (20) into (19)

$$\overrightarrow{M} = \frac{d}{dt}(\overrightarrow{H})|_B + \overrightarrow{\omega}_{ang} \times \hat{J}\overrightarrow{\omega}_{ang} \tag{21}$$

In 21, $\hat{J}$ is depicted as follows.

$$\hat{J} = \begin{bmatrix} I_{xx} & -I_{xy} & -I_{xz} \\ -I_{xy} & I_{yy} & -I_{yz} \\ -I_{xz} & -I_{yz} & I_{zz} \end{bmatrix} \tag{22}$$

The missile's body axis is supposed to be coincident to the principal axis of inertia. As a result, the terms I_{xy}, I_{yz}, I_{xz} for the product of cross inertia disappear, and the inertia matrix

given in 22 can be written as follows:

$$\hat{J} = \begin{bmatrix} I_{xx} & 0 & 0 \\ 0 & I_{yy} & 0 \\ 0 & 0 & I_{zz} \end{bmatrix} \tag{23}$$

In 21, $\overrightarrow{M}$ is represented by the following column vectors.

$$\overrightarrow{M} = \begin{bmatrix} M_x \\ M_y \\ M_z \end{bmatrix} \tag{24}$$

in which M_x, M_y, M_z denote the components of the total moment.

Substituting 22, 23 and 24 into 21 and the above equations can be presented in the following form:

$$\begin{bmatrix} M_x \\ M_y \\ M_z \end{bmatrix} = \begin{bmatrix} I_{xx} & 0 & 0 \\ 0 & I_{yy} & 0 \\ 0 & 0 & I_{zz} \end{bmatrix} \begin{bmatrix} \dot{p} \\ \dot{q} \\ \dot{r} \end{bmatrix} + \begin{bmatrix} p \\ q \\ r \end{bmatrix} \times \begin{bmatrix} I_{xx} & 0 & 0 \\ 0 & I_{yy} & 0 \\ 0 & 0 & I_{zz} \end{bmatrix} \begin{bmatrix} p \\ q \\ r \end{bmatrix} \tag{25}$$

where

$$M_x = I_{xx}(\dot{p}) + \left(I_{zz} - I_{yy}\right) rq \tag{26}$$

$$M_y = I_{yy}(\dot{q}) + \left(I_{xx} - I_{zz}\right) pr \tag{27}$$

$$M_z = I_{zz}(\dot{r}) + \left(I_{yy} - I_{xx}\right) qp \tag{28}$$

Using these equations, one obtains the following results from 26, 27 and 28.

$$\dot{p} = \frac{M_x - qr\left(I_{zz} - I_{yy}\right)}{I_{xx}} \tag{29}$$

$$\dot{q} = \frac{M_y - rp\left(I_{xx} - I_{zz}\right)}{I_{xx}} \tag{30}$$

$$\dot{r} = \frac{M_z - pq\left(I_{yy} - I_{xx}\right)}{I_{xx}} \tag{31}$$

3.1.3.2. Kinematical Equations of Motion Rotational kinematic equations are defined using four fundamental data points. This concept establishes the connections between rotation angle, angular acceleration, angular velocity, and time. In order to obtain the rotational kinematic equations, the following operations will be performed, respectively. Firstly, Euler angles and DCM transformations are used to track the missile's position relative to the ground. DCM transformations are updated using (32).

$$C^{(e,b)} = \int C^{(e,b)} \tilde{w}^{(b)} dt \tag{32}$$

$$\tilde{w} = \left[C^{(e,b)}\right]^T C^{(e,b)} \overrightarrow{w}_{ang} \tag{33}$$

where $\overrightarrow{w}_{ang}$ is given in (13). Since $\overrightarrow{w}_{ang}$ is skew-symmetric, it can be defined as in (34).

$$\tilde{w} = \begin{bmatrix} 0 & -r & q \\ r & 0 & -p \\ -q & p & 0 \end{bmatrix} \tag{34}$$

Equation (32) is arranged, and then rotational kinematics can be described through equations such as the following:

$$\begin{aligned} \dot{\phi} &= p + \tan\theta(q\sin\phi + r\cos\phi) \\ \dot{\theta} &= q\cos\phi - r\sin\phi \\ \dot{\psi} &= \frac{1}{\cos\theta}(q\sin\phi + r\cos\phi) \end{aligned} \tag{35}$$

where θ, ϕ, ψ denote pitch, yaw, and roll angle, respectively.

Translational kinematics equations are described as follows.

$$\begin{aligned} \dot{x} &= V\cos\gamma\cos\kappa \\ \dot{y} &= V\sin\gamma \\ \dot{z} &= -V\cos\gamma\sin\kappa \end{aligned} \tag{36}$$

where γ and κ denote the trajectory inclination angle and deflection angle, respectively.

3.1.4. Aerodynamic Forces and Moments

In addition, this forces and moments must be included in the system to define the movement of the missile in the air. Aerodynamic drag, aerodynamic lateral force, and aerodynamic lift, as well as pitch, yaw, and roll moments, are utilized and the entire set of forces and moments are calculated. Some equations to be used in this calculation are given below.

$$\overrightarrow{F} = \overrightarrow{F}_{aero} + \overrightarrow{F}_{gravity} + \overrightarrow{F}_{thrust} \tag{37}$$

$$\overrightarrow{M} = \overrightarrow{M}_{aero} + \overrightarrow{M}_{gravity} + \overrightarrow{M}_{thrust} \tag{38}$$

This section will focus on the calculation and modeling of forces and moments acting on the equations of motion. Aerodynamic, thrust, gravitational forces and moments act on the

missile. In studies on aircraft and missiles, gravitational acceleration is usually included in the calculations as a constant.

$$\begin{bmatrix} F_X \\ F_Y \\ F_Z \end{bmatrix} = \begin{bmatrix} QSC_X \\ QSC_Y \\ QSC_Z \end{bmatrix} \tag{39}$$

$$\begin{bmatrix} M_x \\ M_y \\ M_z \end{bmatrix} = \begin{bmatrix} QSdC_l \\ QSdC_m \\ QSdC_n \end{bmatrix} \tag{40}$$

where F_x, F_y, F_z are aerodynamic force components, M_x, M_y, M_z are aerodynamic moment components. Also, $C_X, C_Y, C_Y, C_l, C_m, C_n$ are also aerodynamic force and momentum coefficients. Furthermore, Q represents dynamic pressure, ρ represents the density of air, S represents the reference area and d represents the reference length.

Obtaining the missile's aerodynamic forces and moments is quite complex, and the aerodynamic modeling is done by considering computational flow dynamics issues. These calculations are made by taking into account the geometric properties of the missile, its kinematic values, and all other control variables that affect aerodynamics. Some inputs used for aerodynamic data given in Table 3.4.

Variables	**Values**
α	[-30, -25, -20, -15, -12, -10, -8, -6, -4, -2, 0, 2, 4, 6, 8, 10, 12, 15, 20, 25, 30]
β	[-30, -25, -20, -15, -12, -10, -8, -6, -4, -2, 0, 2, 4, 6, 8, 10, 12, 15, 20, 25, 30]
$Mach$	[0.6, 1.2, 1.5, 1.8, 2.2]
δ	[-20, -15, -10, -5, 0, 5, 10, 15, 20]

Table 3.4 Some Variables Affecting Aerodynamic Force

The relations of some aerodynamic coefficients of the missile with each other are shown between Figure 3.9 and Figure 3.17.

From Figure 3.9 to Figure 3.17, variations of aerodynamic force and moment components are shown according to the rudder fin deflection, angle of attack, and Mach velocity. Considering the lift coefficient, drag coefficient, and moment coefficient changes, each figure consisted of 3 sub-figures. These figures are grouped according to the rudder fin deflection value. Looking at the figures in order, the δ_r value in Figure 3.9 is $-20\,^\circ$. In Figure 3.10, the δ_r value is $-15\,^\circ$. In Figure 3.11, the δ_r value is $-10\,^\circ$. In Figure 3.12, the δ_r value is $-5\,^\circ$. In Figure 3.13, the δ_r value is $0\,^\circ$. The δ_r values used between Figure 3.14 and Figure 3.17 are as follows: $\delta_r = 20\,^\circ, \delta_r = 15\,^\circ, \delta_r = 10\,^\circ, \delta_r = 5\,^\circ$. According to Table 3.4, in all figures, the angle of attack varies between -30 and 30, and the Mach velocities are between 0.6 and 2.2

3.1.5. Flight Parameters

There are flight parameters that affect aerodynamic forces and moments. There are four other important variables to consider: dynamic pressure, Mach number, angle of attack, and sideslip angle. These will be briefly explained below.

Dynamic Pressure: The magnitude of the dynamic pressure, whose equation is given below, is proportional to the magnitude of the aerodynamic force on the missile.

$$Q = \frac{1}{2}\rho V^2 \tag{41}$$

in which ρ denotes the density of air, and the formula for calculating ρ with respect to h, which is the altitude, is given below.

$$\rho = \begin{cases} \rho_0(1 - 0.00002256h)^4.256) & : \ h \leq 10000m \\ 0.412e^{-0.000151(h-10000)} & : \ h > 10000m \end{cases} \tag{42}$$

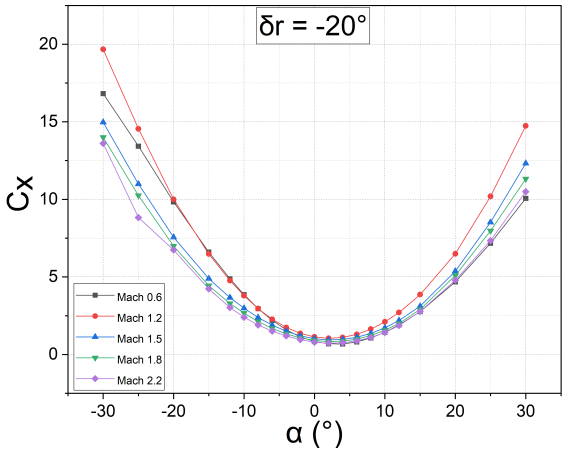

(a)

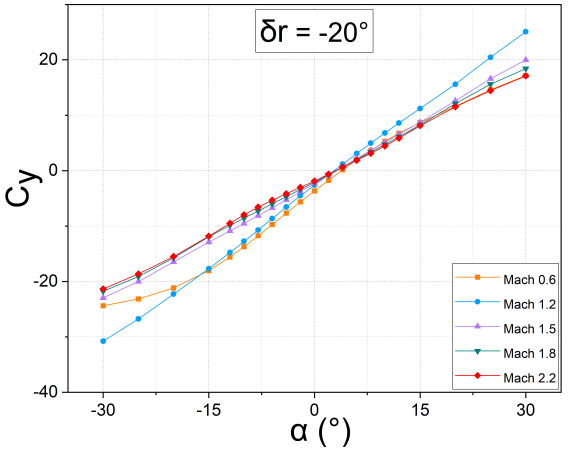

(b)

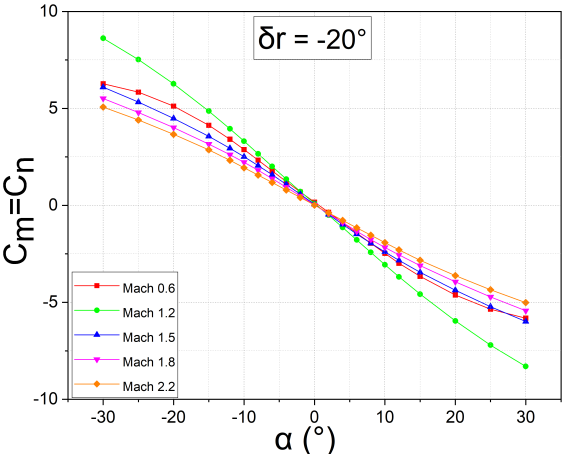

(c)

Figure 3.9 (a) Drag coefficient with $\delta_r = -20^\circ$ bias (b) Lift coefficient with $\delta_r = -20^\circ$ δ_r bias (c) Moment coefficient with $\delta_r = -20^\circ$ δ_r bias

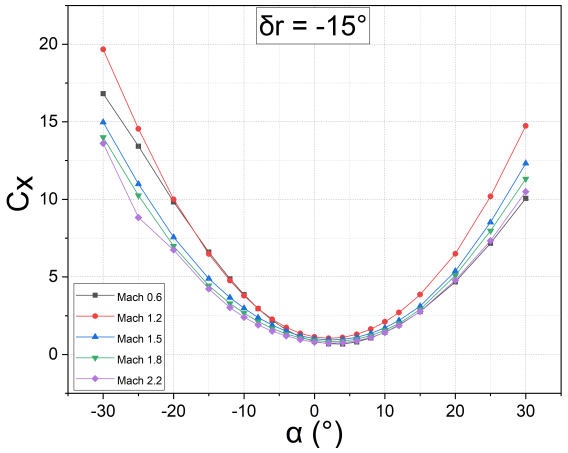

(a)

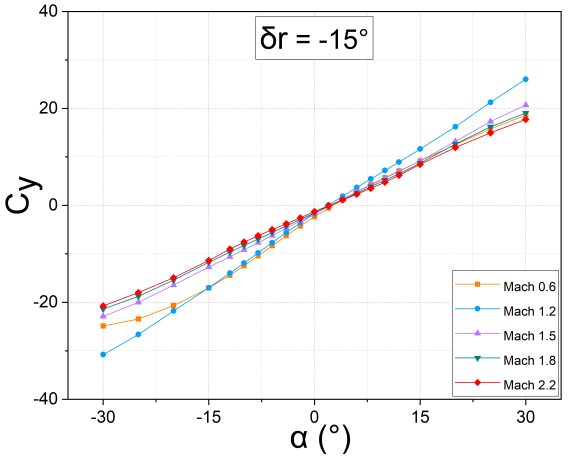

(b)

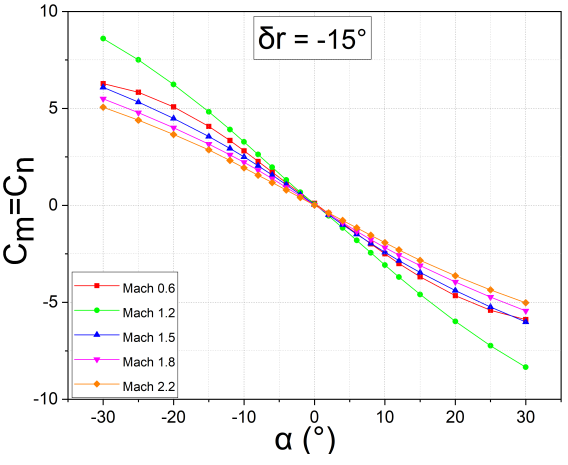

(c)

Figure 3.10 (a) Drag coefficient with $\delta_r = -15^\circ$ bias (b) Lift coefficient with $\delta_r = -15^\circ$ bias (c) Moment coefficient with $\delta_r = -15^\circ$ bias

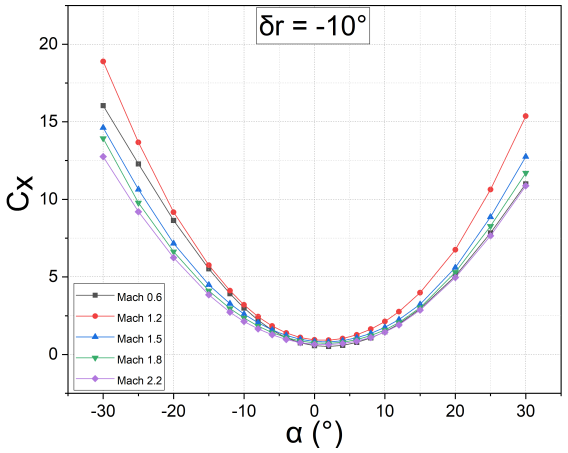

(a)

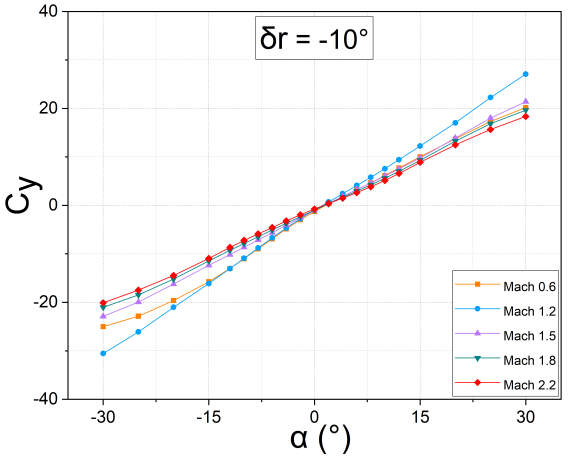

(b)

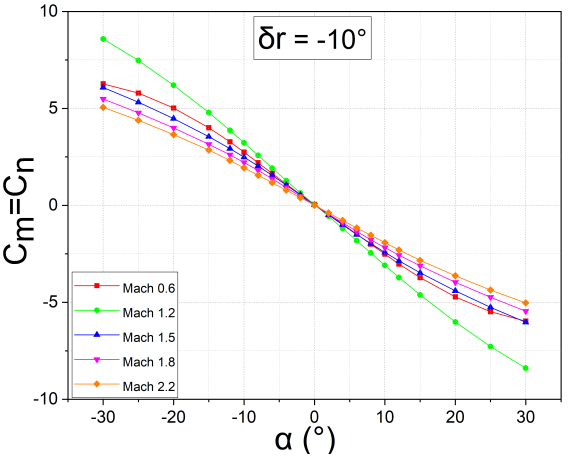

(c)

Figure 3.11 (a) Drag coefficient with $\delta_r = -10^\circ$ bias (b) Lift coefficient with $\delta_r = -10^\circ$ bias (c) Moment coefficient with $\delta_r = -10^\circ$ bias

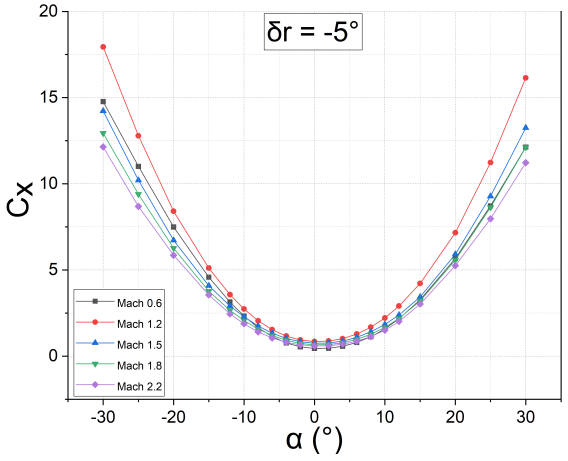

(a)

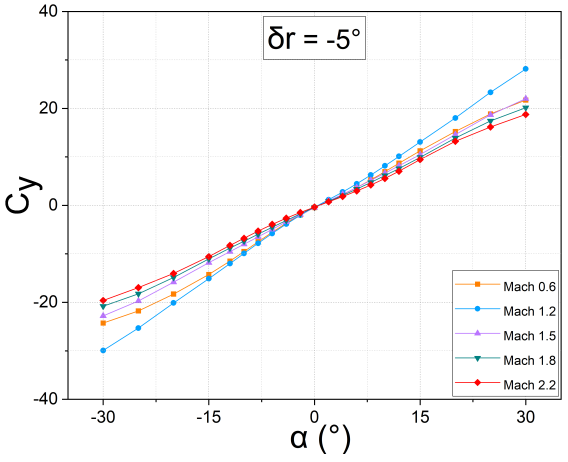

(b)

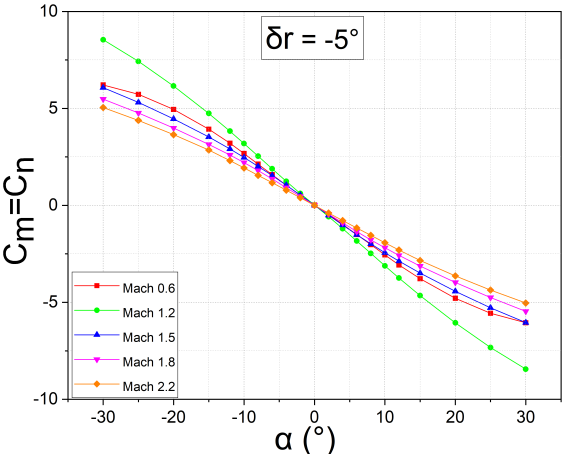

(c)

Figure 3.12 (a) Drag coefficient with $\delta_r = -5^\circ$ bias (b) Lift coefficient with $\delta_r = -5^\circ$ bias (c) Moment coefficient with $\delta_r = -5^\circ$ bias

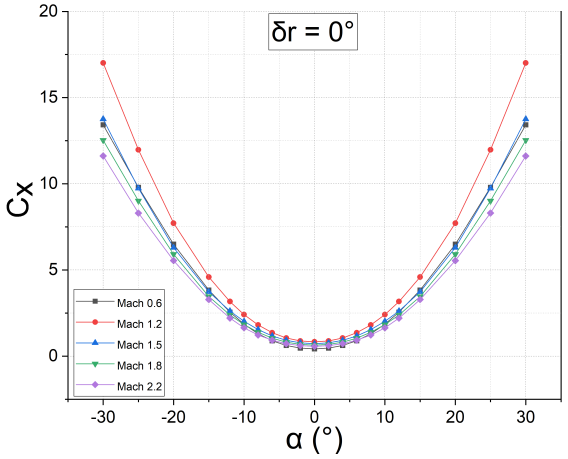

(a)

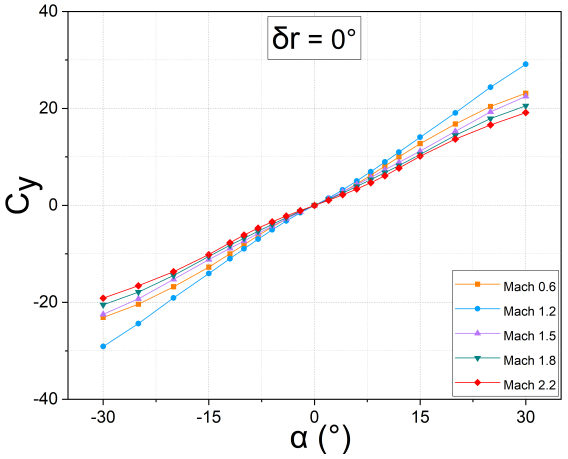

(b)

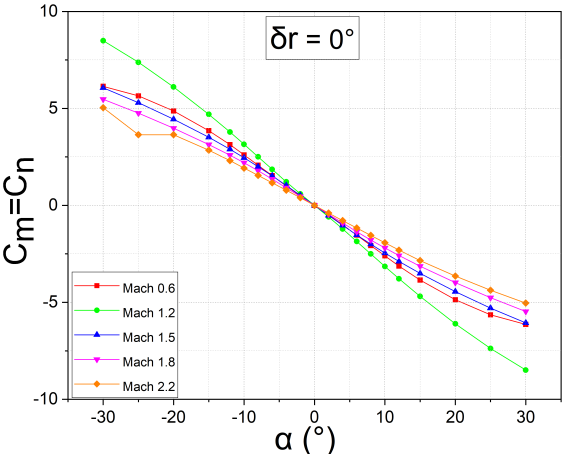

(c)

Figure 3.13 (a) Drag coefficient with $\delta_r = 0\,^\circ$ bias (b) Lift coefficient with $\delta_r = 0\,^\circ$ bias (c) Moment coefficient with $\delta_r = 0\,^\circ$ bias

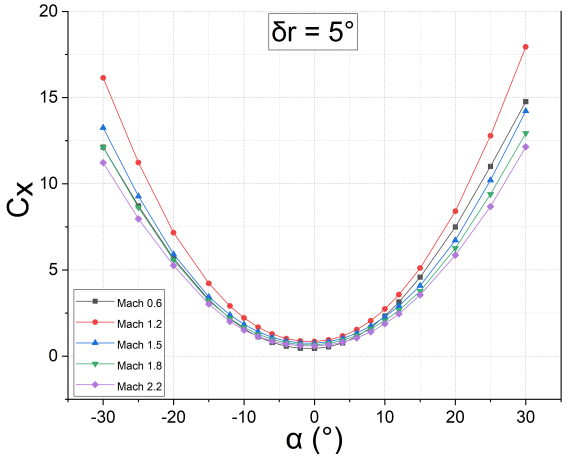

(a)

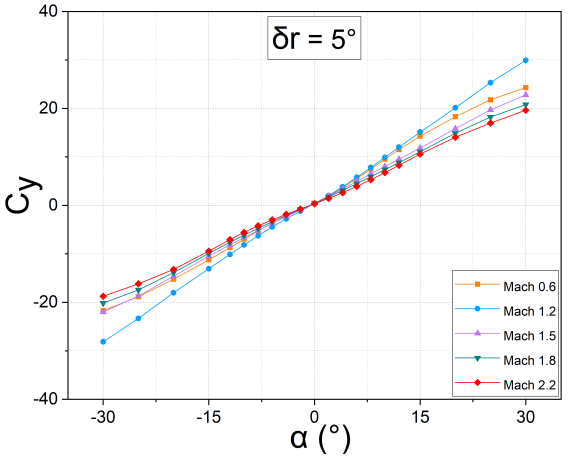

(b)

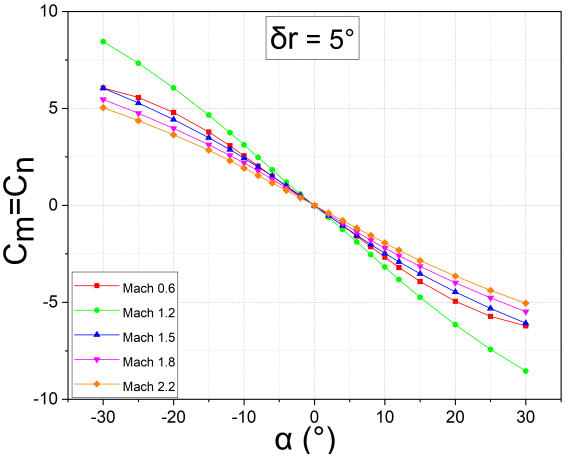

(c)

Figure 3.14 (a) Drag coefficient with $\delta_r = 5\,^\circ$ bias (b) Lift coefficient with $\delta_r = 5\,^\circ$ bias (c) Moment coefficient with $\delta_r = 5\,^\circ$ bias

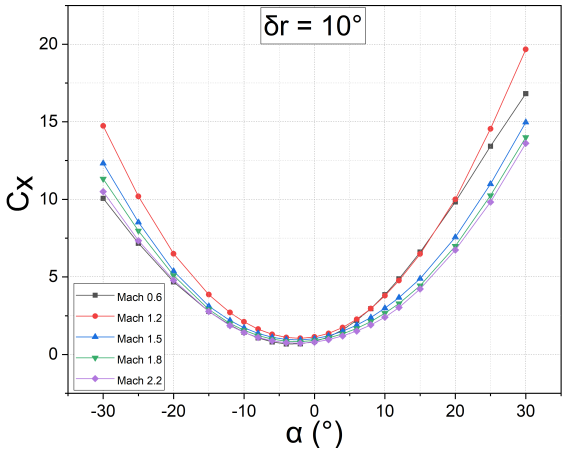

(a)

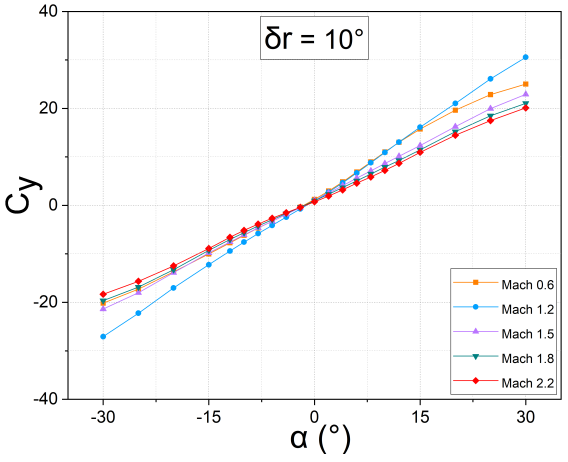

(b)

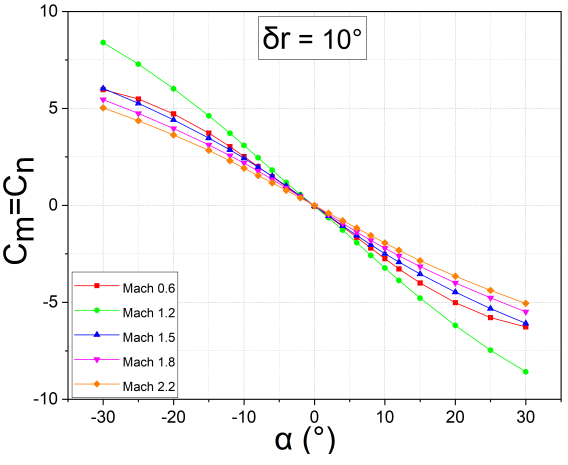

(c)

Figure 3.15 (a) Drag coefficient with $\delta_r = 10^\circ$ bias (b) Lift coefficient with $\delta_r = 10^\circ$ bias (c) Moment coefficient with $\delta_r = 10^\circ$ bias

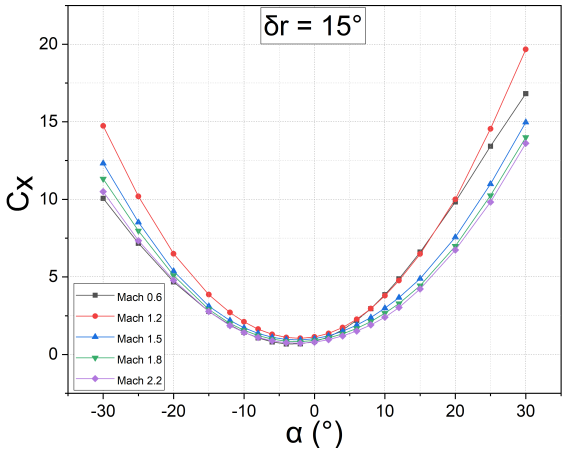

(a)

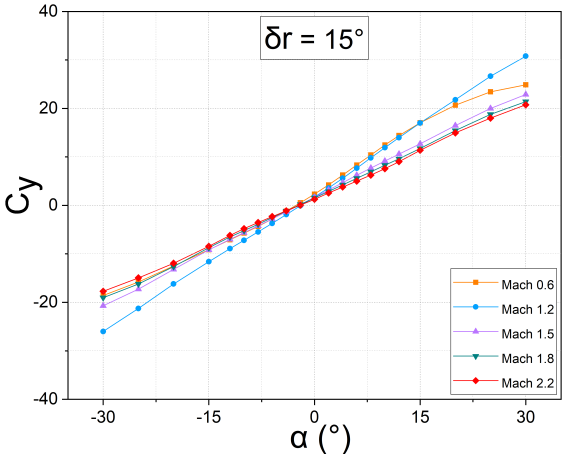

(b)

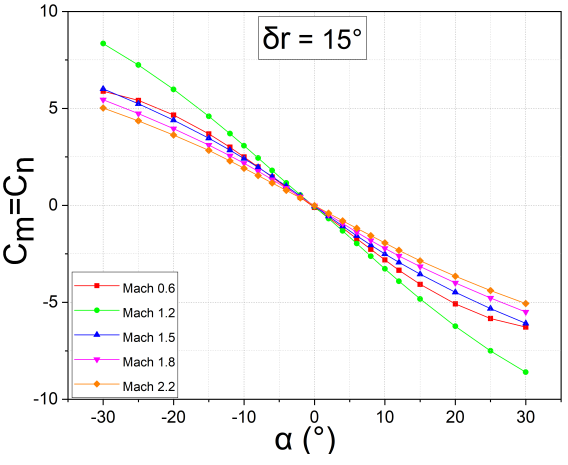

(c)

Figure 3.16 (a) Drag coefficient with $\delta_r = 15^\circ$ bias (b) Lift coefficient with $\delta_r = 15^\circ$ bias (c) Moment coefficient with $\delta_r = 15^\circ$ bias

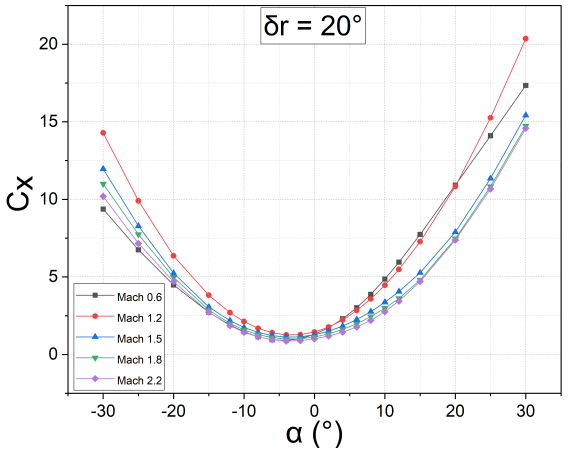

(a)

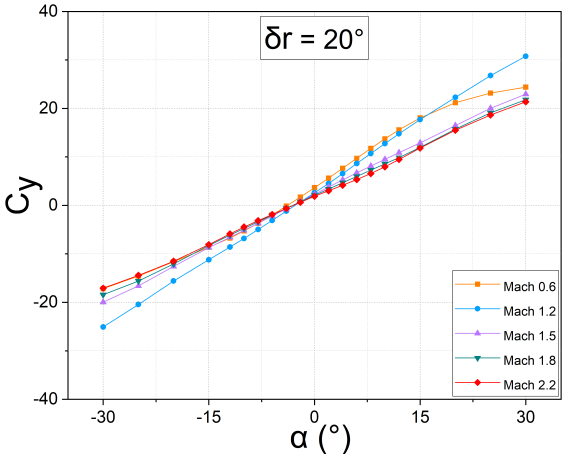

(b)

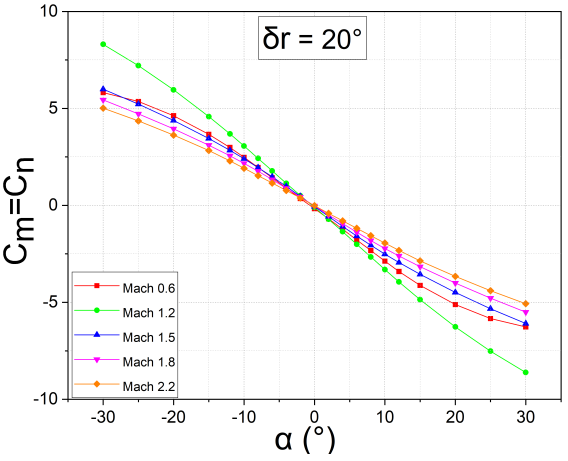

(c)

Figure 3.17 (a) Drag coefficient with $\delta_r = 20^\circ$ bias (b) Lift coefficient with $\delta_r = 20^\circ$ bias (c) Moment coefficient with $\delta_r = 20^\circ$ bias

Mach number: The Mach number is obtained by dividing the speed of the missile by the momentary speed of sound. This number is expressed without units, and its mathematical representation is as in (43).

$$M = \frac{V}{C} \tag{43}$$

in which C denotes the speed of the sound and is given (44).

$$C = \gamma RT \tag{44}$$

in which γ represents the specific heat ratio, R denotes the constant of air gas. Furthermore, the ambient temperature, which varies with altitude, is denoted by T and given as below.

$$T = \begin{cases} T_0(1 - 0.00002256h)) & : \ h \leq 10000m \\ 0.7744T_0 & : \ h > 10000m \end{cases} \tag{45}$$

Angle of Attack: The angle of attack (AOA) can be described as the angle between the x component and the z component of the velocity vector in the missile motion axis set. It is expressed as below.

$$\alpha = \arctan(\frac{w}{u}) \tag{46}$$

The AOA is demonstrated in Figure 3.18. Besides, the flight path angle γ is given in Figure 3.18.

Angle of Sideslip: The angle of sideslip is called the angle between the x-axis component and the y-axis component of the missile velocity vector in the missile axis set and is expressed as in (47).

$$\beta = \arcsin(\frac{v}{V}) \tag{47}$$

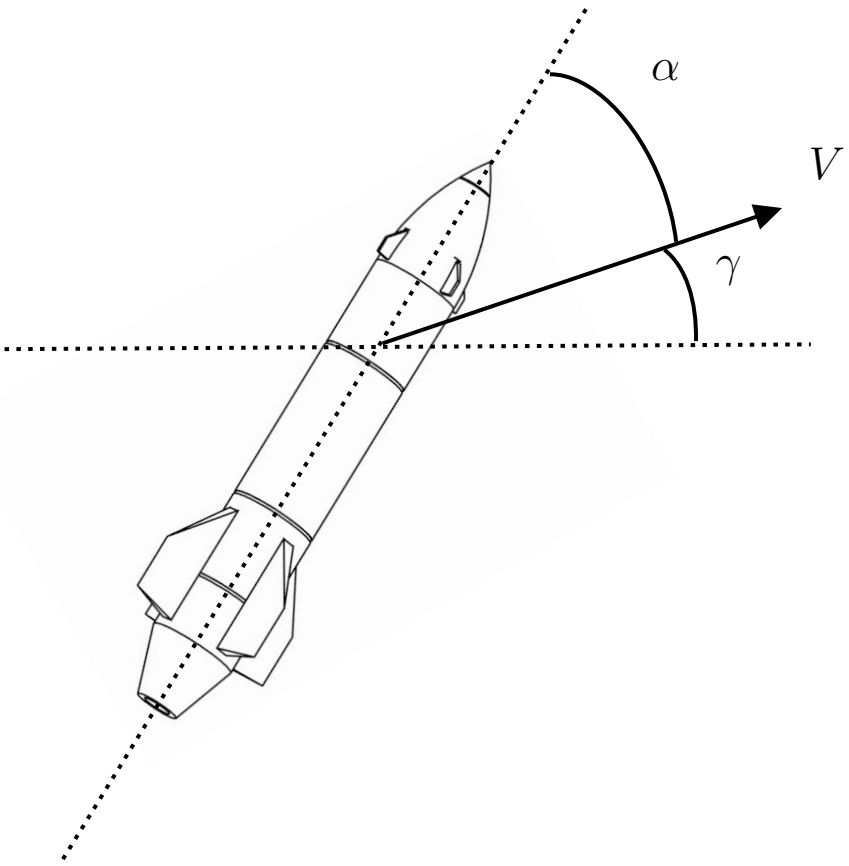

Figure 3.18 Angle of Attack

in which V denotes the total velocity and gives as below.

$$V = \sqrt{u^2 + v^2 + w^2} \tag{48}$$

3.1.6. Deflection Angles of Control Surfaces

The missile's orientation motions are accomplished by tail angles. The forces on the missile are affected by the missile's rapidly shifting tail angles because its geometry changes with the tail angles. Figure 3.19 shows the situation of tail angles with the X configuration, and the formulas for the deflection angles of the tails are given as the following equations. In the literature, those working on aerodynamics preferred new variables called elevator deflection,

rudder deflection, and aileron deflection as control variables instead of physical variables δ_1, δ_2, δ_3, δ_4 [83].

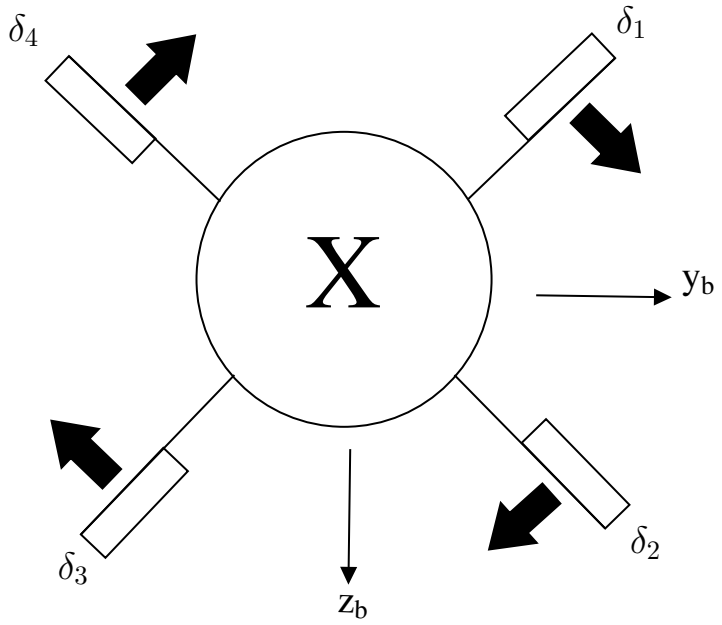

Figure 3.19 X configuration

$$\delta_1 = \delta_e + \delta_r + \delta_a \tag{49}$$

$$\delta_2 = \delta_e - \delta_r + \delta_a \tag{50}$$

$$\delta_3 = -\delta_e - \delta_r + \delta_a \tag{51}$$

$$\delta_4 = -\delta_e + \delta_r + \delta_a \tag{52}$$

By utilizing these angles, control deflection angles are generated as the following equations. Firstly, when used as the positive δ_1, δ_2, δ_3, δ_4, the positive roll motion is obtained in (53).

$$\delta_a = \frac{\delta_1 + \delta_2 + \delta_3 + \delta_4}{4} \tag{53}$$

Secondly, when the positive $\delta 1$, $\delta 2$ and negative $\delta 3$, $\delta 4$ are applied in (54), the pitch motion is obtained and given as below.

$$\delta_e = \frac{\delta_1 + \delta_2 - \delta_3 - \delta_4}{4} \tag{54}$$

Lastly, the yaw motion is produced and presented in the following when the positive $\delta 2$, $\delta 3$, and negative $\delta 1$, $\delta 4$ are applied in (55).

$$\delta_r = \frac{-\delta_1 + \delta_2 + \delta_3 - \delta_4}{4} \tag{55}$$

3.1.7. Control Actuation System

The control actuation system (CAS) is one of the most critical components of a missile and this system manages the missile guidance process according to the commands from the guidance system. Aerodynamic control, thrust vector control, and response control are the three most common forms of control systems. They can be employed separately or in combination in a missile. The control actuation system dynamics can be written

$$\frac{\delta(s)}{\delta_c(s)} = \frac{w_n^2}{s^2 + 2\zeta w_n s + w_n^2} \tag{56}$$

in which w_n, ζ denote the natural frequency and the damping ratio, respectively. Furthermore, the state space of the system is given as below.

$$\frac{d}{dt}\begin{bmatrix}\delta(t) \\ \dot{\delta}(t)\end{bmatrix} = \begin{bmatrix}0 & 1 \\ -w_n^2 & -2\zeta w_n^2\end{bmatrix}\begin{bmatrix}\delta(t) \\ \dot{\delta}(t)\end{bmatrix} + \begin{bmatrix}0 \\ w_n^2\end{bmatrix}\delta_c(t) \tag{57}$$

3.2. Guidance Law Methods

In recent years, a significant amount of literature has come to the fore around the theme of missile guidance law. New methods are constantly being developed in this field. However, it

has been stated in recent literature reviews that new problems have emerged that need to be solved with these methods. These problems have encouraged researchers to undertake more and more studies in this field of study [84–86]

There are two main approaches that draw attention in research on guidance laws: these are the classical guidance laws and modern guidance laws. Classical guidance laws are important methods developed to solve missile guidance problems and appear in a wide variety of scientific and industrial fields. Modern guidance laws have been developed by using control and artificial intelligence methods and in-depth studies on this subject have been carried out by many researchers to achieve superior performance against intelligent and maneuverable targets.

3.2.1. Classical Guidance Laws

The existing literature on guidance laws focuses on classical guidance laws because they are easy to apply, have standardized formulae, and provide reliable results. Traditional guiding laws can be divided into three categories. They are Proportional Navigation Guidance, Pursuit Guidance, and Line of Sight Guidance, and they are examined in detail below.

3.2.1.1. Proportional Navigation Guidance The Proportional Navigation (PN) guidance law is one of the most well-known methods among guidance laws [87–89]. This guidance law was discovered at sea for the first time and then applied to the Lark missiles in 1950. Since then, this law has been frequently encountered in the applications of motive law, sometimes used to derive new methods and sometimes to make comparisons [86, 90, 91].

In this guidance law, the acceleration commands are proportional to the rate of the distance traveled by the missile and the rate of change of the line-of-sight (LOS). Mathematically, it is written in the following equations:

$$a_{M\phi} = N_1 V_c \dot{\phi} \tag{58}$$

$$a_{M\theta} = N_2 V_c \dot{\theta} \tag{59}$$

where $a_{M\phi}$ and $a_{M\theta}$ denotes the acceleration's command $[ft/sec^2]$ or $[m/sec^2]$, N_1 and N_2 are the navigation constant and are positive real numbers. Generally, it is recommended to choose N number between 2 and 6 [90, 91]. V_c is the closing velocity $[ft/sec]$ or $[m/sec]$ of the missile, $\dot{\phi}$ and $\dot{\theta}$ are the LOS rate $[rad/sec]$.

The Proportional Navigation (PN) guidance law can be categorized into pure proportional navigation (PPN) guidance law, true proportional navigation (TPN) guidance law, ideal proportional navigation (IPN) guidance law and augmented proportional navigation (APN) guidance law. [92–94].

- **Pure proportional navigation guidance:**

  In this guidance law, the acceleration command is generated perpendicular to the velocity vector of the missile, and the geometry of the PPN guidance law is demonstrated in Figure 3.20. Moreover, the velocity vector is kept constant and aims to reset the angular velocity of the line-of-sight by rotating the velocity vector towards the target. The PPN guidance law is a realistic model in terms of modeling the physical acceleration that is applied to the missile, and it stands out with this feature among the PN methods [92]. The equations of this law can be stated as

$$a_{M\phi} = N_1 V_c \dot{\phi} \tag{60}$$

$$a_{M\theta} = N_2 V_c \dot{\theta} \tag{61}$$

- **True proportional navigation guidance:**

  In this guidance law, the acceleration command is enforced perpendicular to the LOS vector and the geometry of the TPN guidance law is shown in Figure 3.21. It can change both the direction and the magnitude of the missile speed vector thanks to this law. This guidance law has been used more in literature because it can be expressed

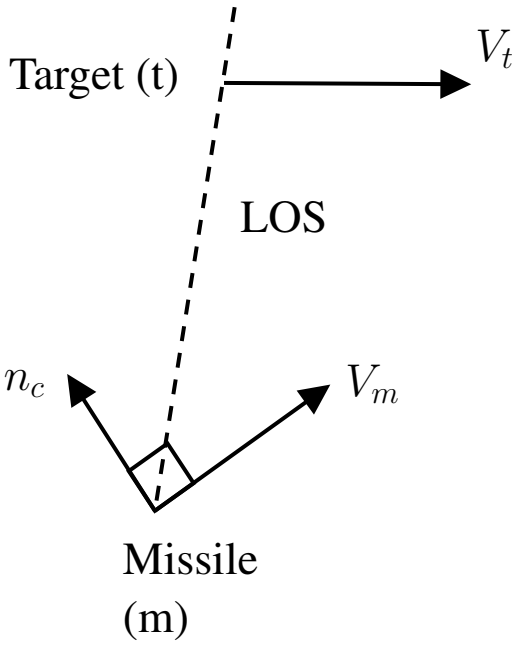

Figure 3.20 Pure proportional navigation guidance geometry

in mathematical terms more conveniently as compared to other proportional guidance laws. However, in terms of modeling real-life dynamics, TPN guidance law falls short of PPN guidance law [94–97]. Mathematically, the TPN guidance law is written as:

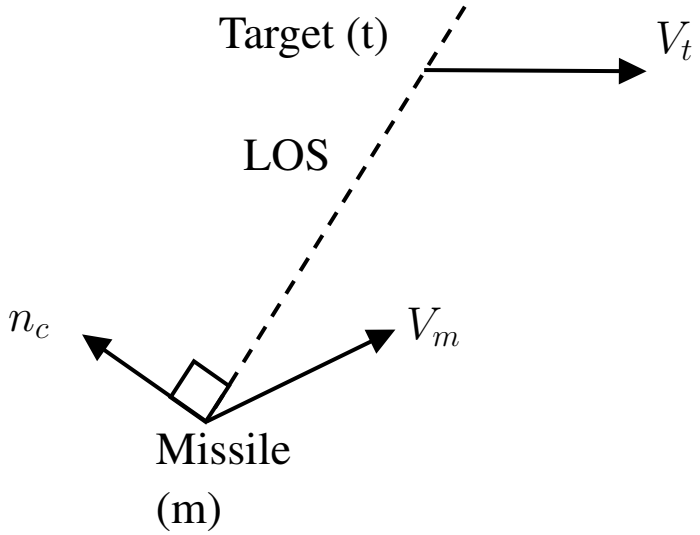

Figure 3.21 True proportional navigation guidance geometry

- **Ideal proportional navigation guidance:**

  In IPN guidance law, the acceleration command is applied perpendicular to the relative velocity vector according to the target of the missile [93]. The equations of this law are given as follows.

$$a_{M\phi} = N_1 V_{relative} \dot{\phi} \tag{62}$$

$$a_{M\theta} = N_2 V_{relative} \dot{\theta} \tag{63}$$

  The variable $V_{relative}$ in the above equations is defined as follows.

$$V_{relative} = V_M - V_T \tag{64}$$

  where V_M respresents the missile velocity and V_T respresents the target velocity.

- **Augmented proportional navigation guidance:**

  The acceleration command is generated by multiplying a proportional coefficient related to the target's acceleration in the APN guidance law. Moreover, this guidance law's purpose is to capture the target with less effort while minimizing the distance between the missile and the target. Mathematically, this law is given as follows.

$$a_{M\phi} = N_1 V_c \dot{\phi} + 0.5 N_3 a_{T\phi} \tag{65}$$

$$a_{M\theta} = N_2 V_c \dot{\theta} + 0.5 N_4 a_{T\theta} \tag{66}$$

  When the studies in the literature are examined, it is seen that the most important advantage of this law is that it can be used against maneuvering targets.

3.2.1.2. Pursuit Guidance The acceleration command is proportional to the lead angle. In this way, the missile velocity vector is steered to show the target in the pursuit guidance law. Moreover, under this law, the missile gets closer to the target at each iteration, and

the target moving at a constant low speed or without maneuvering is a necessity in order to be successful. In addition, the lead angle is a parameter that must be measured sensitively. Due to these limitations, although not preferred nowadays, the guidance law is currently used in laser-guided bombs known as Pawevay I and Pawevay II [90, 98, 99]. Figure 3.22 demonstrates the geometry of this law in planar geometry.

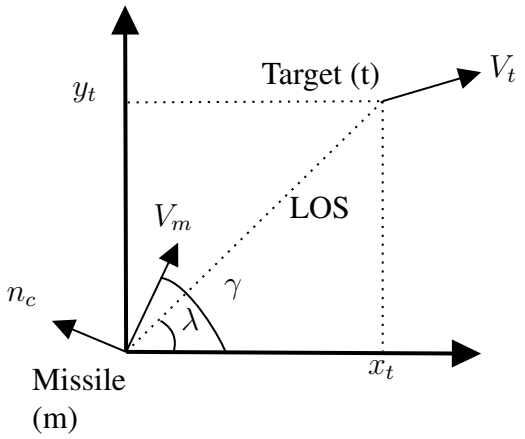

Figure 3.22 Pursuit guidance geometry

3.2.1.3. Line of Sight Guidance The line of sight guidance law aims to maintain the missile on the LOS, which is located between a reference point and the target. Figure 3.23 shows the simple expression of the rule referred to as LOS guidance law [90].

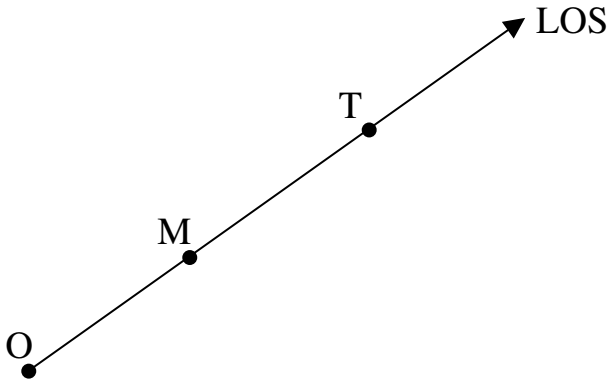

Figure 3.23 Line of sight guidance geometrical rule

As can be seen from the above figure, M is always on the ray starting with reference point O and passing through T, where the target is. According to the way the guiding commands

are executed, this method can be divided into 2 parts: the command to line of sight guidance and the beam riding guidance. These methods will be briefly discussed below.

- **Command to line of sight guidance:**

  The general purpose of this method is to reset the angular difference between the missile and the rays that illuminate the target and so keeping the target close throughout the LOS until the moment of hitting is the main goal. With the use of this method, the seeker cost is eliminated and there is no need for target range information at the same time [90, 100].

- **Beam riding guidance:**

  In beam-riding guidance, in the same way as in the CLOS method, the target is illuminated by the outside monitoring station. The most notable distinction from the CLOS is that the guiding commands are generated by missiles. Beam-riding guidance can be categorized into two types: radar (radio) beam-riding guidance and laser (optical) beam-riding guidance. Laser beam riding guidance is the most well-known method among these types because it has many advantages, such as good accuracy, simple structure and low cost [101, 102].

3.2.2. Guidance Methods based on Classical Control Techniques

In classical control methods, the difference between the reference input of the control system and the measured system output is taken as an error in order to determine the control rule. Then, the error, the integral of the error, and the derivative of the error are appropriately selected and multiplied by the gain coefficients determined in line with the plant dynamics and performance requirements. Thus, the control rule is obtained. If this control rule is multiplied only by the error, the present control method is ”P (Proportional) control”, if the error and the integral of the error are taken into account, ”PI (Proportional and Integral) control”, and if the error and the derivative of the error are considered, ”PD (Proportional and Derivative) control” and the most general classical control rule, in which error, error

derivative and error integral are taken into account, is defined as “PID (Proportional, Integral and Derivative) control”.

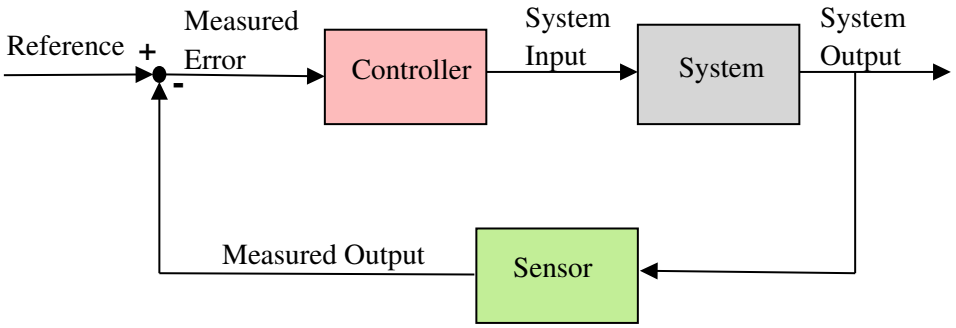

Figure 3.24 Classical control system block diagram

A single-input, single output feedback block diagram for classical control methods is given in Figure 3.24. When the PID method is used as a controller, the controller block is expressed as follows.

$$G_c(s) = K_p + \frac{K_i}{s} + K_d s \tag{67}$$

where $G_c(s)$ denotes the controller block. K_p, K_i and K_d represent the gains. $G_c(s)$ takes the below forms for the P, PI and PD rules, respectively.The block diagram of PID controller is given in Figure 3.25.

$$P: \qquad G_c(s) = K_p \tag{68}$$

$$PI: \qquad G_c(s) = K_p + \frac{K_i}{s} \tag{69}$$

$$PD: \qquad G_c(s) = K_p + K_d s \tag{70}$$

In recent years, the classical control methods have been frequently employed in guidance law design due to their simple structure and easy application [42, 103]. In [103], the new guidance law is designed utilizing the PI control method, and they have presented the results of their methods by comparing them with the PN method. In addition, it has emphasized in the results of the study that the PI control method was more successful. In [42], a new PID guidance law is proposed by using the circle criterion to employ stability. In addition,

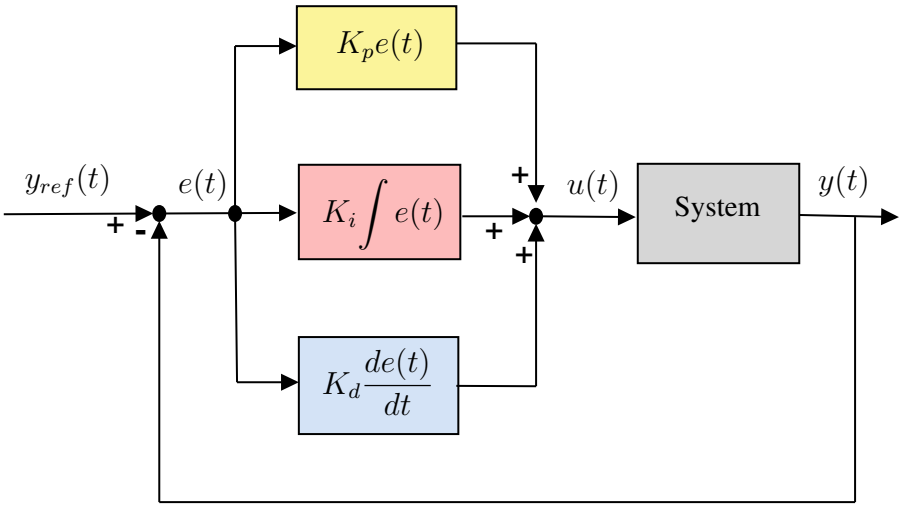

Figure 3.25 The block diagram of PID controller

they compared their results with other guidance laws that they created with different classical control methods. These rules are PD navigation and PI navigation guidance laws. In addition, they have added the PN guidance law to the results.

3.2.3. Guidance Methods based on Robust Control Techniques

Robust control techniques ensure that the system is designed to deliver stable results while system uncertainties, disturbances, and noise caused by external factors occur [104, 105]. The H_∞ criterion and sliding mode control are currently the most popular methods for designing missile guidance laws among robust control techniques.The reason is that these methods try to eliminate or at least reduce the impact of the uncertainties in missile parameters and target maneuvers.

H_∞ control method:

The robust approaches are required when the system's disturbances and uncertainties increase. The H_∞ control approach is one of the most important of these methods. The goal of the H_∞ control approach is to obtain a control system that can run independently without losing its stability under a variety of operating scenarios. Generally, H_∞ controllers designed for single-input, single-output systems are based on linearized system dynamics. After

the control inputs and disturbance inputs are determined, the weight functions are decided. Then the system parameters to be penalized are decided. These parameters are usually the error between the reference input and the measured system output, or the amplitude of the controller signal [106–108]. In Figure 3.26, the generel scheme of H_∞ control design is showed as below.

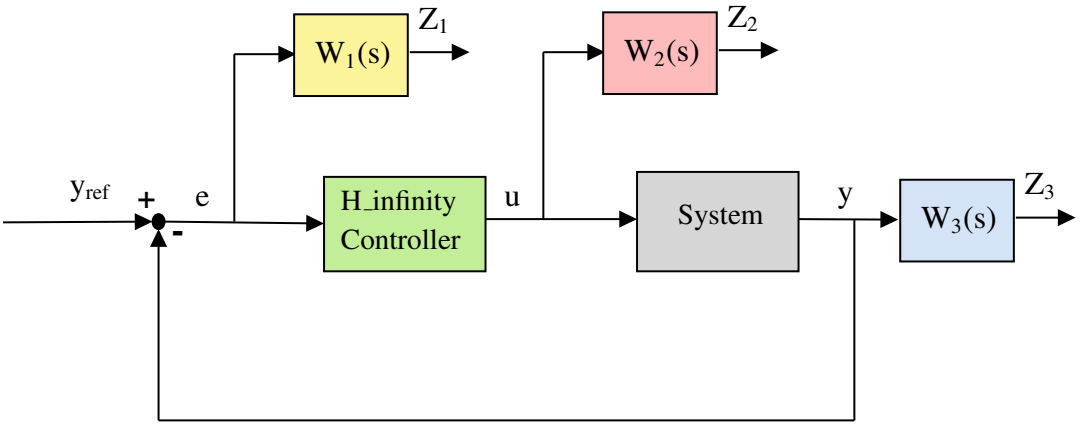

Figure 3.26 General scheme of H_∞ control design

where y_{ref}, e, u and y denotes the reference input, the error, the control signal and the output, respectively. In addition, W_1, W_2, and W_3 represent the weighting transfer functions. The error, the control signal and the output are penalized by utilizing these weighting functions. The appropriate selection of these functions according to the system is both the most important and the most challenging part of the H control method because making the wrong choice affects the entire performance of the system [109].

For many years, by using the H_∞ control method, studies were also carried out in the field of missile guidance law [110, 111]. H_∞ criterion is applied by taking into account the missile-target engagement kinematics. In [110], Savkin and et al. offered results by comparing H_∞ and LQR control methods for precision missile guidance problem. H_∞ methods were applied by used two different methods, such as state feedback without noise and output feedback with sensor noise. In this study, the methods were evaluated in terms of the miss distance and time variation of attack angles. According to the results, H_∞ control method is better than the LQR control methods for the precision missile guidance problem. Yang and Chen [111] proposed a novel 3D missile guidance law with nonlinear

H_∞ control. In their paper, H_∞ guidance law was solved analytically by using the associated Hamilton-Jacobi partial differential inequality and then compared against the results of the LQR controller

Sliding mode control method:

The SMC method emerged in the Soviet Union in the early 1960s. However, it was announced outside of Russia in the mid 1970s through studies by Itkis and Ukin [112]. Since then, the SMC method, which has been the basis of many studies, has become everyone's favorite with its robust performance against disturbance and uncertain system dynamics [113, 114].

In the design procedure of traditional SMC, the method consists of two steps. The first step is to select a sliding manifold and the system states to move towards the sliding manifold, while the second step is to ensure that the system states stay on this sliding surface. These steps are called the reaching phase and sliding-mode phase, respectively. In Figure 3.27, the graphical representation of the SMC method is demonstrated [115].

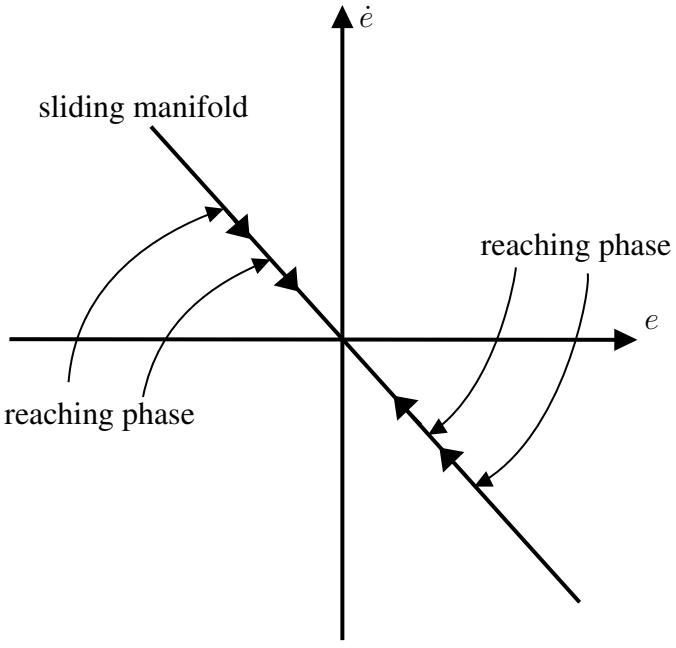

Figure 3.27 Graphical representation of SMC

The basic sliding surface design will be explained briefly. A nonlinear system can be written as below.

$$\ddot{x}_n = f(x,t) + b(x,t)u(t) + d(t) \tag{71}$$

in which $x(t)$ specifies the state vector and $u(t)$ specifies the control input vector to be used for state feedback. $f(x,t)$ and $b(x,t)$ denote uncertain nonlinear function and gain, respectively. $d(t)$ is the unknown disturbance. The sliding manifold can be designed as follow.

$$s(t) = (\frac{d}{dt} + \lambda)^{r-1} e(t) \tag{72}$$

where $\lambda > 0$ must be designed to ensure the Hurwitz criteria. r is the order of the system. In 72, $e(t)$ represents the error and its equation is given below along with its derivative.

$$e(t) = x_d(t) - x(t) \tag{73}$$

$$\dot{e}(t) = \dot{x}_d(t) - \dot{x}(t) \tag{74}$$

After then, the control input (u) is handled in two parts: the equivalent control (u_{eq}) and the switching control (u_{sw}). The equivalent control is obtained the result of $\dot{s}(t) = 0$ and maintains the state trajectory on the sliding manifold. The switching control is calculated generally as $u_{sw} = -K\mathrm{sgn}(s)$. In this way, the value of switching control is alternating between two constant values, crossing the hyperplane $s(t) = 0$, as shown by this equation.

The SMC approach is commonly used in missile guidance research, in addition to being favored in a wide range of fields in industry and academic research. The SMC is generally used for obtaining robust guidance laws when target maneuvers, uncertainties, and disturbances are present [113, 116–118]. In 1999, Zhou et al. [113] published a paper in which they proposed the sliding mode control be used while designing robust homing missile guidance laws. In their study, the missile and target are modeled with 6 DOF and 3 DOF,

respectively. The results of this method were compared with a conventional PNG law, and they stated that, considering the simplicity and robustness the proposed method had, it was suitable for practical applications. Brierley et al. [116] proposed SMC for air-air missile target interception, and their results demonstrated that the performance of the controller was robust enough. A recent study by Fu et al. (2016) proposes a sliding mode guidance law for hypersonic missiles attacking a maneuvering target. They used SMC guidance law as well as back-stepping control law to obtain a robust system.

3.2.4. Guidance Methods with Applications of Artificial Intelligence Techniques

The most known methods of artificial intelligence are genetic algorithms, neural networks, specialized learning schemes, fuzzy logic, and different combinations of these methods. In the missile guidance studies, neural networks and fuzzy logic methods are the most used ones among these methods.

Neural network:

The neural networks are designed as network structures and are inspired by the biological neural system, which consists of hundreds or thousands of neurons connected to each other. Figure 3.28 is demonstrated the structure of a neural network for a neuron. In this figure, the input variables are denoted by $x_i\,(i = 1, 2, ..., k)$, and the output variables are denoted by y. Besides, $w_i\,(i = 1, 2, .., k)$ are the coefficients that determine the weights of the inputs received by the artificial neuron. Each input has its own coefficient. This coefficient demonstrates the importance of the information coming to the artificial neuron and its effect on the neuron. It is then a function that calculates the net input of that neuron by adding the sums of the product of each weight with the inputs it belongs to, with the bias value b. Mathematically, this function is expressed as 75. The activation function is the unit that processes the net information sent to the neuron by the sum function and determines the output that the neuron will produce in response to this input. The output is where the result of the activation function is sent to the outside world or to other neurons. A neuron has only

one output, which is generally expressed as 13. The output of one neuron can be the input of another neuron [119].

$$m = \sum_{i=1}^{k} w_i x_i + b \tag{75}$$

$$y = f(m) \tag{76}$$

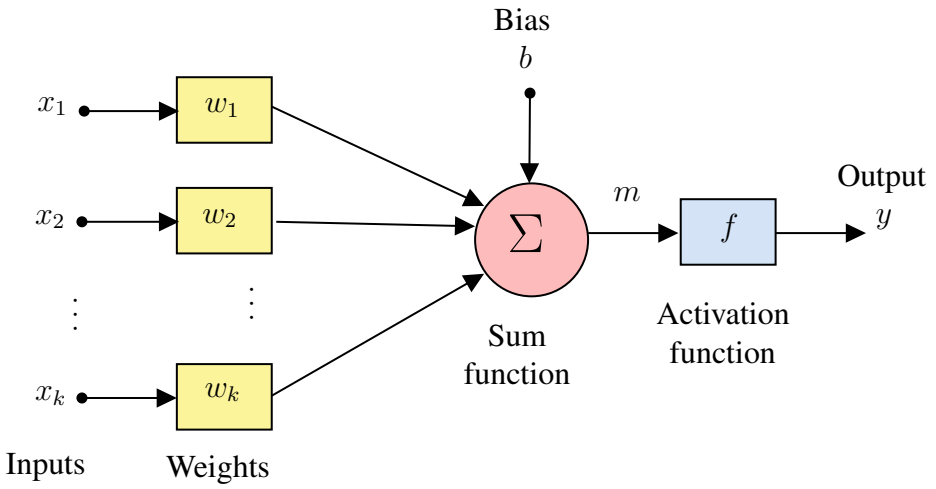

Figure 3.28 The structure of neural network for a neuron

Neural networks are chosen due to their robustness in dealing with noise as well as their versatility in designing advanced guidance laws (Lin and Chen, 1999; Lin and Hua-Wen Su, 2000). Firstly, when neural network guidance methods are designed, input and output variables should be determined. The input variables are the LOS angle and angular rate, the missile velocity, and the target velocity, while the output variable is usually the lateral acceleration command. Lin and Chen (Lin and Chen, 1999) proposed an advanced guidance law that is a combination of the neural network and the conventional proportional navigation guidance law. In their study, the neural network was designed during the terminal phase and it was built on a specialized on-line control architecture that was designed to fix the guidance command provided by Proportional Navigation Guidance (PNG). This way, they aimed to provide a good tracking performance while extending the defensive zone. The simulation results showed that their proposed guidance law was successful and they proposed the advanced guidance law to increase missile performance.

Fuzzy logic method:

In studies using fuzzy logic, in cases where the relationship between inputs and outputs in the system cannot be expressed mathematically precisely, it is tried to be determined expressively, similar to the human decision-making mechanism. The fuzzy logic method consists of three phases called fuzzification, inference, and defuzzification, based on linguistic variables. In the classical logic method, it can have only two values, such as 0 or 1, while in the fuzzy logic method it can take a value in the range of 0 to 1, because some concepts cannot be separated by definite conclusions. Although expert knowledge is required to confirm these intermediate values, this method is encountered in almost every area of the literature. Figure 3.29 demonstrate the general architecture of the fuzzy logic.

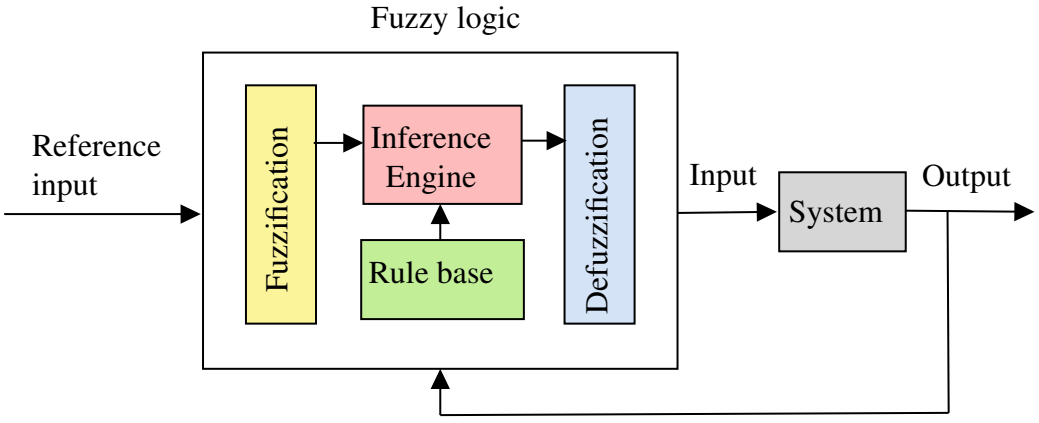

Figure 3.29 General architecture of fuzzy logic

In the literature, the fuzzy logic method can be easily applied to missile guidance laws [45, 120–123]. The inputs of the fuzzy logic guidance system can be selected as the LOS angular rate, seeker angle, the LOS angle, the missile velocity, the missile altitude, and the output is usually selected as the lateral acceleration command [123]. Mishra et al. [120] showed results with fuzzy logic applied to the PNG law and the APNG law. Regarding fuzzy logic applied to PNG in this study, the LOS angle rate and change of the rate were used as input variables and the lateral acceleration command was used as the output variable. And in fuzzy logic applied to APNG, the LOS angle rate and target acceleration command were chosen as input variables, and the output variable was the same as the previous method. Another significant analysis and discussion on the subject was presented by Gonslaves and Caglayan

[45]. In their study, a surface-to-surface missile was modelled and generated. Also, the combination of the PD and PI parts of the guidance commands by using fuzzy rule bases was done. Their results stated that the performance is better than the conventional guidance method in terms of point distance error.

3.2.5. Guidance Methods based on Optimal Control Theory

Optimal control theory is one of the methods that can be applied in various fields such as biology, economics, ecology, engineering, finance, management and medicine and is frequently used by researchers [124–128]. Moreover, the most common among these theories is the LQR method.

The LQR, in short, is just an automated way of finding a suitable state-feedback controller. The general scheme of LQR control design is demonstrated in Figure 3.30, where y_ref is the reference input, u is the control input, y is the system output [124].

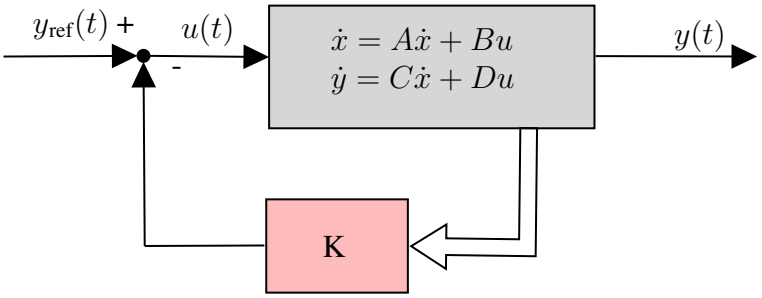

Figure 3.30 General scheme of LQR control design

The LQR technique given 78 creates a linear state feedback rule for a controllable LTI system using a state-space model as stated in 77.

$$\dot{x} = A\dot{x} + Bu \tag{77}$$
$$\dot{y} = C\dot{x} + Du$$

$$u = -Kx(t) \tag{78}$$

in which K is the control gain. Moreover, performance index, through state-space equations, that is utilized to minimize both control effort and states is expressed as below.

$$J = \int_0^\infty (x^T Q x + u^T R u) dt \tag{79}$$

where Q is the symmetric state weighting matrix, which is the positive definite or positive semi-definite. R is the positive definite symmetric state weighting matrix.

$$PA + A^T P + Q - PBR^{-1}B^T P = 0 \tag{80}$$

The P matrix is found using the Riccati Equation and added to the control equation. Thus, the feedback gain K is calculated as shown in Equation 81.

$$K = R^{-1}B^T P \tag{81}$$

As a result, the system is given the LQR feedback gain K and it is provided the optimal control.

Since the mid-1960s, these methods have also been preferred to design the missile guidance laws [110, 129, 130]. These methods can handle the maneuvering targets in a better way than other guidance laws [130]. The LQR is one of the most widely used methods among these methods. Nonlinear optimal control and an LQR correction algorithm used together for a SAM against a hypersonic target [129]; performance comparison of the guidance laws based on LQR and H_∞ control methods [110] are two examples of the LQR method as the guidance law. Although this method provides good results in studies and computer simulations, it is still not used in real missile guidance applications.

3.3. Missile Autopilot Methods

The autopilot is the stability algorithm that produces the wing angle commands that are required to complement the conditions that the commands, generated by the guidance algorithm, require during the flight of the missile. The main objectives of the autopilot can be listed as providing stability, achieving high performance, and flying according to the guidance laws. Moreover, the missile autopilot must be able to produce an accurate and fast response when confronted with problems or alterations.

The design of missile autopilot is complex and a difficult task due to the fact that many factors should be taken into account to control the missile properly [131]. Firstly, the missile can be considered as a nonlinear and time-varying system because of the rotational and translational motions of the missile. Furthermore, this system can be unstable due to the non-measurable and/or uncertain parameters, which can be caused by several aerodynamic parameters [132]. In addition, the system can have significant constraints such as the noise and the finite bandwidth.

For the reasons listed above, it is very important to determine the correct controller for missiles. The control methods can best be treated under four headings: classical control methods, modern control methods, robust control methods and intelligent control methods.

Classical Control Methods:

The classical control method can be easily used if the roll motion of the missile is stable and control is provided for pitch and yaw motion. Fromion et al. [133] examined the nonlinear behavior of the PI controller in detail and its application to the missile autopilot design. They stated that the desired results were obtained by utilizing a nonlinear closed-loop controller. In 2012, Ki and Tahk [134] proposed a nonlinear controller structure, including an outer loop for the missile. In their paper, the inner loop controller was designed using an SMC that was based on asymptotic output. Tracking was designed by using the angle of attack control and the outer loop was designed by using the PI controller. Moreover, two different estimator structures for the angle of attack were designed.

Robust Control Methods:

Robust control methods are the most popular methods in designing the missile autopilot which can have uncertainties and disturbances. The most popular robust control methods are divided into three categories: backstepping control, sliding mode control, and the H_∞ norm.

- Backstepping Method

  The backstepping method based on the Lyapunov theorem is a nonlinear control method that has also become attractive due to the recursive design methodology. The foremost advantage of this method is that when the actual control input is determined, the stability of the system is guaranteed [135]. The reason for this is that the appropriate control input is recursively derived until the actual control input can be determined. This method has been studied by many researchers for designing missile autopilots [131, 136–138]. Lin and Fan [137] proposed the backstepping control method for air-to-air dogfight missiles and compared their results with the classical three-loop topology. Pal et al. [136] investigated the effects of the backstepping method and dynamic inversion, which is the nonlinear controller, on the 3 DOF of the missile autopilot. They stated that the most prominent difference between these methods was the response speed of the missile. However, since the backstepping method works recursively and considering the fact that the flight parameters are constantly updated, the control inputs must be continuously updated as well. For this reason, this method is rarely preferred in missile applications.

- Sliding mode control

  Since the mid-1970s, many of the studies on control emphasize sliding mode control because this control method can be designed for almost every system. Salamcı et al. [139] proposed an acceleration autopilot design for missiles by using the SMC method. The most important part of the article was that the State Dependent Riccati Equations (SDRE) method was utilized to design a sliding manifold that could be adapted to change over time so that a movable sliding manifold could be obtained. In

2000, Salamcı and Özgören [140] reported a new method in which the SMC method with optimally selected sliding manifolds for recursive linear-time varying systems was considered. The method was applied to a missile autopilot, which was expected to comply with given acceleration commands. Although the results of the studies in the literature are successful, this method is generally not preferred. The fact that the sliding manifold is determined by changing flight conditions means that it would produce slower results than conventional methods.

Intelligent Control Methods:

Generally, for this missile autopilot design, the two most popular methods are discussed: neural networks and fuzzy logic methods.

- Neural network

  A neural network controller is used as an inverse plant model in the control system. When designing a missile autopilot with the neural network method, the output variable is usually the lateral acceleration command. It generates different output values for different input values, and the system trains with these values. This trained network is used as a controller in the system. In a study conducted by McFarland et al. [141], it was shown that the nonlinear controller was improved by using neural networks with on-line learning. A bank-to-turn autopilot design for an agile anti-air missile was selected as the system to show the results of the proposed method.

- Fuzzy logic

  In the missile autopilot studies, the fuzzy logic controller generally produces the fin deflection commands as an output. The biggest disadvantage of this method is that it cannot provide stability for the system. Some examples of the fuzzy logic controller utilized to the design of the autopilot are, for example, a nonlinear autopilot by using fuzzy logic for a supersonic missile [142], fuzzy-feedback linearization controller for the missile model using a multiobjective evolutionary algorithm [143].

4. GUIDANCE LAW BASED ON CONTROL METHODS

It has been mentioned in the previous sections that the general purpose of guidance is to apply appropriate acceleration commands to the missile to ensure that the distance between the missile and the target reaches zero or a minimum value in a finite time. In this section, in addition to the two classical guidance laws, PPN and APN, guidance rules are designed with two control methods, which are PID and SMC.

Initially, before describing the guidance law design, the missile target engagement geometry are given in subsection 4.1.. Then, the PID guidance law and SM guidance law are designed and these laws are presented in 4.2.. After then, simulation studies on 3D geometry of all the guidance laws given were carried out for two different targets and the results are given in detail in 4.3..

4.1. Missile-Target Engagement Geometry

In this subsection, the relative motion between a missile and a target in 3D environment is briefly explained and is presented in Figure 4.1.

In practice, the target-missile relative motion happens in a 3D environment. The mathematical model of this environment comes from second-order nonlinear and coupling differential equations. Many studies exist in which the guidance laws are designed in planar geometries [65, 144, 145]. In this way, the cross-coupling effects are ignored, and the design and analysis of the missile-target relative motion are very easily achieved thanks to these simplifications and some assumptions. However, if it is expected to get closer results to the real system, the guidance law should be designed by taking the 3D engagement geometry into account. At present, many 3D guidance laws have been studied by many researchers [146–149].

In Figure 4.1, T and M denote the target and the missile, respectively. R is the range between missile and target. The elevation angle and the azimuth angle of the line-of-sight are θ and

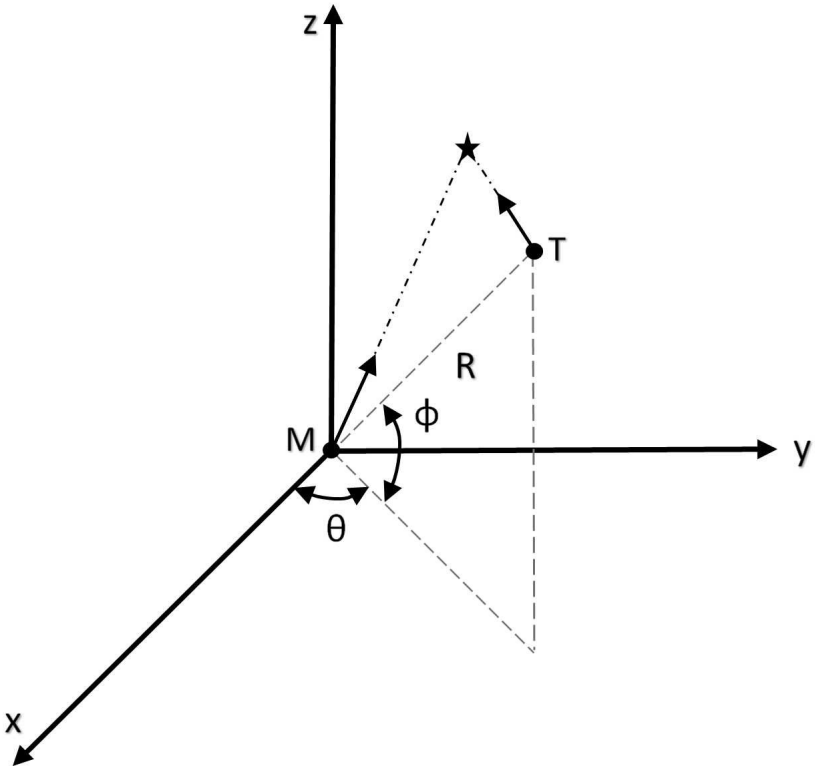

Figure 4.1 Missile-Target engagement geometry

ϕ. The second-order nonlinear differential equations of the relative motion in [150] can be described as

$$\ddot{R} - R\dot{\phi}^2 - R\dot{\theta}^2 \cos^2\phi = a_{TR} - a_{MR} \tag{82}$$

$$R\ddot{\phi} + 2\dot{R}\dot{\phi} + R\dot{\theta}^2 \sin\phi\cos\phi = a_{T\phi} - a_{M\phi} \tag{83}$$

$$R\ddot{\theta}\cos\phi + 2\dot{R}\dot{\theta}\cos\phi - 2R\dot{\phi}\dot{\theta}\sin\phi = a_{M\theta} - a_{T\theta} \tag{84}$$

in which $a_{TR}, a_{T\theta}, a_{T\phi}$ define the accelerations of target and $a_{MR}, a_{M\theta}, a_{M\phi}$ define the accelerations of missile in the LOS frame. Equations (85) and (86), which refer to the 3D nonlinear coupled LOS motion equations of missile and target, are used in the design of the guidance laws.

$$\ddot{\phi} = -\frac{2\dot{R}}{R}\dot{\phi} - \dot{\theta}^2 \sin\phi\cos\phi - \frac{a_{M\phi}}{R} + \frac{a_{T\phi}}{R} \tag{85}$$

$$\ddot{\theta} = -\frac{2\dot{R}}{R}\dot{\theta} + 2\dot{\theta}\dot{\phi}\tan\phi + \frac{a_{M\theta}}{R\cos\phi} - \frac{a_{T\theta}}{R\cos\phi} \tag{86}$$

Remark. According to the literature [151] , there was $\cos\phi > 0$ during the terminal guidance phase if we choose an appropriate reference inertial coordinate.

4.2. Design of the Guidance Law

4.2.1. PID Guidance Law

For a wide range of scientific and industrial control processes, the conventional PID controller approach is quite important [8, 152, 153]. Although PID has been used over many years, it remains popular today because of their simple functionality, easy implementation. The control law of the PID method is described as below.

$$u_t = K_p e(t) + K_i \int e(t)dt + K_d \frac{de}{dt} \tag{87}$$

in which $e(t)$ denotes the tracking error. K_p, K_i and K_d are the proportional, the integral and the derivative gain, respectively. The overall effects of each controller parameter (K_p, K_d, K_i) on a system are different and given briefly in the Table 4.1. Therefore, using one or more of these terms, different controllers can be developed according to the needs of the system.

Parameter	**Rise Time**	**Overshoot**	**Settling Time**
$\boldsymbol{K_p}$	Decrease	Increase	Small Change
$\boldsymbol{K_i}$	Decrease	Increase	Increase
$\boldsymbol{K_d}$	Small Change	Decrease	Decrease

Table 4.1 The overall effects of each controller parameter (K_p, K_d, K_i) on a system

In the light of what has been explained above, the control parameters K_p and K_i will be used while designing the guidance law in this section [42]. Thus, the PI guidance law scheme has been developed and its equations given as the following.

$$a_{M\theta} = N_p V_c \dot{\theta} + N_i V_c \theta \tag{88}$$

$$a_{M\phi} = N_p V_c \dot{\phi} + N_i V_c \phi \tag{89}$$

where N_p and N_i are the proportional gain and the integral gain, respectively. V_c denotes the closing velocity, $\dot{\theta}$ and θ are the elevation LOS rate and angle, and also $\dot{\phi}$ and ϕ are the azimuth LOS rate and angle, respectively.

4.2.2. Sliding Mode Guidance Law

The traditional SMC method is a robust control method that has been implemented in almost every control application under uncertainties and disturbances and the interest in the SMC method is also increasing more and more, thanks to its robust results against parameter uncertainties and external disturbances [154–156]. However, it has a notable disadvantage, which is called the chattering phenomenon. The chattering phenomenon is a high-frequency change occurring in the control signal during the sliding mode and is given in Figure 4.2. This phenomenon adversely affects the performance of the system and may potentially cause instability. Moreover, it may damage the actuator or other parts of the system. In order to reduce or completely eliminate this oscillation, various studies have been carried out in the literature, methods have been proposed, and it has been intensively studied to find a solution while maintaining the features of the sliding mode [157, 158].

The classical SMC method is composed of two phases. The first phase is to design the switching function in which sliding motion occurs. The other phase is to determine a control law in order to maintain system states on that sliding surface. Here, u_{sw} denotes the switching control and u_{eq} denotes the equivalent control. It is denoted as the r^{th} order sliding mode

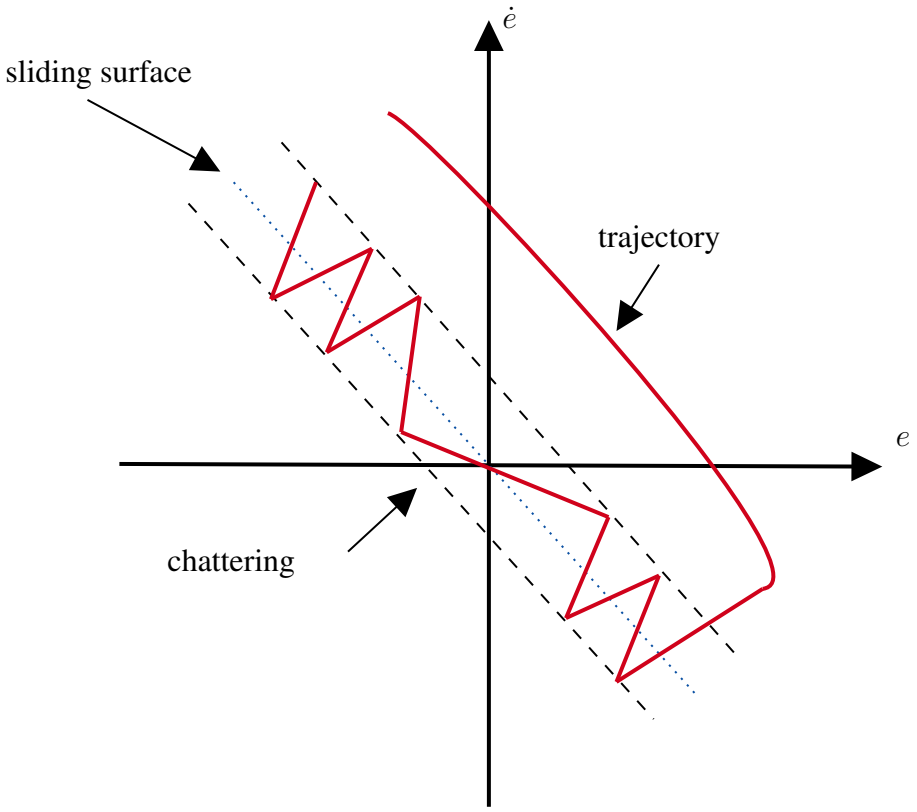

Figure 4.2 Sliding surface and the chattering phenomenon

and is stated in terms of the degree of derivative of the SMC sliding variable. It is expressed in terms of the order of derivative of the SMC sliding variable. $(r-1)^{th}$ order derivative of sliding variable mean up the r^{th} order sliding mode. The order derivative of sliding variable is described as below.

$$s = \dot{s} = \ddot{s} = \cdots = s^{r-1} = 0 \tag{90}$$

In the literature, the SMC method appears in two different forms as the first order and the high order. The high order SMC method plays an important role in solving the chattering phenomenon mentioned earlier.

Lyapunov stability analysis is utilized to determine stability of the sliding manifold. For this purpose, a positive definite Lyapunov function $V(t,x)$ with a negative time derivative is first chosen. Then, the first derivative of Lyapunov function $\dot{V}(t,x) < 0$.

This section, the first order SMC method is used to design the guidance law for 3D missile-target engagement geometry. Firstly, the sliding surface is determined to design the SM guidance law. In here, two sliding surfaces are designed to zero both LOS angular rate of elevation and LOS angular rate of azimuth at the same time.

The system dynamics in (85)-(86) can be rewritten as follows:

$$x_1 = \phi, \quad x_2 = \dot{\phi}$$

$$x_3 = \theta, \quad x_4 = \dot{\theta}$$

For the nonlinear SM guidance law, a sliding manifold vector is described as bellows.

$$s = \begin{pmatrix} s_1 \\ s_2 \end{pmatrix} = \begin{pmatrix} x_2 \\ \\ x_4 cos x_1 \end{pmatrix} \tag{91}$$

For the presented guidance law, the first time derivative of the sliding surfaces that are expressed by s_1 and s_2 are:

$$\dot{s} = \begin{pmatrix} \dot{s}_1 \\ \dot{s}_2 \end{pmatrix} = \begin{pmatrix} \dot{x}_2 \\ \\ \dot{x}_4 cos x_1 - x_4 x_2 cos x_1 sin x_1 \end{pmatrix} \tag{92}$$

Consider a suitable Lyapunov candidate function is selected by:

$$V_1 = \frac{1}{2} s_1^2 + \frac{1}{2} s_2^2 \tag{93}$$

The first time derivative of V_1 is obtained as given below:

$$\dot{V}_1 = s_1 \dot{s}_1 + s_2 \dot{s}_2 \tag{94}$$

According to the Lyapunov stability rule, to guarantee a finite time convergence to the sliding surface, $\dot{V}_1 \leqslant 0$ must be ensured.

The conclusion of the above condition, the SM guidance law is explained as follows.

$$\begin{pmatrix} a_{M\phi} \\ a_{M\theta} \end{pmatrix} = \begin{pmatrix} NV_c x_2 + \epsilon_1 \mathrm{sgn}(x_1) \\ NV_c x_4 + \epsilon_2 \mathrm{sgn}(x_3) \end{pmatrix} \tag{95}$$

where the target accelerations $\left|a_{T\phi}\right| \leq \epsilon_1$ and $|a_{T\theta}| \leq \epsilon_2$ and sgn is the signum function described by

$$\mathrm{sgn}(s) = \begin{cases} 1 & : \ s \geq 0 \\ 0 & : \ s = 0 \\ -1 & : \ s < 0 \end{cases} \tag{96}$$

The saturation function is used instead of signum function to minimize the chattering phenomenon. Consequently, this guidance law is more robust against uncertainties and external disturbances. The SM guidance law is rewritten as below.

$$\begin{pmatrix} a_{M\phi} \\ a_{M\theta} \end{pmatrix} = \begin{pmatrix} NV_c x_2 + \epsilon_1 \mathrm{sat}(x_1) \\ NV_c x_4 + \epsilon_2 \mathrm{sat}(x_3) \end{pmatrix} \tag{97}$$

As a result, the control signal's undesirable high frequency chattering is reduced.

At mentioned previously, the PI guidance law given Equation (88)-(89) and the SM guidance law given Equation (97) are presented in this section. In the next subsection, the numerical results of these guidance laws will be examined.

4.3. Results of the Numerical Simulations

In this subsection, the numerical simulations for the missile-target intercepting in a 3D environment are presented. A performance comparison between PID guidance law, SM

guidance law, classical PN, and APN guidance law is conducted to highlight the robustness of the methods. Through numerical validation, the performance of the presented guidance system is carried out, and the results are presented in detail here.

4.3.1. Simulation Scenarios Setting

The speed of the target is constant and the target has two different actions, they being non-maneuvering and maneuvering actions. The simulations are performed in MATLAB/Simulink and is used the ode4 (Runge-Kutta) with fixed step size of 0.001 s in the simulation. The system performance is investigated by adding an external disturbance, which is the band limited white noise with the power 25e-5.

The missile and target parameters used in simulation are as follows. The missile initial position is $x_{M0} = 0$ m, $y_{M0} = 5000$ m and $z_{M0} = 0$ m. Its initial velocity is $V_{M0} = 204$ m/s. The target initial position is $x_T0 = 2500$ m, $y_T0 = 5000$ m and $z_T0 = 0$ m and its initial velocity is $V_T0 = 200$ m/s. The table below is given three different cases that take account of target accelerations, and these cases will be used to indicate the effectiveness of the presented guidance laws. Two separate scenarios that account for target accelerations are presented in the table below, and these cases will be utilized to display the effectiveness of the designed guidance laws.

Interception Scenarios	**Azimuth acceleration**	**Elevation acceleration**
non-maneuvering	0	0
time-varying maneuvering	$3g + \sin 2\pi t$	$3g + \sin 4\pi t$

Table 4.2 Accelerations setting of target in interception scenarios

The guidance law parameters are taken different for each scenario. For first scenario, the parameter of the PN given Equation 58-59 is $N = 4$. The parameters of the APN guidance law are $N_1 = 3$ and $N_2 = 4$ given Equation 65-66. For PI guidance law, the parameters are determined to be $N_p = 5$ and $N_i = 0.73$ in Equation 88-89. Moreover, the guidance

law parameters based on SMC method given 97 are $N = 4$, $\epsilon_1 = 10$ and $\epsilon_2 = 10$. For another scenario, the parameters of PN Equation 58-59 is $N = 4$. The parameters of the APN guidance law are $N_1 = 3$ and $N_2 = 2$ in Equation 65-66. For PI guidance law, the navigation constants are preferred $N_p = 5$ and $N_i = 0.73$ given Equation 88-89. Moreover, the guidance parameters of SM-based law are $N = 4$, $\epsilon_1 = 10$ and $\epsilon_2 = 18$ in Equation 97.

4.3.2. Simulation Results

There are important conditions that must be fulfilled to demonstrate that the proposed guidance law is successful.The miss distance should be as small as possible and the LOS rates should be close to zero at finite time. Two simulation scenarios are constructed so as to ensure the performance of the designed guidance laws. Figures 4.3-4.18 demonstrate the simulation results. These figures are examined in two parts. The first part is to be presented between Figure 4.3 and Figure 4.10.

It can be clearly seen from Figure 4.3 that the relative range decreases to zero at the intercept time in all the guidance laws. And also in Figure 4.4 it is shown that LOS angles become stable at zero in finite time. From Figure 4.5, it can be observed that all of them can verify that LOS angular rates $\dot{\theta}$ and $\dot{\phi}$ decrease to zero in finite time. Two figures related to SM based guidance law are examined in Figure 4.6. These figures are observed that the sliding surfaces become stable at zero in finite time. Thus, the sliding surface variables are understood to be smooth and stable. As shown in Figure 4.7-4.8, the missile successfully intercepts the target in the implementation of the whole guidance laws. However, the presented PI-based guidance law follows a different trajectory. Finally, Figure 4.9 gives the change of Mach number over time and Figure 4.10 presents the change of the closing velocity.

Miss distances and final times for non-maneuvering target are given in the Table 4.3. It is clearly observed that the presented guidance law yields successful results in terms of miss distances and target tracking ability.

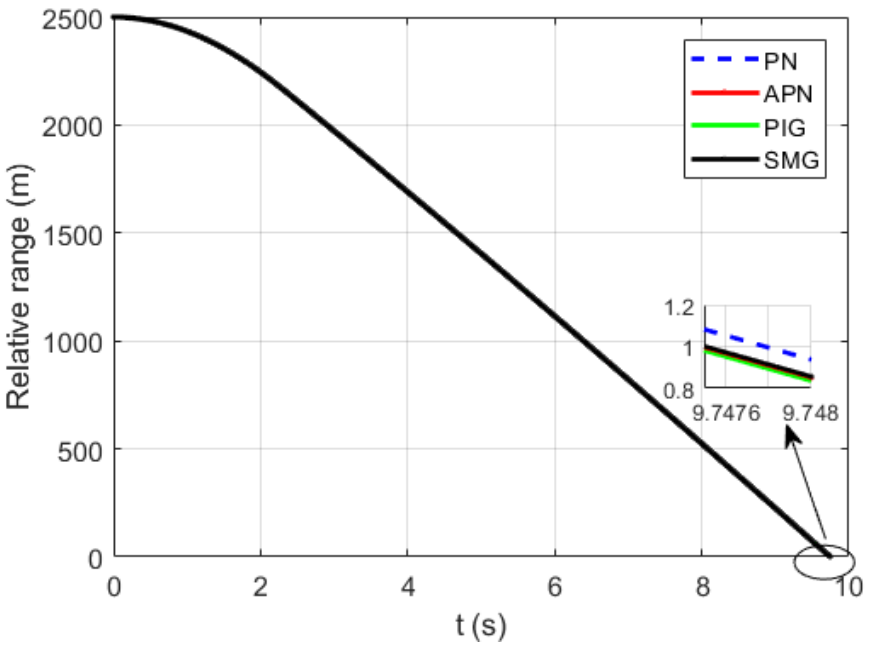

Figure 4.3 Results of Case 1: Relative range

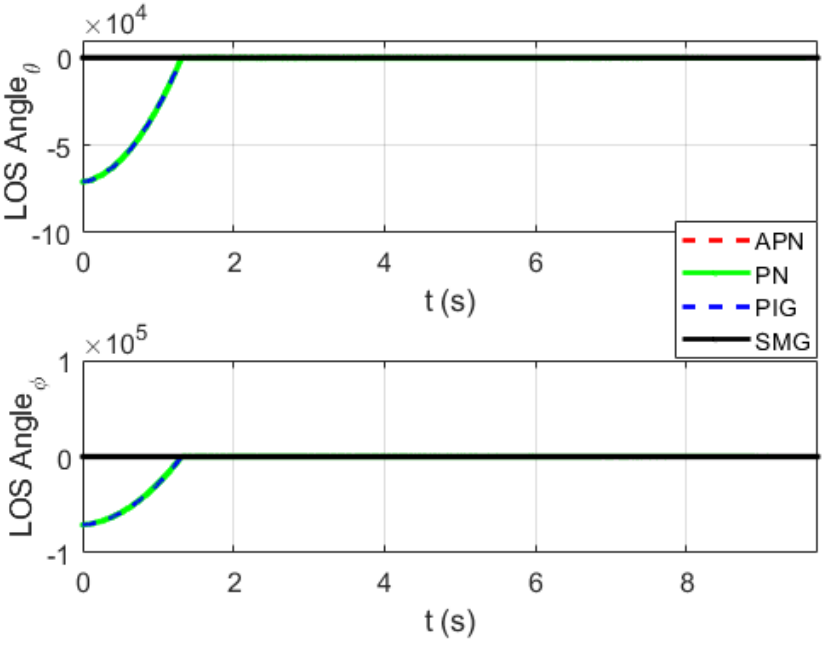

Figure 4.4 Results of Case 1: LOS angles

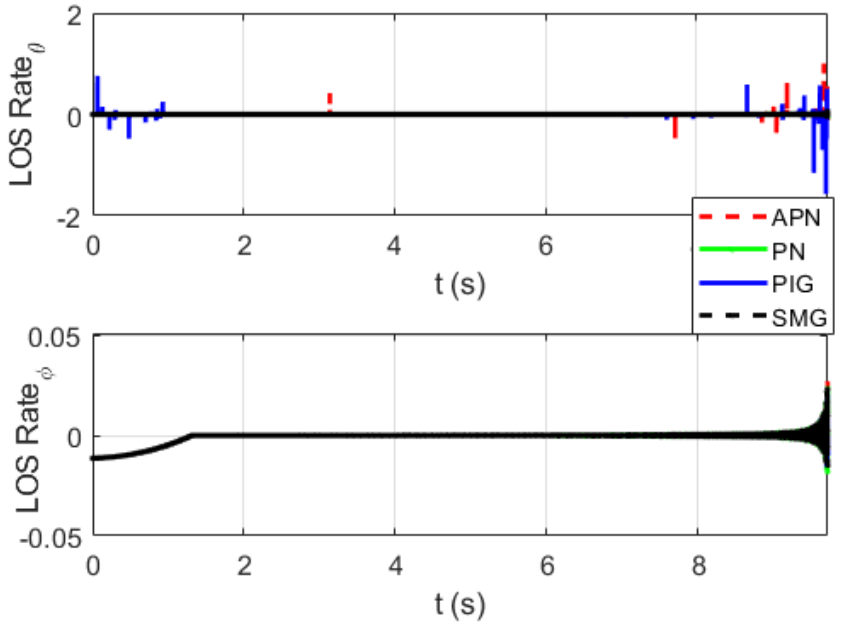

Figure 4.5 Results of Case 1: LOS angular rates

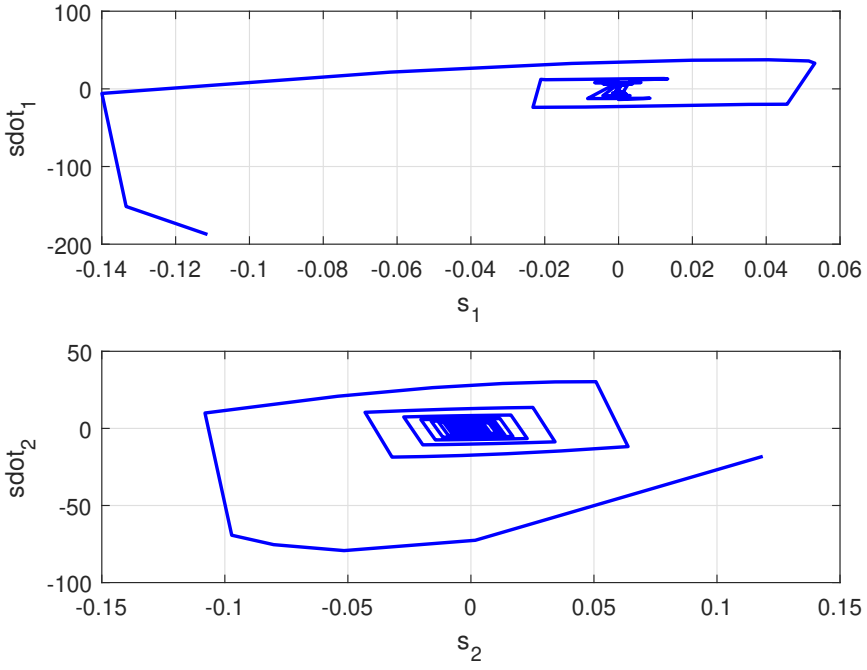

Figure 4.6 Results of Case 1: Phase space behavior

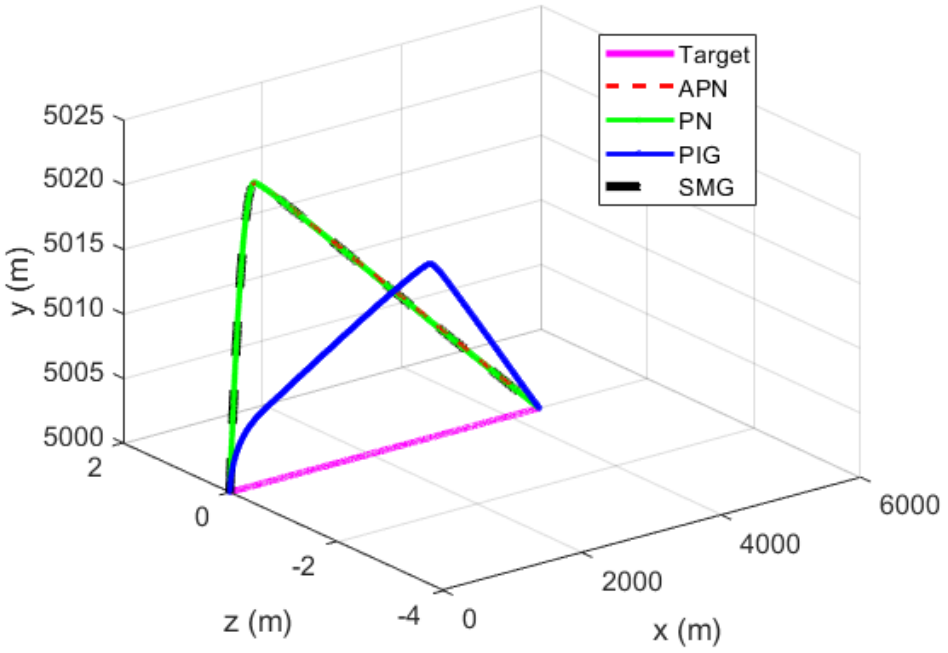

Figure 4.7 Results of Case 1: Missile and target trajectories

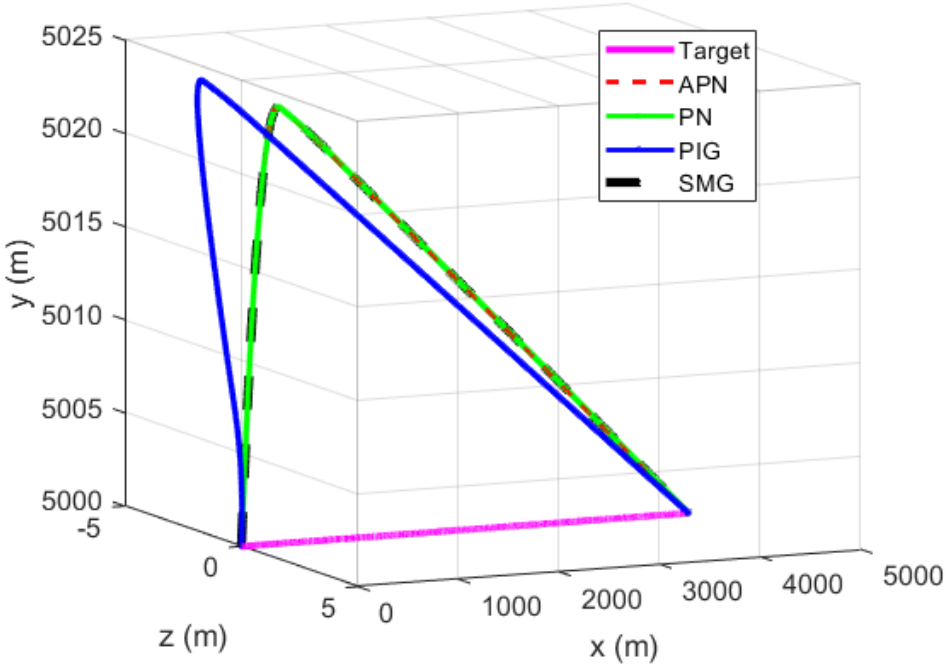

Figure 4.8 Results of Case 1: Missile and target trajectories

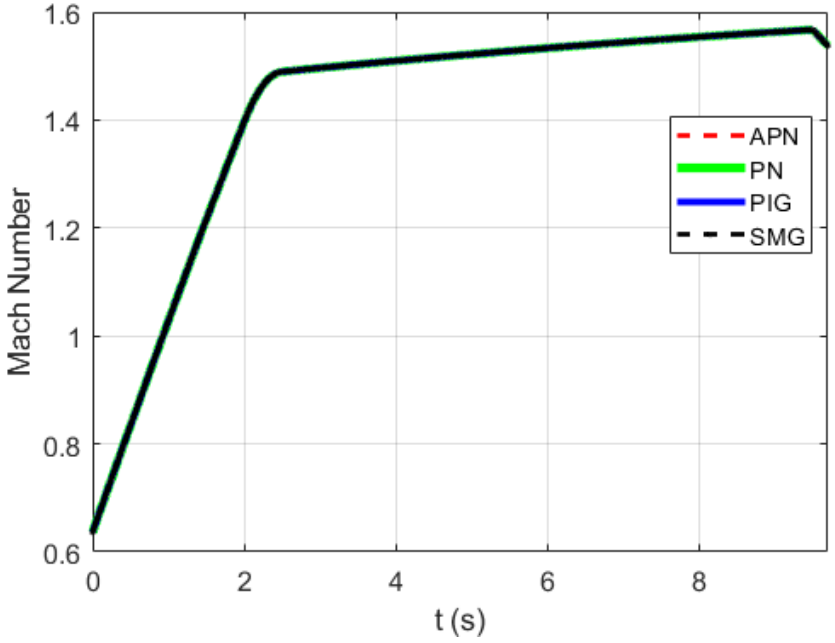

Figure 4.9 Results of Case 1: Mach number

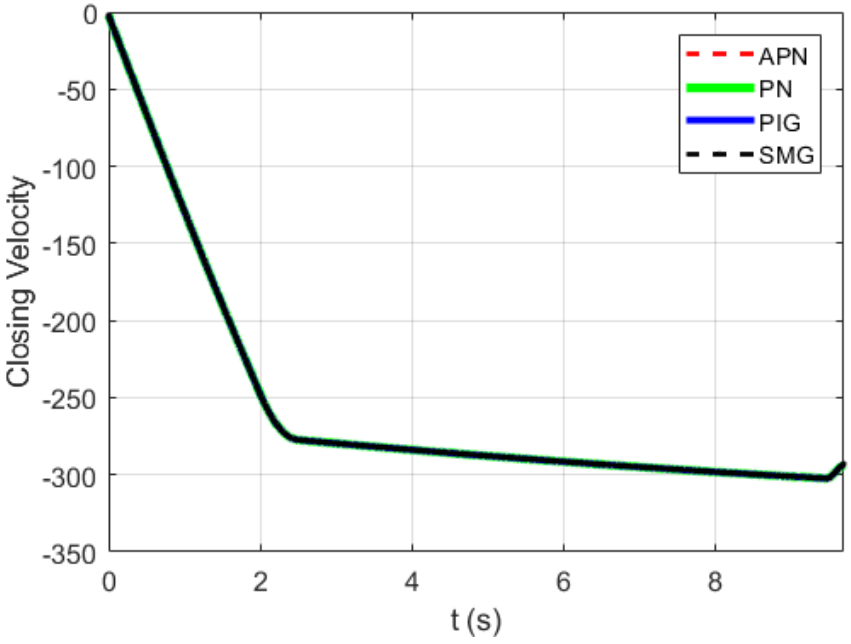

Figure 4.10 Results of Case 1: Closing velocity

Target Scenario	Guidance law	Miss distance (m)	Interception time (s)
non-maneuvering	PN Guidance law	0.8511	9.7480
	APN Guidance law	0.9372	9.7480
	PI Guidance law	0.7955	9.7480
	SM Guidance law	0.8491	9.7480

Table 4.3 Miss distance and Interception time for non-maneuvering target

In the second part, the results of the guidance rules against a maneuvering target are demonstrated in Figure 4.11 and Figure 4.18. The relative range presented in Figure 4.11 declines to zero at the intercept time, as expected from all of the guidance laws. As shown in Figure 4.12 and Figure 4.13, $\dot{\theta}$ and $\dot{\phi}$ which are known as LOS angular rates converge to zero and the same can be said for the LOS angles. In addition, the sliding surfaces have become stable at zero, as in the first scenario for the SM-based guidance law. It is observed in Figure 4.14 that the presented guidance law is stable and smooth when the target is capable of maneuvering. In Figure 4.15-4.16, the missile successfully intercepted the target for each of the guidance laws presented in this paper. Figure 4.17-4.18 show the change of Mach number over time and the closing velocity, respectively.

For the maneuvering target, miss distances and final times are presented in Table 4.4. It can be clearly observed that the designed guidance law yields successful results in terms of miss distances as well as target tracking ability.

Target Scenario	Guidance law	Miss distance (m)	Interception time (s)
maneuvering	PN Guidance law	0.8598	9.6040
	APN Guidance law	0.8111	9.6040
	PI Guidance law	0.8369	9.6040
	SM Guidance law	0.7601	9.6040

Table 4.4 Miss distance and Interception time for maneuvering target

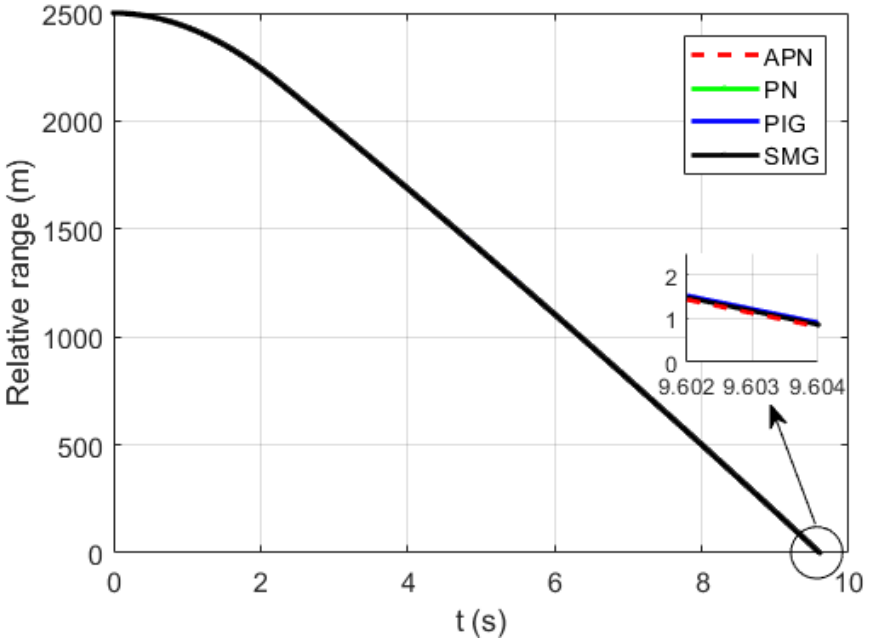

Figure 4.11 Results of Case 2: Relative range

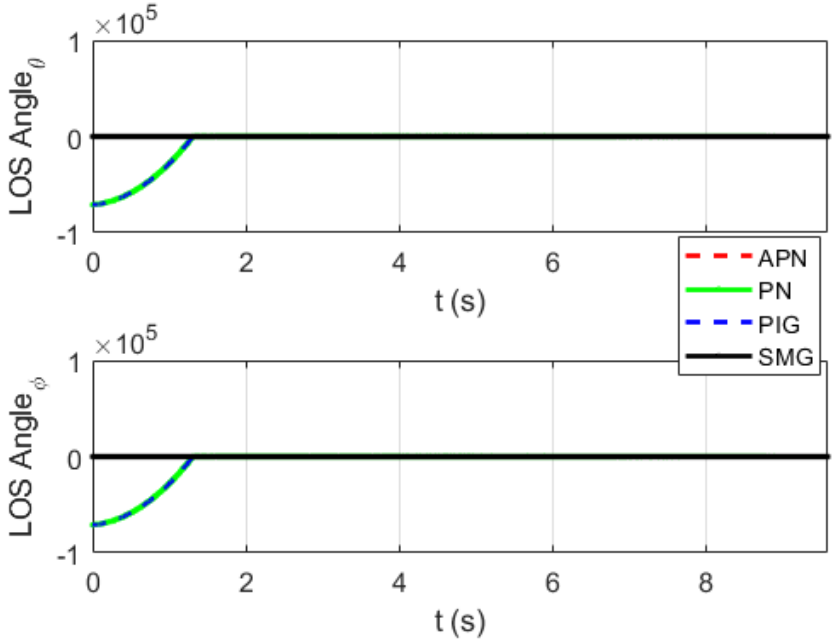

Figure 4.12 Results of Case 2: LOS angles

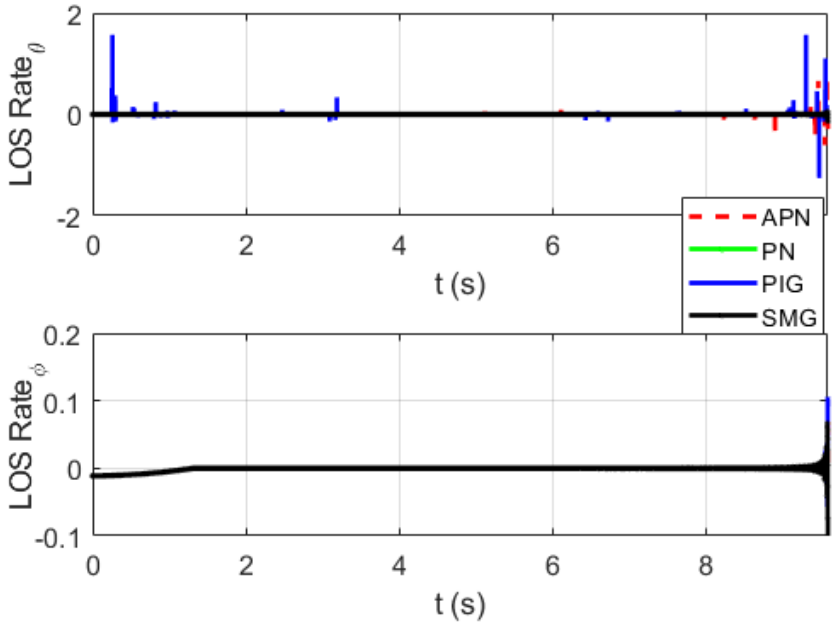

Figure 4.13 Results of Case 2: LOS angular rates

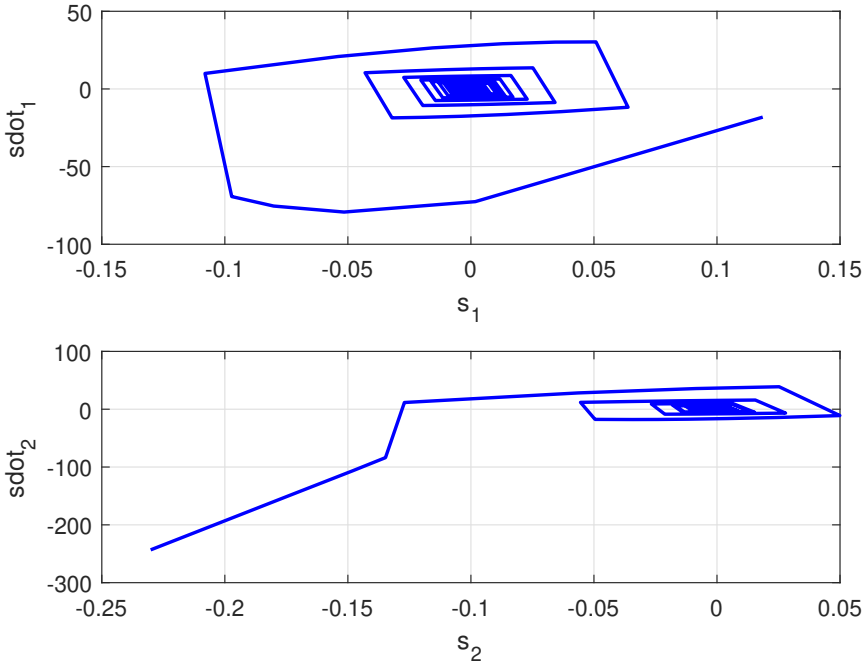

Figure 4.14 Results of Case 2: Phase space behavior

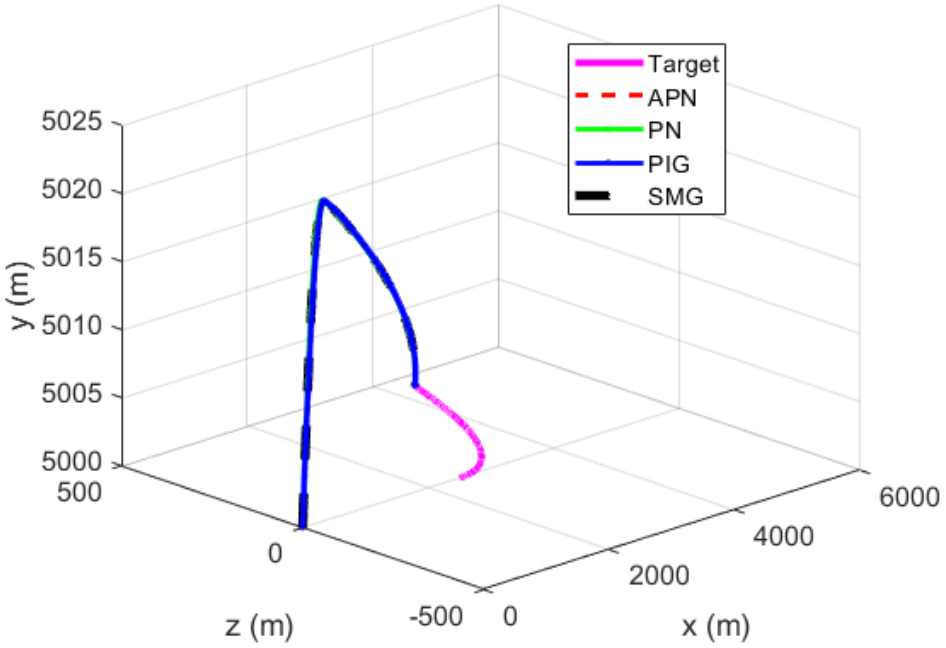

Figure 4.15 Results of Case 2: Missile and target trajectories

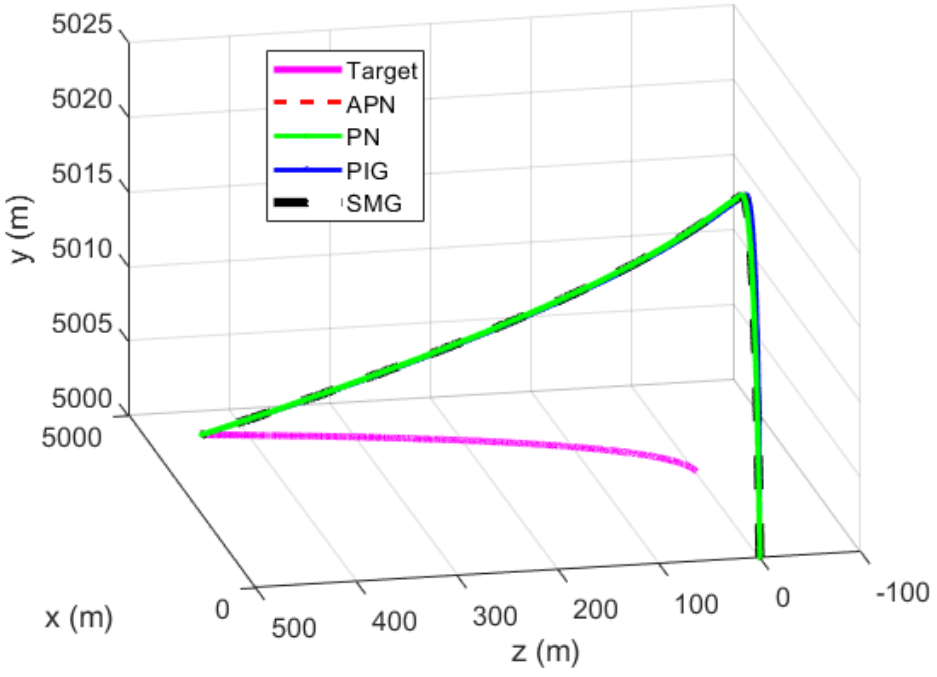

Figure 4.16 Results of Case 2: Missile and target trajectories

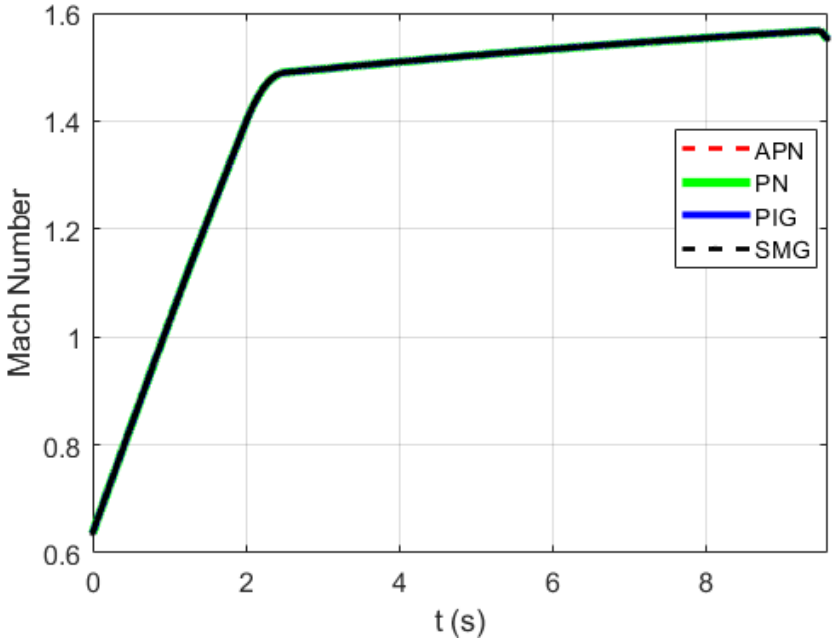

Figure 4.17 Results of Case 2: Mach Number

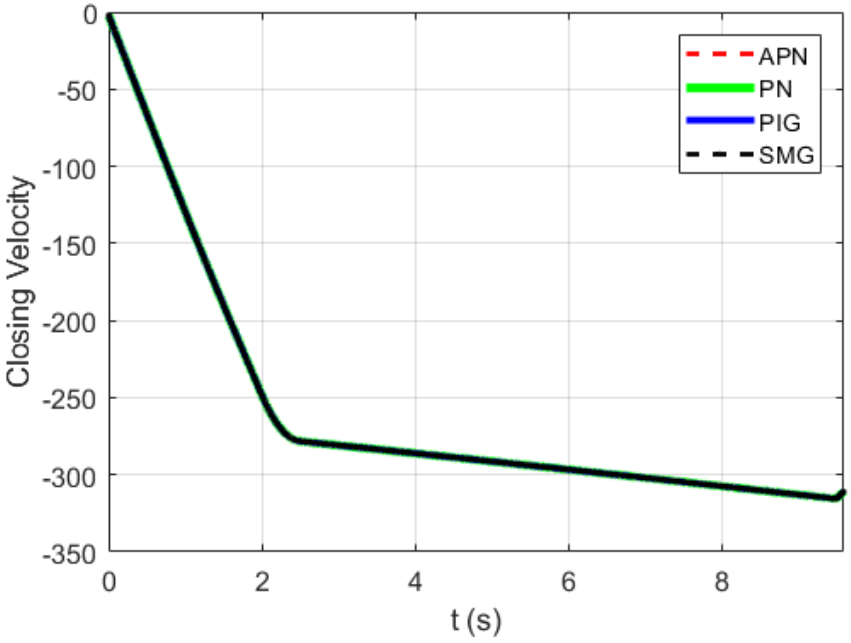

Figure 4.18 Results of Case 2: Closing velocity

4.4. Summary

In this section, controller-based guidance laws are developed in order to design a missile guidance law that intercepts the target in a 3D environment with less sensitivity to external disturbances, and their comparative results with classical guidance laws are presented. Here, the following steps have been followed.

- PPN and APN, which are classical guidance law methods, are preferred.
- For designing control-based guidance laws, the PID and SMC methods, which are the most preferred control methods from the past to the present, have been selected.
- These guidance laws are investigated by taking two scenarios into account, which are according to two different models of the target: non-maneuverable and maneuverable target.

It is clearly understood from the results of numerical simulations that the designed control methods based guidance laws are able to give better results than the classical guidance laws in terms of miss distance in all two target models. Furthermore, the relative range, the LOS angles, as well as the LOS angular rates converge to zero in finite time, as expected from all of the guidance laws presented.

5. ADAPTIVE INTEGRAL SLIDING MODE GUIDANCE LAW WITH A NONLINEAR DISTURBANCE OBSERVER

In this section, a novel composite 3D (3D) guidance law for missiles is presented. This composite guidance law is based on an adaptive integral sliding mode (AISM) control method utilizing a nonlinear disturbance observer (NDOB) technique. Generally, in the subsections, AISM guidance law will be explained in design steps, and the NDOB method will be introduced and used to improve guidance law. Finally, a new design and analysis of the composite guidance law will be discussed at the end of this part.

5.1. Design the Guidance Law

5.1.1. Mathematical Preliminaries

In this subsection, some basic mathematical preliminaries, which will be used in this section, are introduced.

Lemma 1. [159] Let $b_i \in \mathbb{R}$ for $(i = 1, 2, ..., n)$. Following inequality is satisfied for $0 < q < 1$.

$$\left(|b_1| + |b_2| + \cdots + |b_n|\right)^q \leq |b_1|^q + |b_2|^q + \cdots + |b_n|^q \tag{98}$$

Lemma 2. [160] Let k_i for $(i = 1, 2, ..., n)$ are all positive numbers. Following inequality is satisfied for $0 < q < 2$.

$$\left(k_1^2 + k_2^2 + \cdots + k_n^2\right)^q \leq \left(k_1^q + k_2^q + \cdots + k_n^q\right)^2 \tag{99}$$

Lemma 3. [160] Let $V(t)$ be a continuous positive definite Lyapunov function as well as t_0 is the initial time. If $\dot{V}(t) \leq -\kappa_1 V(t) - \kappa_2 V(t)^{\xi}$ $(\forall t > t_0)$, where $\kappa_1, \kappa_2 > 0$, $0 < \xi < 1$. Then, $V(t)$ converges to the equilibrium point in finite time if given by Lemma 2

$$t_f \leqslant t_0 + \frac{1}{\kappa_1(1-\xi)} \ln\left(\frac{\kappa_1 V(t_0)^{1-\xi} + \kappa_2}{\kappa_2}\right) \tag{100}$$

Lemma 4. [161] A necessary condition for a polynomial $D(x) = x^n + a_n x^{n-1} + \cdots + a_2 x + a_1$ of a complex variable x to be Hurwitz is $a_1, a_2, ...a_n > 0$.

For an n-th order system with input u,

$$\dot{y}_1 = y_2, \dot{y}_2 = y_3, \cdots, \dot{y}_{n-1} = y_n, \qquad \dot{y}_n = u \tag{101}$$

there exists an $\varepsilon \in (0,1)$ such that, for every $\alpha \in (1-\varepsilon, 1)$ the equilibrium at origin is reached in finite time under the following feedback law for the system given in (101).

$$u = -a_1 \mathrm{sgn}(y_1) |y_1|^{\alpha_1} - \cdots - a_n \mathrm{sgn}(y_n) |y_n|^{\alpha_n} \tag{102}$$

where $\alpha_1, \alpha_2, \cdots, \alpha_n$ satisfy $\alpha_{i-1} = \frac{\alpha_i \alpha_{i+1}}{2\alpha_{i+1} - \alpha_i}$ $(i = 2, ..., n)$, $\alpha_n = \alpha$, $\alpha_{n+1} = 1$.

Lemma 5. [162, 163] (Input-to-State Stability Theorem, ISS Theorem) Consider the nonlinear system of the following form:

$$\dot{x}(t) = f(x, u, t) \tag{103}$$

If the system $\dot{x} = f(x, 0, t)$ is globally asymptotically stable and also $\lim_{t\to\infty} u = 0$, this system's states converge asymptotically to zero, i.e. $\lim_{t\to\infty} x = 0$.

Assumption 1. [31] It is assumed that the target accelerations $\left|a_{T\phi}\right| \leq \epsilon_1$ and $|a_{T\theta}| \leq \epsilon_2$, where ϵ_1 and ϵ_2 are two positive yet unknown constants.

Assumption 2. [164, 165] We assume that the final values of the time derivative of target accelerations $\dot{a}_{T\theta}$ and $\dot{a}_{T\phi}$ are zero, i.e. $\lim_{t\to\infty} \dot{a}_{T\theta} = 0$ and $\lim_{t\to\infty} \dot{a}_{T\phi} = 0$.

Assumption 3. $e_{T\theta}$ and $e_{T\phi}$, which are the disturbance prediction errors, are bounded. Let $\Delta := [\Delta_1; \Delta_2]$ and also Δ_1 and Δ_2 are two positive constants such that

$$\begin{aligned} \left|e_{T\theta}(t)\right| &= |a_{T\theta} - \hat{a}_{T\theta}| \leq \Delta_1 \\ \left|e_{T\phi}(t)\right| &= \left|a_{T\phi} - \hat{a}_{T\phi}\right| \leq \Delta_2 \end{aligned} \tag{104}$$

for $t \geq 0$. This assumption emphasizes that the physical systems can produce finite accelerations thereby ensuring their difference to be finite in magnitude.

5.1.2. Integral Sliding Mode Approach for Guidance Law Design

The nonlinear integral sliding mode (ISM) guidance law is presented for 3D missile-target interception systems under the external disturbances in this section. However, when designing the ISM guidance law needs the upper bound of the acceleration of the target. For this reason, the adaptive law is utilized to estimate the upper bound of the target's accelerations denoted by ϵ_1 and ϵ_2. The stability of the given system is proven via the use of Lyapunov's stability theorem.

According to these definitions $x_1 = \phi,\ x_2 = \dot{\phi},\ x_3 = \theta,\ x_4 = \dot{\theta}$, the guidance system dynamics in (85)-(86) and can be rewritten as follows:

$$\begin{aligned} \dot{x}_1 &= x_2 \\ \dot{x}_2 &= -\frac{2\dot{R}}{R}x_2 - x_4^2 \sin x_1 \cos x_1 - \frac{a_{M\phi}}{R} + \frac{a_{T\phi}}{R} \\ \dot{x}_3 &= x_4 \end{aligned} \tag{105}$$

$$\dot{x}_4 = -\frac{2\dot{R}}{R}x_4 + 2x_4x_2\tan x_1 + \frac{a_{M\theta}}{R\cos x_1} - \frac{a_{T\theta}}{R\cos x_1} \tag{106}$$

For the nonlinear ISM guidance law, a sliding manifold vector is described [32, 68] as follows:

$$s = \begin{pmatrix} s_1 \\ \\ s_2 \end{pmatrix} = \begin{pmatrix} x_2 - x_2(t_0) + \int_0^t (a_1 \mathrm{sgn}(x_1)\,|x_1|^{\alpha_1} + a_2 \mathrm{sgn}(x_2)\,|x_2|^{\alpha_2})dt \\ \\ x_4 - x_4(t_0) + \int_0^t (b_1 \mathrm{sgn}(x_3)\,|x_3|^{\beta_1} + b_2 \mathrm{sgn}(x_4)\,|x_4|^{\beta_2})dt \end{pmatrix} \tag{107}$$

where $a_1, a_2, b_1, b_2 > 0, 0 < \alpha_1 < 1, 0 < \beta_1 < 1$, $\alpha_2 = \frac{2\alpha_1}{\alpha_1+1}, \beta_2 = \frac{2\beta_1}{\beta_1+1}$ are the parameters to be designed. Besides, $a_1, a_2, b_1, b_2 > 0$ ensure that the two polynomials $\lambda^2 + a_2\lambda + a_1$ and $\lambda^2 + b_2\lambda + b_1$ are Hurwitz. In addition, it need to be acknowledged that sliding mode starts from the initial time instance since $s_1(t_0) = 0$, $s_2(t_0) = 0$ at $t = t_0$.

The first time derivative of the sliding surfaces given in (107) is obtained as follows.

$$\dot{s} = \begin{pmatrix} \dot{s}_1 \\ \dot{s}_2 \end{pmatrix} = \begin{pmatrix} \dot{x}_2 + (a_1 \mathrm{sgn}(x_1)\,|x_1|^{\alpha_1} + a_2 \mathrm{sgn}(x_2)\,|x_2|^{\alpha_2}) \\ \\ \dot{x}_4 + (b_1 \mathrm{sgn}(x_3)\,|x_3|^{\beta_1} + b_2 \mathrm{sgn}(x_4)\,|x_4|^{\beta_2}) \end{pmatrix} \tag{108}$$

Substituting $\dot{x}_2$ and $\dot{x}_4$ given in (105)-(106) into (108), the following derivative is obtained

$$\dot{s} = \begin{pmatrix} \dot{s}_1 \\ \dot{s}_2 \end{pmatrix} = \begin{pmatrix} -\frac{2\dot{R}}{R}x_2 - x_4^2 \sin x_1 \cos x_1 - \frac{a_{M\phi}}{R} + \frac{a_{T\phi}}{R} \\ +(a_1 \mathrm{sgn}(x_1)\,|x_1|^{\alpha_1} + a_2 \mathrm{sgn}(x_2)\,|x_2|^{\alpha_2}) \\ \\ -\frac{2\dot{R}}{R}x_4 + 2x_4x_2\tan x_1 + \frac{a_{M\theta}}{R\cos x_1} - \frac{a_{T\theta}}{R\cos x_1} \\ +(b_1 \mathrm{sgn}(x_3)\,|x_3|^{\beta_1} + b_2 \mathrm{sgn}(x_4)\,|x_4|^{\beta_2}) \end{pmatrix} \tag{109}$$

Equation (109) can be rewritten as given by (110).

$$\dot{s} = A + B \begin{pmatrix} a_{M\phi} \\ a_{M\theta} \end{pmatrix} + C \begin{pmatrix} a_{T\phi} \\ a_{T\theta} \end{pmatrix} \tag{110}$$

where

$$A = \begin{pmatrix} -\frac{2\dot{R}}{R} x_2 - x_4^2 \sin x_1 \cos x_1 + (a_1 \mathrm{sgn}(x_1) \left|x_1\right|^{\alpha_1} + a_2 \mathrm{sgn}(x_2) \left|x_2\right|^{\alpha_2}) \\ \\ -\frac{2\dot{R}}{R} x_4 + 2x_4 x_2 \tan x_1 + (b_1 \mathrm{sgn}(x_3) \left|x_3\right|^{\beta_1} + b_2 \mathrm{sgn}(x_4) \left|x_4\right|^{\beta_2}) \end{pmatrix}$$

$$B = \begin{pmatrix} -\frac{1}{R} & 0 \\ 0 & \frac{1}{R\cos x_1} \end{pmatrix}$$

$$C = \begin{pmatrix} \frac{1}{R} & 0 \\ 0 & -\frac{1}{R\cos x_1} \end{pmatrix}$$

Theorem 5.1. Let (111) be the chosen control law for the 3D missile guidance system whose dynamics are expressed in (105) and (106). Under Assumption 1, the elevation angular rate $\dot{\theta}$ and the azimuth angular rate $\dot{\phi}$ of LOS converge to zero in finite time.

$$\begin{pmatrix} a_{M\phi} \\ a_{M\theta} \end{pmatrix} = B^{-1} \left(-A - \rho s - \begin{pmatrix} \gamma_1 \mathrm{sgn}(s_1) \\ \gamma_2 \mathrm{sgn}(s_2) \end{pmatrix} \right) \tag{111}$$

Proof. The Lyapunov function is selected as

$$V_1 = \frac{1}{2} s^T s \tag{112}$$

The derivative of this Lyapunov function as follows:

$$
\begin{aligned}
\dot{V}_1 &= s^T \dot{s} \\
&= s^T \left(A + B \begin{pmatrix} a_{M\phi} \\ a_{M\theta} \end{pmatrix} + C \begin{pmatrix} a_{T\phi} \\ a_{T\theta} \end{pmatrix} \right) \\
&= s^T \left(-\rho s + C \begin{pmatrix} a_{T\phi} \\ a_{T\theta} \end{pmatrix} - \begin{pmatrix} \gamma_1 \mathrm{sgn}(s_1) \\ \gamma_2 \mathrm{sgn}(s_2) \end{pmatrix} \right) \\
&= -\rho s^T s + s^T \begin{pmatrix} c_{11} a_{T\phi} + c_{12} a_{T\theta} - \gamma_1 \mathrm{sgn}(s_1) \\ c_{21} a_{T\phi} + c_{22} a_{T\theta} - \gamma_2 \mathrm{sgn}(s_2) \end{pmatrix} \\
&= -\rho s^T s + (c_{11} a_{T\phi} + c_{12} a_{T\theta}) s_1 - \gamma_1 \left| (s_1 \right| + (c_{21} a_{T\phi} + c_{22} a_{T\theta}) s_2 - \gamma_2 \left| (s_2 \right| \\
&\leqslant -\rho s^T s + (\epsilon_1 |c_{11}| + \epsilon_2 |c_{12}|) |s_1| - \gamma_1 \left| (s_1 \right| + (\epsilon_1 |c_{21}| + \epsilon_2 |c_{22}|) |s_2| - \gamma_2 \left| (s_2 \right| \\
&\leqslant -\rho s^T s - w_1 \left| (s_1 \right| - w_2 \left| (s_2 \right|
\end{aligned}
\tag{113}
$$

Let's assume that $w = min\{w_1, w_2\}$. The above equation (113) can be rewritten as follows.

$$
\dot{V}_1 \leqslant -\rho s^T s - w \left| s_1 \right| - w \left| s_2 \right| \tag{114}
$$

According to Lemma 1, it can be obtained that $\left(|s_1| + |s_2| \right) \leq \left(|s_1|^2 + |s_2|^2 \right)^{1/2}$. Thus, the above equations can be rewritten as below.

$$
\begin{aligned}
\dot{V}_1 &\leqslant -\rho s^T s - w (|s_1|^2 - |s_2|^2)^{\frac{1}{2}} \\
&= -2\rho V_1 - 2^{\frac{1}{2}} w V_1^{\frac{1}{2}}
\end{aligned}
\tag{115}
$$

According to Lemma 3, the final inequality above stipulates that the switching variables converge to zero in finite time .

Finally, there is one more step that needs to be proved in this section. It is known that x_2 and x_4 given in (105) and (106) are system states. In (109), if $\dot{x}_2$ and $\dot{x}_4$ are separated, the following equations can be written as:

$$\dot{x}_2 = -(a_1 \text{sgn}(x_1) |x_1|^{\alpha_1} + b_1 \text{sgn}(x_2) |x_2|^{\alpha_2}) \tag{116}$$

$$\dot{x}_4 = -(a_1 \text{sgn}(x_3) |x_3|^{\beta_1} + b_1 \text{sgn}(x_4) |x_4|^{\beta_2}) \tag{117}$$

According to the information given in Lemma 4, in the closed loop, the states x_2 and x_4 converge to zero in finite time. It can be stated as a conclusion that the LOS angular rates $\dot{\theta}$ and $\dot{\phi}$ will converge to zero in finite time and can be realized by the chosen guidance approach as shown. Thus, this completes the proof. □

In the designed guidance system using ISM, the upper bounds of the target accelerations need to be known numerically according to Assumption 1. In a practical operation scenario, it is impossible to know the upper bound of the target acceleration a priori. The adaptive control scheme is a good alternative for solving the problem. As a result, as defined by Song et al. [32], the robust guidance law is designed by utilizing an adaptive law and the ISM guidance law. At this point, the adaptive law of the proposed guidance aims to estimate the upper bound for the target accelerations.

5.1.3. Adaptive Integral Sliding Mode Approach for Guidance Law Design

Theorem 5.2. Let (118) be the chosen control law for the 3D missile guidance system whose dynamics are expressed in (105) and (106).

$$\begin{pmatrix} a_{M\phi} \\ a_{M\theta} \end{pmatrix} = B^{-1}\left(-A - \rho_1 s - \rho_2 \begin{pmatrix} |s_1|^{\gamma}\,\mathrm{sgn}(s_1) \\ |s_2|^{\gamma}\,\mathrm{sgn}(s_2) \end{pmatrix} - \sum_{j=1}^{2} \begin{pmatrix} \left|c_{1j}\right|\mathrm{sgn}(s_1) \\ \left|c_{2j}\right|\mathrm{sgn}(s_2) \end{pmatrix} \eta_j \widehat{\epsilon}_j \right) \quad (118)$$

where $\rho_1, \rho_2 > 0$, $0 < \gamma < 1$, $\eta_1, \eta_2 > 1$ and $\widehat{\epsilon}_j$ is an adaptive estimate of ϵ_j $(j = 1, 2)$.

Define the estimation error as $\tilde{\epsilon}_j := \epsilon_j - \widehat{\epsilon}_j$ and the adaptive law for $\widehat{\epsilon}_j$ as follows.

$$\dot{\widehat{\epsilon}}_j = \eta_j \left(\sum_{i=1}^{2} \left|c_{ij}\right| |s_i| \right), \quad \widehat{\epsilon}_j(0) > 0, \quad j = 1, 2 \quad (119)$$

Under these conditions $\dot{\theta}$ and $\dot{\phi}$, which are the LOS angular rates, will converge to zero in finite time.

Proof. This guidance law can be studied in three steps. These steps are given below.

- *Step 1:* The switching variables given in (107) and estimation errors $\tilde{\epsilon}_j$ are bounded.
- *Step 2:* The switching variables given in (107) converge to zero in finite time.
- *Step 3:* The states x_2 and x_4 given in (105) and (106) converge to zero in finite time.

In the light of the above, each step will be evaluated individually.

Step 1: Choose the Lyapunov function candidate as below:

$$V_1 = \frac{1}{2} s^T s + \frac{1}{2} \sum_{j=1}^{2} \tilde{\epsilon}_j^2 \quad (120)$$

The first time derivative of the Lyapunov function V_1 is obtained as obtained as follows:

$$\dot{V}_1 = s^T \dot{s} + \sum_{j=1}^{2} \tilde{\epsilon}_j \dot{\tilde{\epsilon}}_j \tag{121}$$

Equation (121) along the guidance system in (118) and the adaptive law in (119) is

$$\begin{aligned}
\dot{V}_1 &= s^T \dot{s} + \sum_{j=1}^{2} \tilde{\epsilon}_j \dot{\tilde{\epsilon}}_j \\
&= s^T \left(A + B \begin{pmatrix} a_{M\phi} \\ a_{M\theta} \end{pmatrix} + C \begin{pmatrix} a_{T\phi} \\ a_{T\theta} \end{pmatrix} \right) + \sum_{j=1}^{2} \tilde{\epsilon}_j \dot{\tilde{\epsilon}}_j \\
&= s^T (-\rho_1 s - \rho_2 \begin{pmatrix} |s_1|^\gamma \operatorname{sgn}(s_1) \\ |s_2|^\gamma \operatorname{sgn}(s_2) \end{pmatrix} - \sum_{j=1}^{2} \begin{pmatrix} |c_{1j}| \operatorname{sgn}(s_1) \\ |c_{2j}| \operatorname{sgn}(s_2) \end{pmatrix} \eta_j \widehat{\epsilon}_j + C \begin{pmatrix} a_{T\phi} \\ a_{T\theta} \end{pmatrix}) + \sum_{j=1}^{2} \tilde{\epsilon}_j \dot{\tilde{\epsilon}}_j \\
&= \left(-\rho_1 s^T s - \rho_2 \sum_{i=1}^{2} |s_i|^{\gamma+1} - \sum_{j=1}^{2} \left(\sum_{i=1}^{2} |c_{ij}| \, |s_i| \right) \eta_j \widehat{\epsilon}_j \right) + \left(\sum_{i=1}^{2} c_{i1} s_i \right) a_{T\phi} + \left(\sum_{i=1}^{2} c_{i2} s_i \right) a_{T\theta} \\
&\quad - \sum_{j=1}^{2} \left(\sum_{i=1}^{2} |c_{ij}| \, |s_i| \right) \eta_j (\epsilon_j - \widehat{\epsilon}_j) \\
&= -\rho_1 s^T s - \rho_2 \sum_{i=1}^{2} |s_i|^{\gamma+1} + \left(\sum_{i=1}^{2} c_{i1} s_i \right) a_{T\phi} + \left(\sum_{i=1}^{2} c_{i2} s_i \right) a_{T\theta} - \sum_{j=1}^{2} \left(\sum_{i=1}^{2} |c_{ij}| \, |s_i| \right) \eta_j \epsilon_j \\
&\leqslant -\rho_1 s^T s - \rho_2 \sum_{i=1}^{2} |s_i|^{\gamma+1} + \sum_{j=1}^{2} \left(\sum_{i=1}^{2} |c_{ij}| \, |s_i| \right) \epsilon_j - \sum_{j=1}^{2} \left(\sum_{i=1}^{2} |c_{ij}| \, |s_i| \right) \eta_j \epsilon_j \\
&= -\rho_1 s^T s - \rho_2 \sum_{i=1}^{2} |s_i|^{\gamma+1} + \sum_{j=1}^{2} \left(\sum_{i=1}^{2} |c_{ij}| \, |s_i| \right) \epsilon_j (1 - \eta_j) \\
&\leqslant -\rho_1 s^T s - \rho_2 \sum_{i=1}^{2} |s_i|^{\gamma+1}
\end{aligned} \tag{122}$$

According to (122), for $V_1 > 0$, $\dot{V}_1 \leqslant 0$ is obtained and s and $\tilde{\epsilon}_j (j = 1, 2)$ are bounded. This completes the claim in the first step.

Step 2. In this step, the Lyapunov function is selected as

$$V_2 = \frac{1}{2} s^T s \tag{123}$$

The derivative of this Lyapunov function as follows:

$$\begin{aligned}
\dot{V}_2 &= s^T \dot{s} \\
&= s^T \left(A + B \begin{pmatrix} a_{M\phi} \\ a_{M\theta} \end{pmatrix} + C \begin{pmatrix} a_{T\phi} \\ a_{T\theta} \end{pmatrix} \right) \\
&= s^T \left(-\rho_1 s - \rho_2 \begin{pmatrix} |s_1|^\gamma \operatorname{sgn}(s_1) \\ |s_2|^\gamma \operatorname{sgn}(s_2) \end{pmatrix} - \sum_{j=1}^{2} \begin{pmatrix} \left|c_{1j}\right| \operatorname{sgn}(s_1) \\ \left|c_{2j}\right| \operatorname{sgn}(s_2) \end{pmatrix} \eta_j \widehat{\epsilon}_j + C \begin{pmatrix} a_{T\phi} \\ a_{T\theta} \end{pmatrix} \right) \\
&\leqslant -\rho_1 s^T s - \rho_2 \sum_{i=1}^{2} |s_i|^{\gamma+1} - \sum_{j=1}^{2} \left(\sum_{i=1}^{2} \left|c_{ij}\right| |s_i| \right) \eta_j \widehat{\epsilon}_j + \sum_{j=1}^{2} \left(\sum_{i=1}^{2} \left|c_{ij}\right| |s_i| \right) \epsilon_j \\
&= -\rho_1 s^T s - \rho_2 \sum_{i=1}^{2} |s_i|^{\gamma+1} + \sum_{j=1}^{2} \left(\sum_{i=1}^{2} \left|c_{ij}\right| |s_i| \right) (\epsilon_j - \eta_j \widehat{\epsilon}_j)
\end{aligned} \tag{124}$$

Since $\widehat{\epsilon}_j(0) > 0$ and $\dot{\widehat{\epsilon}}_j \geq 0$, we have $\widehat{\epsilon}_j(t) \geq \widehat{\epsilon}_j(0) \geq 0$. If $\widehat{\epsilon}_j(0)$ is large enough, i.e. $\widehat{\epsilon}_j(0) > |\tilde{\epsilon}_j(0)|$, η_j satisfies the following inequality as given in [166, 167].

$$\eta_j \geq 1 + \frac{\sqrt{\widehat{\epsilon}_j^2(0) + s_j^2(0)}}{\widehat{\epsilon}_j(0)}, \qquad j = 1, 2 \tag{125}$$

Accordingly, the following inequalities can be written by considering $\widehat{\epsilon}_j(t) \geq \widehat{\epsilon}_j(0) \geq 0$.

$$
\begin{aligned}
\epsilon_j(0) - \eta_j\widehat{\epsilon}_j(0) &\leq \epsilon_j(0) - \widehat{\epsilon}_j(0) - \sqrt{\widehat{\epsilon}_j^2(0) + s_j^2(0)} \\
&\leq \tilde{\epsilon}_j(0) - \sqrt{\widehat{\epsilon}_j^2(0) + s_j^2(0)} \\
&\leq \left|\tilde{\epsilon}_j(0)\right| - \sqrt{\widehat{\epsilon}_j^2(0) + s_j^2(0)} \\
&\leq \sqrt{\tilde{\epsilon}_j^2(0)} - \sqrt{\widehat{\epsilon}_j^2(0) + s_j^2(0)} \\
&\leq \sqrt{\widehat{\epsilon}_j^2(0)} - \sqrt{\widehat{\epsilon}_j^2(0) + s_j^2(0)} \\
&\leq 0
\end{aligned}
\tag{126}
$$

Equation (124) can be obtained by using (126).

$$
\dot{V}_2 \leq -\rho_1 s^T s - \rho_2 \sum_{i=1}^{2} |s_i|^{\gamma+1} \tag{127}
$$

Based on Lemma 2, $\left(s_1^2 + s_2^2\right)^q \leq \left(s_1^q + s_2^q\right)^2$ is known. By using (124) and (126), equation (127) can be written as below.

$$
\dot{V}_2 \leq -2\rho_1 V_2 - 2^{\frac{\gamma+1}{2}} \rho_2 V_2^{\frac{\gamma+1}{2}} \tag{128}
$$

According to Lemma 3, the final inequality above stipulates that the switching variables converge to zero in finite time . This completes the claim in the second step.

Step 3: Finally, the states x_2 and x_4 given in (105) and (106) are given. It is clearly known that $[s_1;\ s_2] = [0;\ 0]$ and $[\dot{s}_1;\ \dot{s}_2] = [0;\ 0]$ on the sliding surface. In (109), if $\dot{x}_2$ and $\dot{x}_4$ are separated, the following equations are obtained.

$$\dot{x}_2 = -(a_1 \text{sgn}(x_1) |x_1|^{\alpha_1} + b_1 \text{sgn}(x_2) |x_2|^{\alpha_2}) \tag{129}$$

$$\dot{x}_4 = -(a_1 \text{sgn}(x_3) |x_3|^{\beta_1} + b_1 \text{sgn}(x_4) |x_4|^{\beta_2}) \tag{130}$$

According to the information given in Lemma 4, in the closed loop, the states x_2 and x_4 converge to zero in finite time, that is, the LOS angular rates $\dot{\theta}$ and $\dot{\phi}$ will converge to zero in finite time as a result of the chosen guidance strategy. □

5.2. Composite Guidance Law Design

This section will show how the composite guidance law can be designed with AISM guidance law and NDOB method as a novel guidance system. The use of the theory of NDOB for the design of the guidance law will be included in the first subsection. The next other subsection will show how NDOB and AISM control strategy can be used when designing a composite guidance law for guidance strategy had less miss distance and shorter stopping time.

5.2.1. Design of Nonlinear Disturbance Observer

The guidance system in (85) - (86) can be rewritten as follows.

$$\dot{x}_2 = A_1 + B_1 \left(a_{M\phi} - a_{T\phi}\right) \tag{131}$$

$$\dot{x}_4 = A_2 + B_2 \left(a_{M\theta} - a_{T\theta}\right) \tag{132}$$

where

$$A = \begin{pmatrix} A_1 \\ A_2 \end{pmatrix} = \begin{pmatrix} -\frac{2\dot{R}}{R}x_2 - x_4^2 \sin x_1 \cos x_1 \\ \\ -\frac{2\dot{R}}{R}x_4 + 2x_4 x_2 \tan x_1 \end{pmatrix}$$

$$B = \begin{pmatrix} B_1 \\ B_2 \end{pmatrix} = \begin{pmatrix} -\frac{1}{R} \\ \\ \frac{1}{R\cos x_1} \end{pmatrix}.$$

Theorem 5.3. [164] Let Assumption 2 holds true and let the NDOB dynamics is given by the following equations. The predicted target accelerations asymptotically converge to the target accelerations if $z_1(0) = x_2(0)$ and $z_2(0) = x_4(0)$ hold true.

$$\begin{aligned} \dot{z}_1 &= A_1 + B_1 \left(a_{M\phi} - \widehat{a}_{T\phi}\right) \\ \widehat{a}_{T\phi} &= \omega_1 \left(x_2 - z_1\right) \end{aligned} \tag{133}$$

$$\begin{aligned} \dot{z}_2 &= A_2 + B_2 \left(a_{M\theta} - \widehat{a}_{T\theta}\right) \\ \widehat{a}_{T\theta} &= \omega_2 \left(x_4 - z_2\right) \end{aligned} \tag{134}$$

where $\omega_1 > 0$ and $\omega_2 < 0$.

Proof. Let $e_{T\phi}$ and $e_{T\theta}$ be the disturbance prediction errors and are expressed as below.

$$e_{T\phi} := a_{T\phi} - \widehat{a}_{T\phi} \tag{135}$$

$$e_{T\theta} := a_{T\theta} - \widehat{a}_{T\theta} \tag{136}$$

Then, their derivatives are obtained as follows.

$$\dot{e}_{T\phi} := \dot{a}_{T\phi} - \dot{\widehat{a}}_{T\phi} \tag{137}$$

$$\dot{e}_{T\theta} := \dot{a}_{T\theta} - \dot{\widehat{a}}_{T\theta} \tag{138}$$

Derivatives of $\widehat{a}_{T\phi}$ and $\widehat{a}_{T\theta}$ variables given in (133) and (134) are taken. Then, these substitute into (137) and (138).

$$\begin{aligned} \dot{e}_{T\phi} &= \dot{a}_{T\phi} - \dot{\widehat{a}}_{T\phi} \\ &= \dot{a}_{T\phi} - \omega_1 \left(\dot{x}_2 - \dot{z}_1 \right) \end{aligned} \tag{139}$$

$$\begin{aligned} \dot{e}_{T\theta} &= \dot{a}_{T\theta} - \dot{\widehat{a}}_{T\theta} \\ &= \dot{a}_{T\theta} - \omega_2 \left(\dot{x}_4 - \dot{z}_2 \right) \end{aligned} \tag{140}$$

Substituting (131) and (132) into (139) and (140)

$$\begin{aligned} \dot{e}_{T\phi} &= \dot{a}_{T\phi} - \omega_1 \left(\dot{x}_2 - \dot{z}_1 \right) \\ &= \dot{a}_{T\phi} - \omega_1 \left(A_1 + B_1 (a_{M\phi} - a_{T\phi}) - \dot{z}_1 \right) \end{aligned} \tag{141}$$

$$\begin{aligned} \dot{e}_{T\theta} &= \dot{a}_{T\theta} - \omega_2 \left(\dot{x}_4 - \dot{z}_2 \right) \\ &= \dot{a}_{T\theta} - \omega_2 \left(A_2 + B_2 (a_{M\theta} - a_{T\theta}) - \dot{z}_2 \right) \end{aligned} \tag{142}$$

Substituting (133) and (134) into (141) and (142), respectively yields the following two equations.

$$\begin{aligned}\dot{e}_{T\phi} &= \dot{a}_{T\phi} - \omega_1 \left(A_1 + B_1(a_{M\phi} - a_{T\phi}) - \dot{z}_1\right) \\ &= \dot{a}_{T\phi} - \omega_1((A_1 + B_1(a_{M\phi} - a_{T\phi}) - A_1 - B_1 \left(a_{M\phi} - \widehat{a}_{T\phi}\right)) \\ &= \dot{a}_{T\phi} + \omega_1 B_1 \left(a_{T\phi} - \widehat{a}_{T\phi}\right) \\ &= \dot{a}_{T\phi} + \omega_1 B_1 e_{T\phi} \end{aligned} \tag{143}$$

$$\begin{aligned}\dot{e}_{T\theta} &= \dot{a}_{T\theta} - \dot{\widehat{a}}_{T\theta} \\ &= \dot{a}_{T\theta} - \omega_2 \left(\dot{x}_4 - \dot{z}_2\right) \\ &= \dot{a}_{T\theta} - \omega_2((A_2 + B_2(a_{M\theta} - a_{T\theta}) - A_2 - B_2 \left(a_{M\theta} - \widehat{a}_{T\theta}\right)) \\ &= \dot{a}_{T\theta} + \omega_2 B_2 \left(a_{T\theta} - \widehat{a}_{T\theta}\right) \\ &= \dot{a}_{T\theta} + \omega_2 B_2 e_{T\theta} \end{aligned} \tag{144}$$

According to Assumption 2 and Lemma 5, $\lim_{t\to\infty} e_{T\phi} = 0$ and $\lim_{t\to\infty} e_{T\theta} = 0$ are obtained. Thus, the predicted target accelerations,$\widehat{a}_{T\theta}$ and $\widehat{a}_{T\phi}$, will converge to the actual target accelerations asymptotically. □

5.2.2. Composite Guidance Law Based on Nonlinear Disturbance Observer

Composite guidance law consists of the AISM guidance law in (118) and the NDOB technique in (133) and (134). The theorem of the composite guidance law and its proof will be given in detail in this subsection.

Theorem 5.4. Let the chosen guidance system is given by (105)-(106) and let Assumption 3 holds true. If the switching gains satisfy $\eta_i > \Delta_i$, $i = 1, 2$, $\dot{\theta}$ and $\dot{\phi}$, which are the LOS angular rates, converge to zero in finite time.

The proposed composite guidance law is indicated as below.

$$\begin{pmatrix} a_{M\phi} \\ a_{M\theta} \end{pmatrix} = B^{-1}\Bigg(-A - \rho_1 s - \rho_2 \begin{pmatrix} |s_1|^{\gamma}\operatorname{sgn}(s_1) \\ |s_2|^{\gamma}\operatorname{sgn}(s_2) \end{pmatrix} - \sum_{j=1}^{2}\begin{pmatrix} \left|c_{1j}\right|\operatorname{sgn}(s_1) \\ \left|c_{2j}\right|\operatorname{sgn}(s_2) \end{pmatrix}\eta_j\widehat{\epsilon}_j\Bigg) + \begin{pmatrix} \hat{a}_{T\phi} \\ \hat{a}_{T\theta} \end{pmatrix}. \quad (145)$$

Proof. The stability proof is given here similar to those of Theorem 5.2. Firstly, choose the Lyapunov function candidate as $V_3 = \frac{1}{2}s^T s + \frac{1}{2}\sum_{j=1}^{2}\tilde{\epsilon}_j^2$.

Substituting (105)-(106) and (145) into (108) yields the following time derivative of the Lyapunov function.

$$\begin{aligned}
\dot{V}_3 &= s^T\dot{s} + \sum_{j=1}^{2}\tilde{\epsilon}_j\dot{\tilde{\epsilon}}_j \\
&= \left(-\rho_1 s^T s - \rho_2\sum_{i=1}^{2}|s_i|^{\gamma+1} - \sum_{j=1}^{2}\left(\sum_{i=1}^{2}\left|c_{ij}\right||s_i|\right)\eta_j\widehat{\epsilon}_j\right) \\
&+ \left(\sum_{i=1}^{2}c_{i1}s_i\right)a_{T\phi} + \left(\sum_{i=1}^{2}c_{i2}s_i\right)a_{T\theta} - \left(\sum_{i=1}^{2}c_{i1}s_i\right)\widehat{a}_{T\phi} \\
&- \left(\sum_{i=1}^{2}c_{i2}s_i\right)\widehat{a}_{T\theta} - \sum_{j=1}^{2}\left(\sum_{i=1}^{2}\left|c_{ij}\right||s_i|\right)\eta_j(\epsilon_j - \widehat{\epsilon}_j) \\
&= \left(-\rho_1 s^T s - \rho_2\sum_{i=1}^{2}|s_i|^{\gamma+1} - \sum_{j=1}^{2}\left(\sum_{i=1}^{2}\left|c_{ij}\right||s_i|\right)\eta_j\epsilon_j\right) + \sum_{j=1}^{2}\left(\sum_{i=1}^{2}\left|c_{ij}\right||s_i|\right)\begin{pmatrix} a_{T\phi} - \widehat{a}_{T\phi} \\ a_{T\theta} - \widehat{a}_{T\theta} \end{pmatrix} \\
&\leqslant -\rho_1 s^T s - \rho_2\sum_{i=1}^{2}|s_i|^{\gamma+1} - \sum_{j=1}^{2}\left(\sum_{i=1}^{2}\left|c_{ij}\right||s_i|\right)\eta_j\epsilon_j + \sum_{j=1}^{2}\left(\sum_{i=1}^{2}\left|c_{ij}\right||s_i|\right)\Delta \\
&\leqslant -\rho_1 s^T s - \rho_2\sum_{i=1}^{2}|s_i|^{\gamma+1} - \sum_{j=1}^{2}\left(\sum_{i=1}^{2}\left|c_{ij}\right||s_i|\right)\left(\eta_j\epsilon_j - \Delta\right) \\
&\leqslant 0
\end{aligned} \quad (146)$$

It can be seen that $\dot{V}_3 \leqslant 0$. Thus, $V_3(t) \leqslant V_3(0)$ and $V_3(t)$ is bounded. Therefore, s and $\tilde{\epsilon}_j (j = 1, 2)$ are bounded.

At this stage, we will choose a new Lyapunov function to show that the sliding variables converge to zero in finite time and this function is $V_4 = \frac{1}{2} s^T s$.

The derivative of this Lyapunov function is satisfied as follows.

$$
\begin{aligned}
\dot{V}_4 &= s^T \dot{s} \\
&= \left(-\rho_1 s^T s - \rho_2 \sum_{i=1}^{2} |s_i|^{\gamma+1} - \sum_{j=1}^{2} \left(\sum_{i=1}^{2} \left| c_{ij} \right| |s_i| \right) \eta_j \widehat{\epsilon}_j \right) \\
&+ \left(\sum_{i=1}^{2} c_{i1} s_i \right) a_{T\phi} + \left(\sum_{i=1}^{2} c_{i2} s_i \right) a_{T\theta} - \left(\sum_{i=1}^{2} c_{i1} s_i \right) \widehat{a}_{T\phi} - \left(\sum_{i=1}^{2} c_{i2} s_i \right) \widehat{a}_{T\theta} \\
&= \left(-\rho_1 s^T s - \rho_2 \sum_{i=1}^{2} |s_i|^{\gamma+1} - \sum_{j=1}^{2} \left(\sum_{i=1}^{2} \left| c_{ij} \right| |s_i| \right) \eta_j \widehat{\epsilon}_j \right) + \sum_{j=1}^{2} \left(\sum_{i=1}^{2} \left| c_{ij} \right| |s_i| \right) \begin{pmatrix} a_{T\phi} - \widehat{a}_{T\phi} \\ a_{T\theta} - \widehat{a}_{T\theta} \end{pmatrix} \\
&\leqslant -\rho_1 s^T s - \rho_2 \sum_{i=1}^{2} |s_i|^{\gamma+1} - \sum_{j=1}^{2} \left(\sum_{i=1}^{2} \left| c_{ij} \right| |s_i| \right) \eta_j \widehat{\epsilon}_j + \sum_{j=1}^{2} \left(\sum_{i=1}^{2} \left| c_{ij} \right| |s_i| \right) \Delta \\
&\leqslant -\rho_1 s^T s - \rho_2 \sum_{i=1}^{2} |s_i|^{\gamma+1} - \sum_{j=1}^{2} \left(\sum_{i=1}^{2} \left| c_{ij} \right| |s_i| \right) \left(\eta_j \widehat{\epsilon}_j - \Delta \right)
\end{aligned}
\tag{147}
$$

where $\eta_i > \Delta_i$, it can be obtained that

$$
\dot{V}_4 \leqslant -\rho_1 s^T s - \rho_2 \sum_{i=1}^{2} |s_i|^{\gamma+1} \tag{148}
$$

Based on Lemma 2, we can be rewritten as

$$
\dot{V}_4 \leqslant -2\rho_1 V_4 - 2^{\frac{\gamma+1}{2}} \rho_2 V_4^{\frac{\gamma+1}{2}} \tag{149}
$$

According to Lemma 3, the sliding variables converges to zero in finite time. Since the remaining steps of the proof are similar to those in Theorem 5.2, they are not shown again here. Thus, in the light of all this, it is obtained that the LOS angular rates $\dot{\theta}$ and $\dot{\phi}$ converge to zero in finite time, respectively. □

In conclusion, the novel composite guidance law is proposed in 3D engagement geometry. Compared to *Theorem 5.2*, *Theorem 5.4* has $\hat{a}_{T\theta}$ and $\hat{a}_{T\phi}$ obtained using the NDOB technique and these are given in the guidance system as the feed forward compensation term. This composite guidance law is proposed in order to improve performance of missile-target interception and to obtain robust results while the chattering is diminished. Besides, knowledge of the upper bound of the target acceleration uncertainties is also not necessary.

5.3. Results of the Numerical Simulations

This section demonstrates the conditions of the simulations, for instance, the missile-target inputs and considered scenario models, and the results are given in detail in the following part. Three guidance laws (a classical APN guidance law, an AISM guidance law, and the proposed robust guidance law based on the AISM guidance law and an NDOB method (AISM+NDOB)) are compared in different scenarios to demonstrate the features of the proposed method [168]. Mathematically, the classical APN guidance law is described as below.

$$a_{M\phi} = N_1 V_c \dot{\phi} + 0.5 N_2 a_{T\phi} \tag{150}$$

$$a_{M\theta} = N_1 V_c \dot{\theta} + 0.5 N_2 a_{T\theta} \tag{151}$$

where V_c is the closing velocity and N_1, N_2 are positive constants. The AISM guidance law is given in (118), [32, 68].

5.3.1. Simulation Scenarios Setting and Initial Conditions

All of the simulations were run using MathWork's Matlab and Simulink software is used the ode4 (Runge-Kutta) with fixed step size of 0.001 s in the simulation. The initial conditions of the guidance system are chosen as follows. The initial velocity of the missile is $V_{M0} = 800$ m/s and the initial position of the missile is $x_{M0} = 0$ m, $y_{M0} = 5000$ m and $z_{M0} = 0$ m. The initial velocity of the target is $V_{M0} = 400$ m/s and the initial position of the target is $x_{M0} = 1100$ m, $y_{M0} = 5000$ m and $z_{M0} = 0$ m. In addition to these, the initial flight-path angle of the missile is $\phi_{M0} = 0\,^\circ$ and the heading angle of the missile is $\theta_{M0} = 8\,^\circ$. For the target, initial flight-path angle is $\phi_{T0} = 10\,^\circ$ and the heading angle is $\theta_{T0} = 5\,^\circ$. $g = 9.8$ m/s^2 is used as the gravitational constant [164].

In order to optimize the control parameters used in the presented guidance laws and to obtain high performance, the trial and error method was used. The parameters of the AISM guidance law (118) and the proposed composite guidance law (145) are chosen as $a_1 = b_1 = 0.005$, $a_2 = b_2 = 0.02$, $\alpha_1 = \beta_1 = 0.33$, $\alpha_2 = \beta_2 = 0.5$, $\rho_1 = 0.05$, $\rho_2 = 0.01$. Moreover, the parameters of NDOB (133) and (134) are selected as $\omega_1 = 3000$ and $\omega_2 = -3000$.

The table below gives three different cases that take account of target accelerations, and these cases will be used to demonstrate the effectiveness of the presented guidance laws. Additionally, the simulations are carried out under the presence of external disturbances to assess the performance of the guidance law fairly.

Interception Scenarios	**Azimuth acceleration**	**Elevation acceleration**
non-maneuvering	0	0
constant maneuvering	$4g$	$4g$
time-varying maneuvering	$3g + \sin 2\pi t$	$3g + \sin 4\pi t$

Table 5.1 Accelerations setting of target in interception scenarios

5.3.2. Simulation Results

Case 1: Non-maneuvering target

According to the assumption in Case 1, the target has a non-maneuvering motion and the missile aims to intercept this target. For Case 1, the final miss distance and the time of interception are given in Table 5.2. The relative distance r, the response of LOS angle θ and ϕ, the response of LOS angular rates $\dot{\theta}$ and $\dot{\phi}$, phase space behavior, target acceleration estimation errors for $a_{T\phi}$ and $a_{T\theta}$, missile and target trajectories are demonstrated from Figure 5.1 to 5.6, respectively.

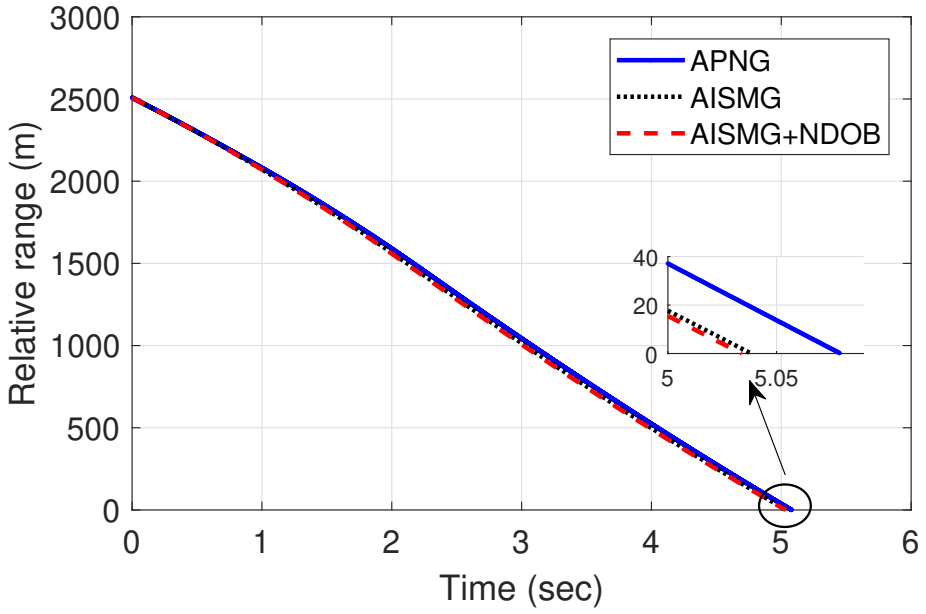

Figure 5.1 Results of Case 1: Target acceleration estimation errors

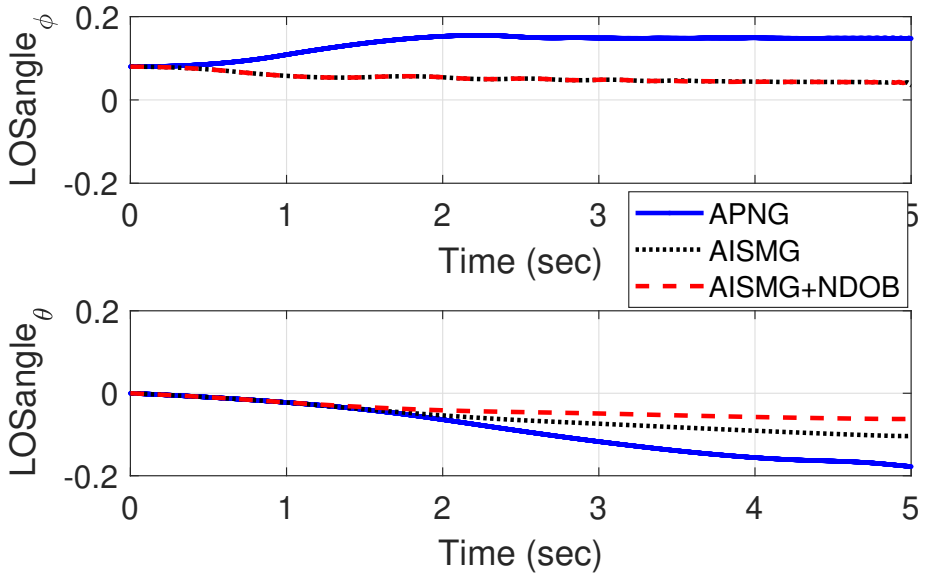

Figure 5.2 Results of Case 1: Missile and target trajectories

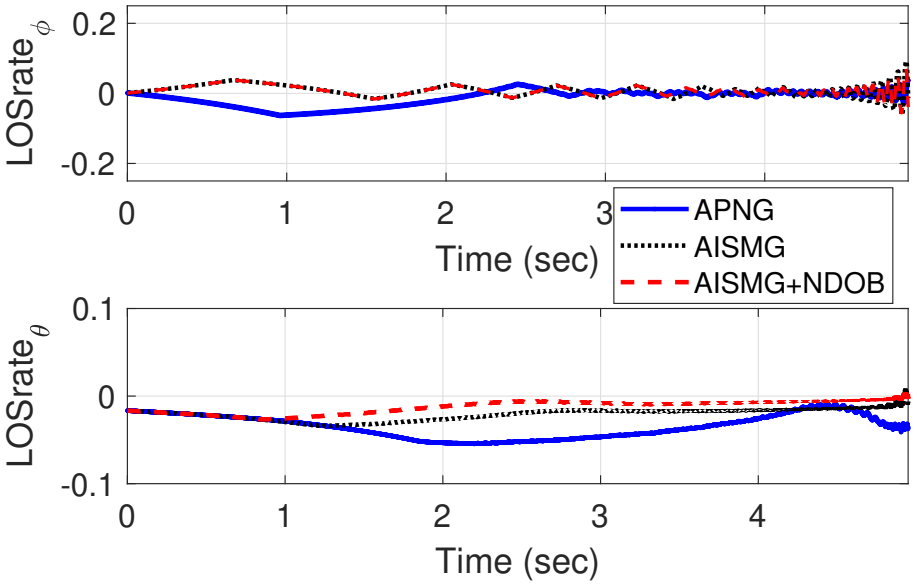

Figure 5.3 Results of Case 1: LOS angular rates

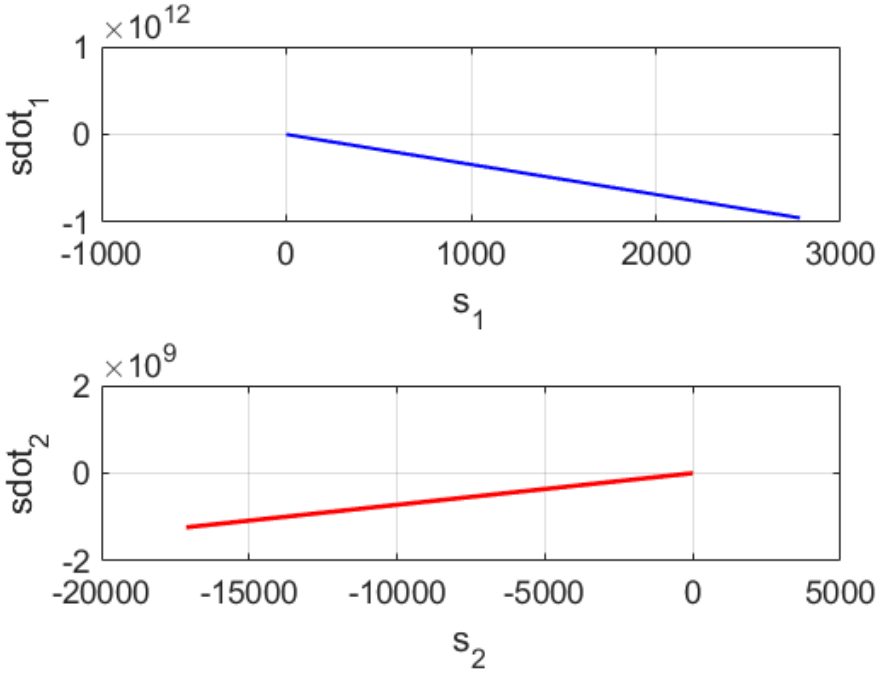

Figure 5.4 Results of Case 1: Phase space behavior

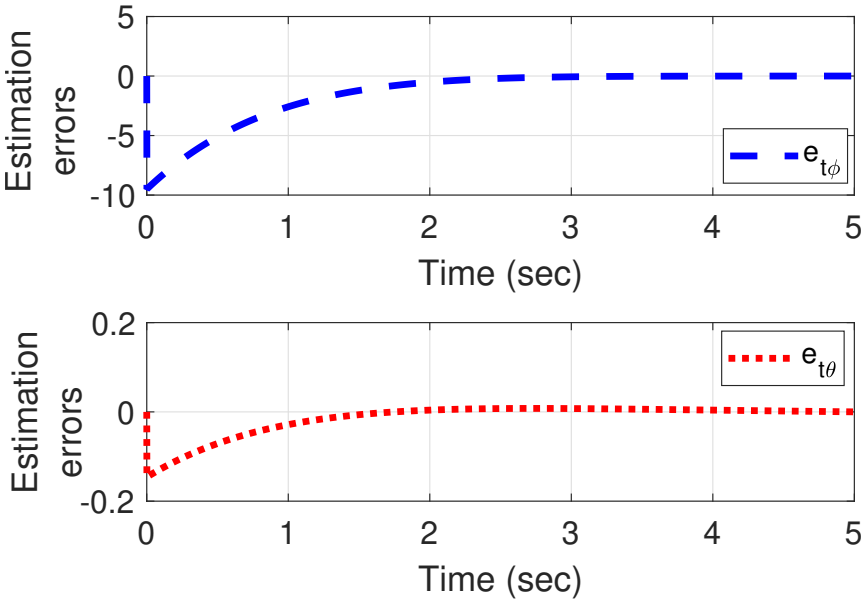

Figure 5.5 Results of Case 1: Target acceleration estimation errors

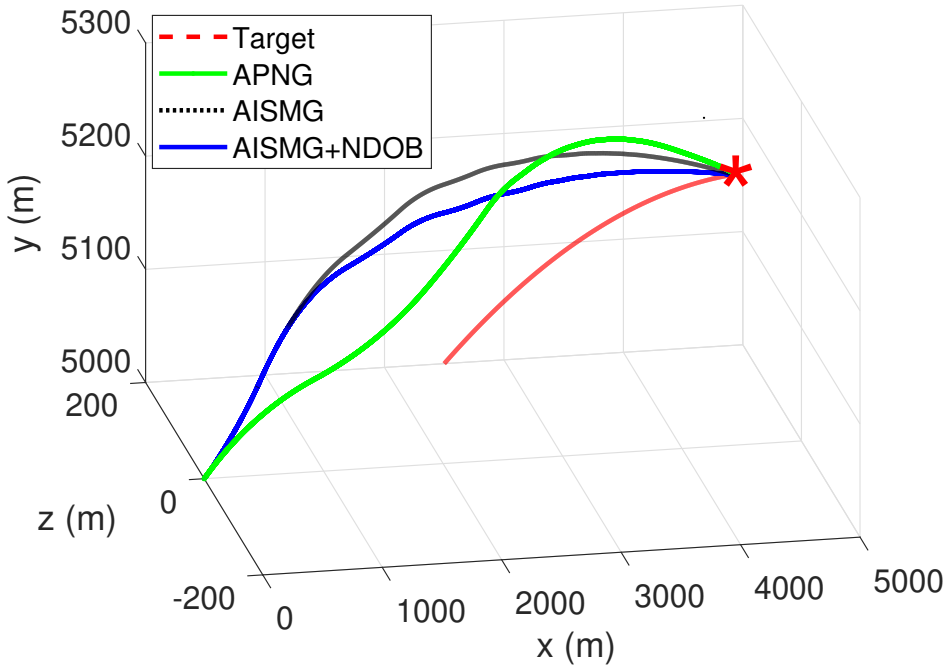

Figure 5.6 Results of Case 1: Missile and target trajectories

Case 2: Constant maneuvering target

According to the assumption in this case, the target has a constant maneuver motion and the missile aims to intercept this target. For Case 2, the final miss distance and the time of interception are presented in Table 5.2. The relative distance r, the response of LOS angle θ and ϕ, the response of LOS angular rates $\dot{\theta}$ and $\dot{\phi}$, phase space behavior, target acceleration estimation errors for $a_{T\phi}$ and $a_{T\theta}$, missile and target trajectories are showed from Figure 5.7 to 5.12, respectively.

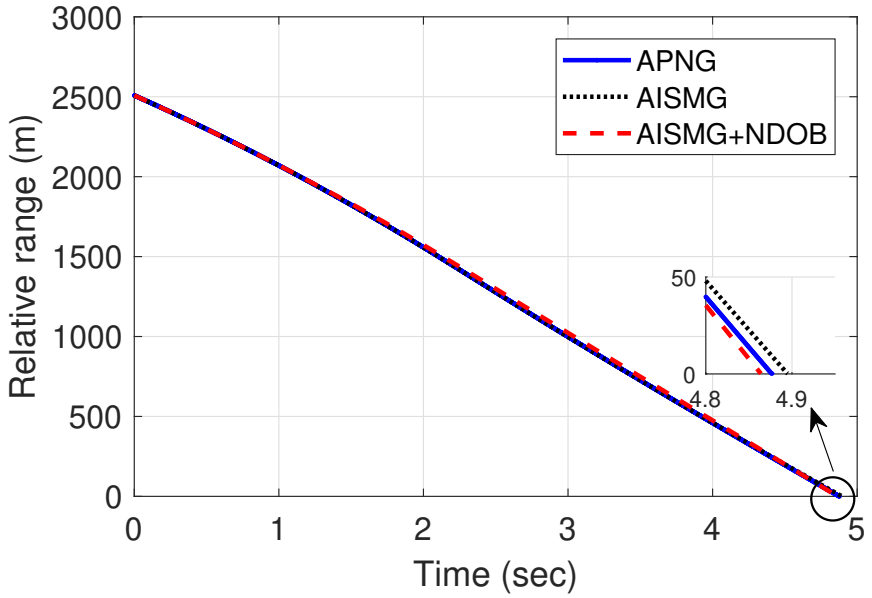

Figure 5.7 Results of Case 2: Relative range

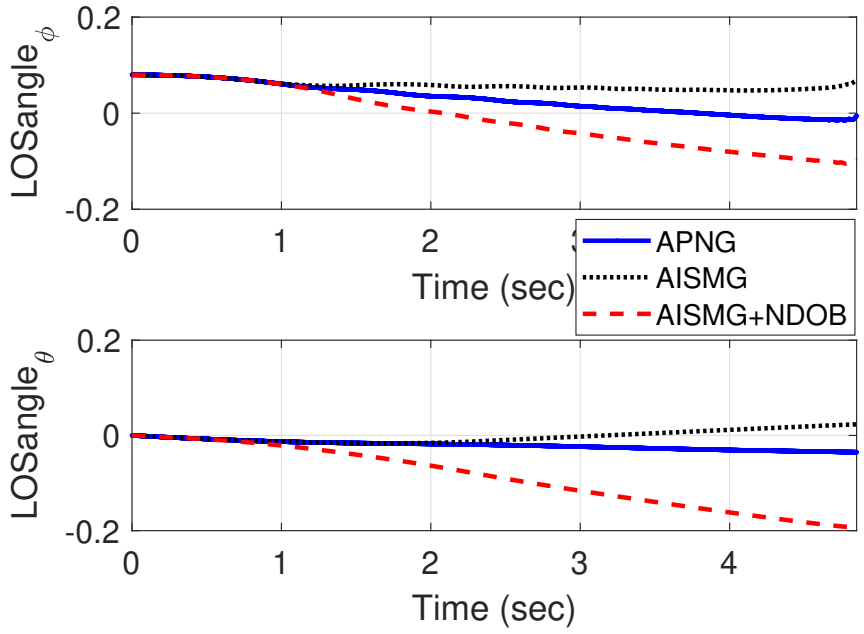

Figure 5.8 Results of Case 2: LOS angles

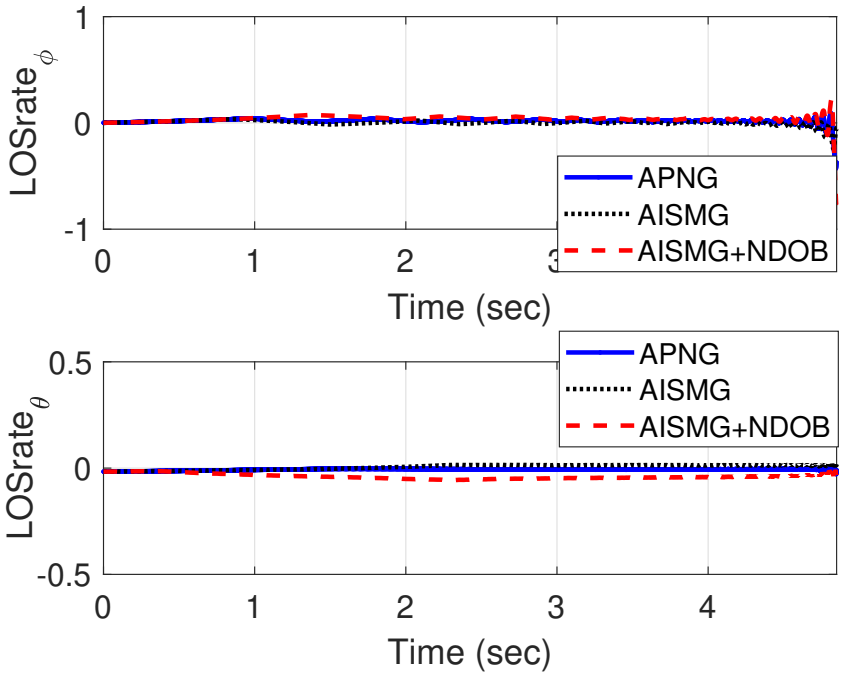

Figure 5.9 Results of Case 2: LOS angular rates

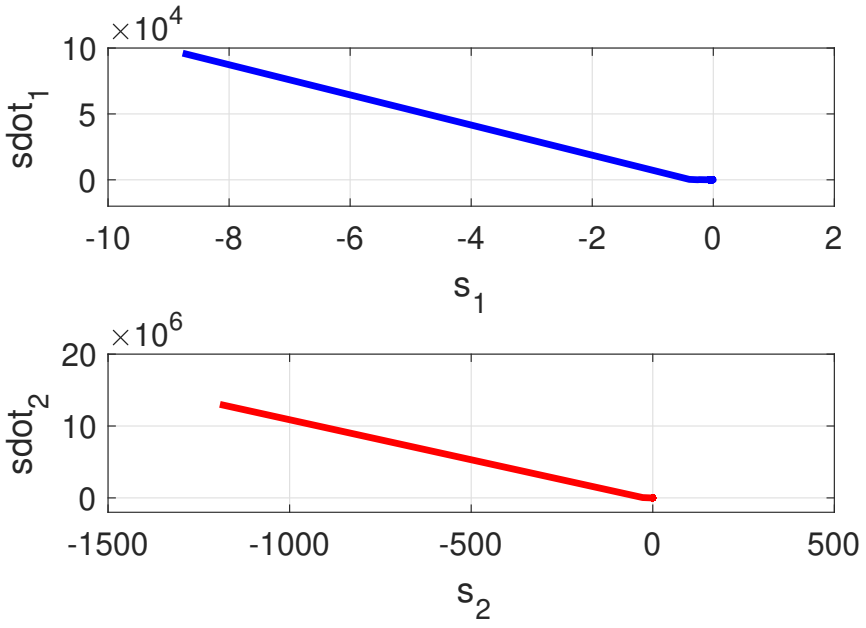

Figure 5.10 Results of Case 2: Phase space behavior

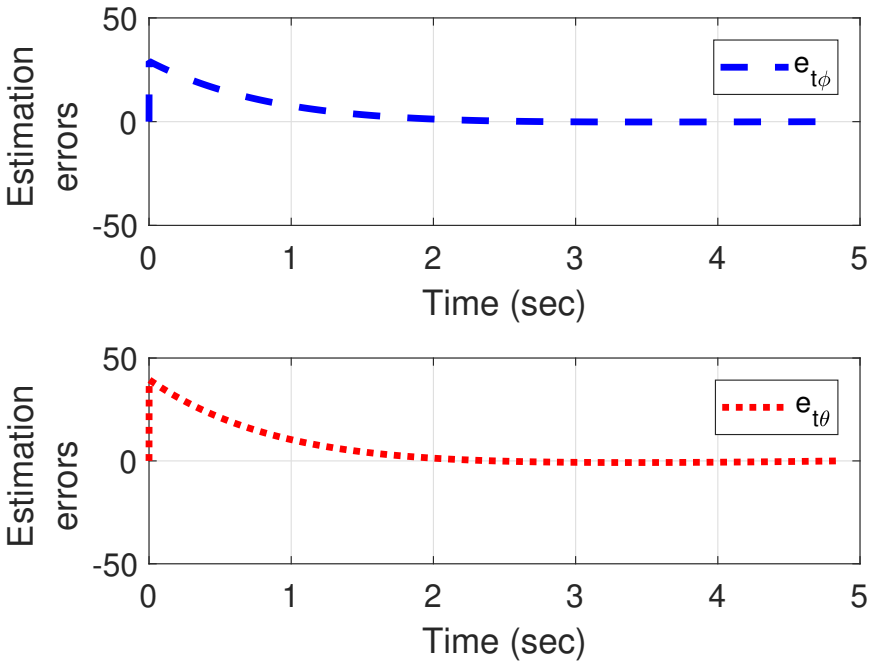

Figure 5.11 Results of Case 2: Target acceleration estimation errors

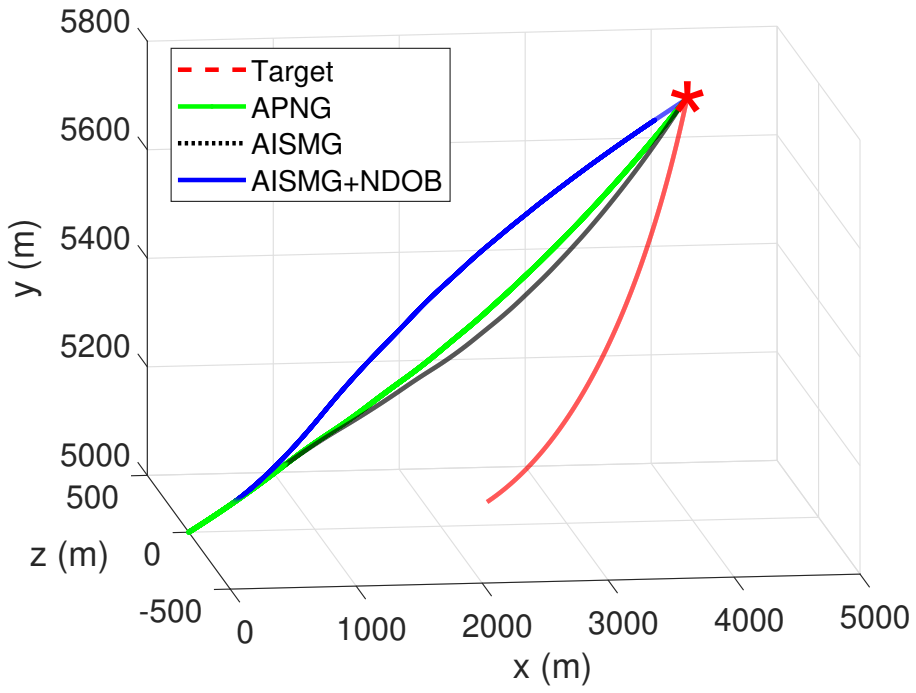

Figure 5.12 Results of Case 2: Missile and target trajectories

Case 3: Time-varying maneuvering target

According to the assumption in Case 3, the target has a time-varying maneuvering movement, which is different from the second case, in which the missile intercepts this target. For Case 3, the final miss distance and the time of interception are given in Table 5.2. The relative distance r, the response of LOS angle θ and ϕ, the response of LOS angular rates $\dot{\theta}$ and $\dot{\phi}$, phase space behavior, target acceleration estimation errors for $a_{T\phi}$ and $a_{T\theta}$, missile and target trajectories are demonstrated in from Figure 5.13 to Figure 5.18, respectively.

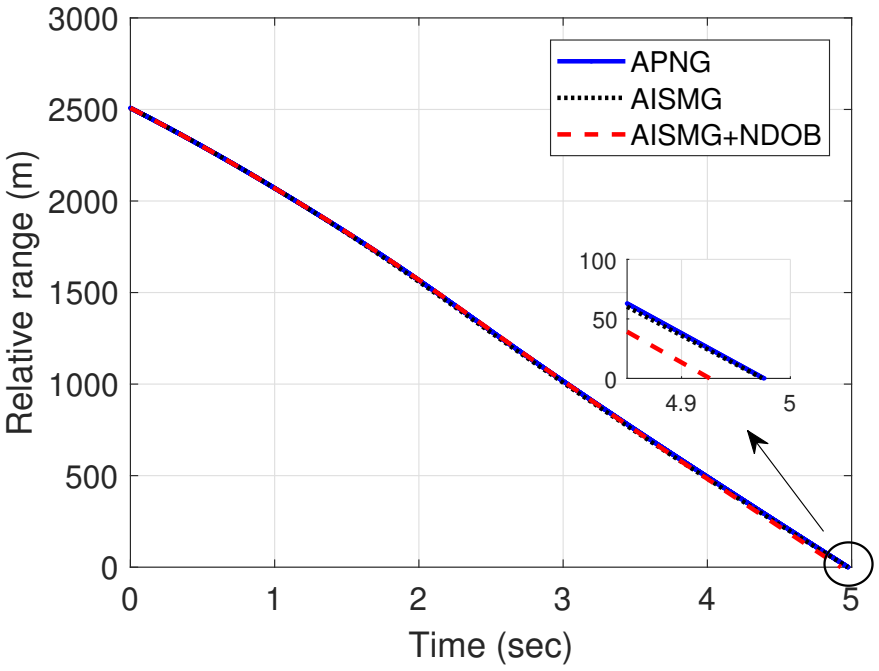

Figure 5.13 Results of Case 3: Relative range

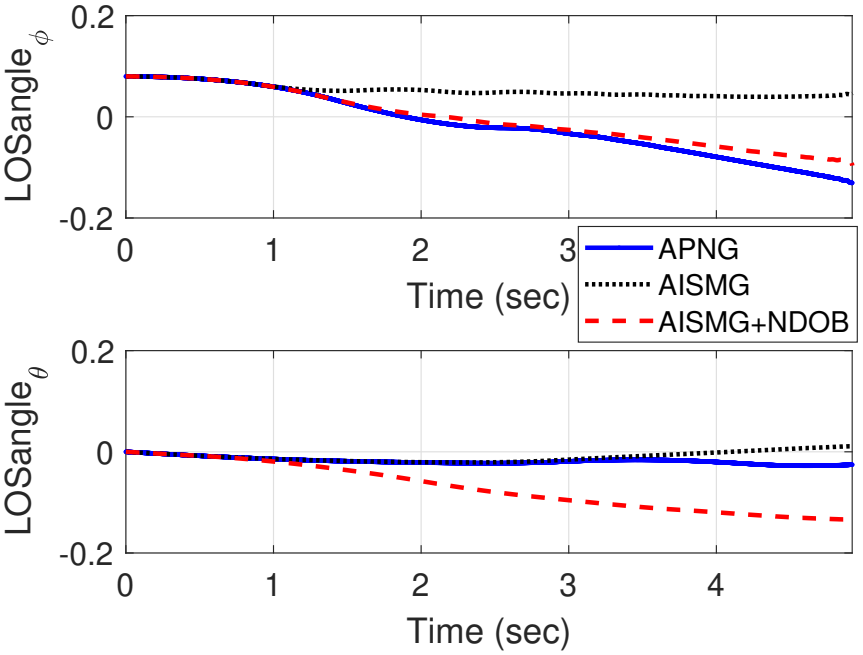

Figure 5.14 Results of Case 3: LOS angles

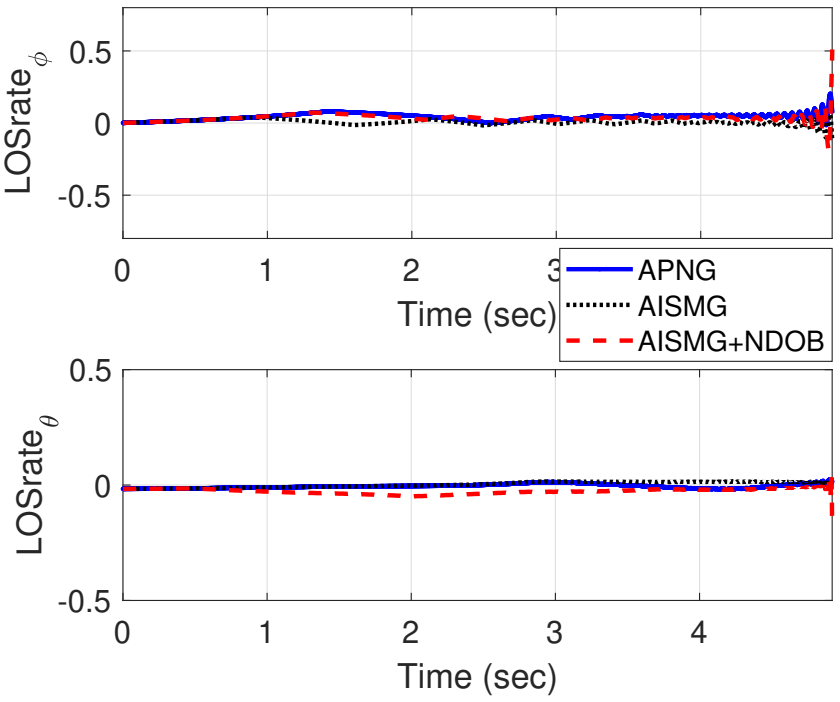

Figure 5.15 Results of Case 3: LOS angular rates

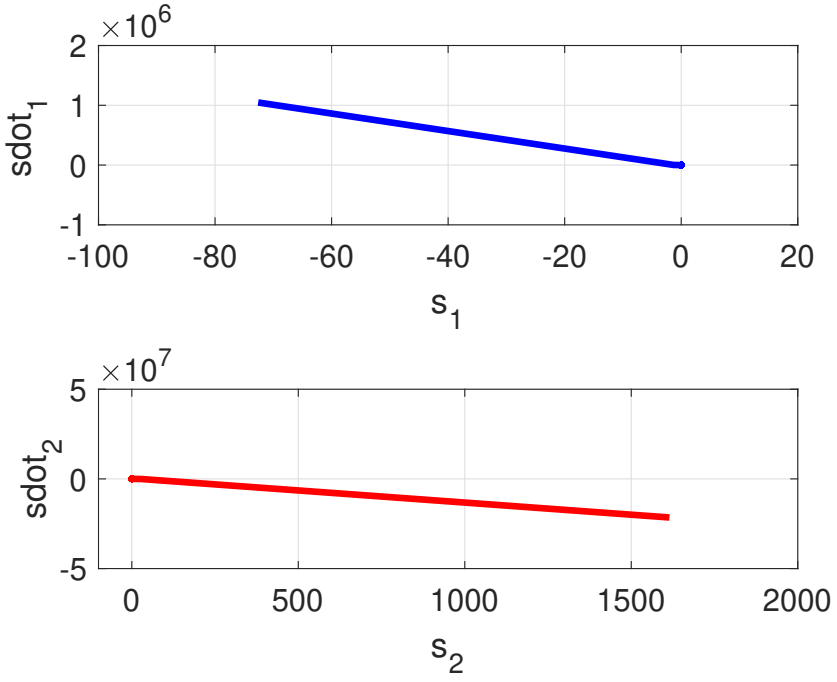

Figure 5.16 Results of Case 3: Phase space behavior

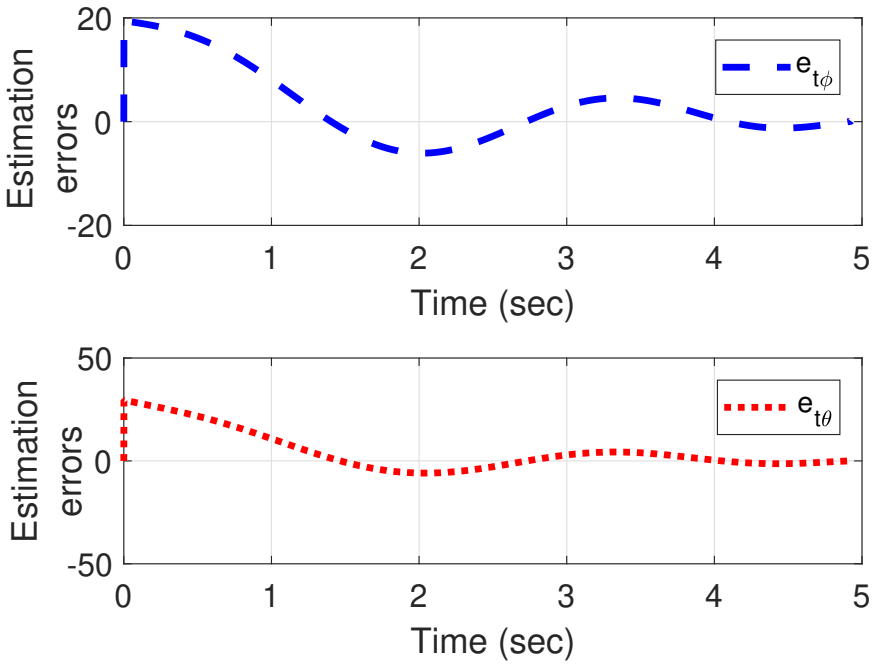

Figure 5.17 Results of Case 3: Target acceleration estimation errors

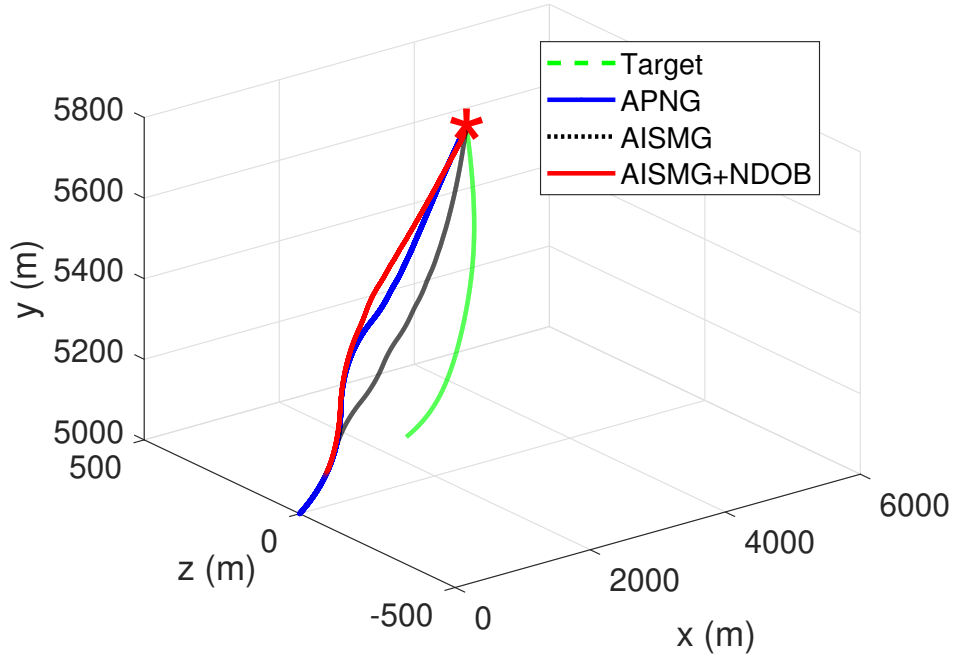

Figure 5.18 Results of Case 3: Missile and target trajectories

It can be seen in Figure 5.1, Figure 5.7 and Figure 5.13 that the relative range decreases to zero at intercept time in all of the guidance laws for each case. It can be understood from here that these guidance laws can guarantee to intercept the target successfully. However, the APN guidance law and the AISM guidance law approach zero over a longer period of time than the NDOB-based AISM guidance law, resulting in additional cost in terms of convergence time. Figure 5.2, Figure 5.8 and Figure 5.14 show the response of the LOS angles. Figure 5.3, Figure 5.9 and Figure 5.15 show the response of LOS angular rates. It has also been reported that the LOS angular rates come close to zero for all of the guidance laws in cases where the missile is intercepting the target that has a non-maneuvering movement. Figure 5.4, Figure 5.10 and Figure 5.16 illustrate the controlled phase space behavior of the switching manifold defined by the elevation angle and the azimuth angle for the proposed guidance law. Figure 5.5, Figure 5.11 and Figure 5.17 demonstrate the disturbance estimation errors obtained using the NDOB technique. The estimated accelerations by the NDOB converge to the real target's accelerations and so the estimation errors finally reach zero. As are demonstrated in Figure 5.6, Figure 5.12 and Figure 5.18, the presented all guidance laws can intercept the target successfully. Also, with the proposed guidance law, it can be seen that the missile has shorter trajectories.

The miss distances and the time of flight for all the presented cases are provided in Table 5.2. As can be seen from the table, the presented guidance laws guarantee the miss distance to be below 0.25 m in the three cases considered. This means that the missile successfully intercepts the targets using the hit-to-kill strategy [118]. The results have shown that the proposed novel guidance law outperforms the classical APN guidance law and the AISM guidance law and it it has a shorter interception time and a lower miss distance compared to others. Besides, when the missile intercepts a target that has large maneuverability, the performance of the proposed guidance law is observed to be even better.

Scenario	Guidance law	Miss distance (m)	Interception time (s)
Case 1	APNGL	0.1918	5.080
	AISMGL	0.1704	5.039
	NDOB-based AISMGL	0.0114	5.035
Case 2	APNGL	0.1915	4.978
	AISMGL	0.2175	4.896
	NDOB-based AISMGL	0.0986	4.865
Case 3	APNGL	0.1487	4.977
	AISMGL	0.2116	4.975
	NDOB-based AISMGL	0.0759	4.927

Table 5.2 Miss distance and Interception time for all cases

5.4. Summary

A novel 3D composite guidance law by using the AISM control method and the NDOB technique is presented for missile guidance systems. The steps are taken to design the new guidance law will be briefly summarized below in order.

- At the outset, an ISM guidance law is presented to eliminate the reaching phase of the traditional SMC method.
- Then, the AISM guidance law is presented for the case in which the target acceleration profile's upper bound is unavailable. The results have shown that the reaching phase is eliminated and a robust guidance law is obtained without the need for an upper bound on the target accelerations. Moreover, since the case in which the target acceleration profile's upper bound is unavailable, compared with the APN guidance law and the AISM guidance approaches, it is clear that the developed method is a more applicable method.

- The NDOB technique has been utilized to generate an estimate by considering the target accelerations as disturbances. The estimated accelerations of the target are provided to the system as a compensation term.
- Thus, the chattering phenomenon that is one of the disadvantages of SMC is eliminated by using the proposed composite guidance law.
- Additionally, it is analytically demonstrated in our study that the LOS angular rates converge to zero in finite time, as expected from a guidance law.

The numerical simulation results presented above demonstrate that with the NDOB method and the AISM guidance law, the new composite guidance law can be a viable solution to design. Moreover, these simulations of the missile guidance system proved the effectiveness and feasibility of the proposed guidance law compared to its alternatives.

6. ADAPTIVE HIGH-ORDER SLIDING MODE GUIDANCE LAW WITH FUZZY LOGIC SYSTEM

The design of a 3D missile guidance law based on a SOSMC technique using an adaptive tuning law and a fuzzy gain planning is described and discussed in this section. This proposed law is referred to as the adaptive fuzzy super-twisting sliding mode (AFSTWSM) guidance law throughout the section.

Before describing the guidance law design, the mathematical preliminaries are given as the first step in subsection 6.1.1.. The AFSTWSM guidance law consist of the STWSM guidance law, an adaptive law and a fuzzy module. The motivation for the use of these three methods is explained in detail in 6.1.2., 6.1.3., 6.2., together with their applications, taking into account the guidance system. Finally, in section 6.3., simulation scenarios that take into account the target movements are designed and the efficiency and importance of the proposed guidance law are presented in comparison with the other three methods, the traditional SM guidance law, the traditional STWSM guidance law and the ASTWSM guidance law.

6.1. Design the Guidance Law

6.1.1. Mathematical Preliminaries

This subsection is devoted to introducing necessary some basic mathematical preliminaries, which will be used to design the presented guidance laws within this section.

Lemma 6. [159] Let $L_j \in \mathbb{R}$ for $j = 1, 2, ..., n$. The inequality

$$\big(|L_1| + |L_2| + \cdots + |L_n|\big)^q \leq |L_1|^q + |L_2|^q + \cdots + |L_n|^q \tag{152}$$

is satisfied for $0 < q < 1$.

Lemma 7. [169] Let V be a positive definite Lyapunov function. There exist real numbers $\tau > 0$ and $0 < \sigma < 1$, such that $\dot{V}(t) \leq -\tau V^{\sigma}(t)$. Then, V converges to zero in finite time. The settling time is given as

$$t_f \leq t_0 + \frac{2V^{1-\sigma}(t_0)}{\tau(1-\sigma)} \tag{153}$$

where t_0 stands for the initial time.

Assumption 4. It is assumed that $d(t)$ is the the total disturbance acting on the system and the $\dot{d}(t)$ is bounded, that is

$$\left|\dot{d}(t)\right| \leq \delta_f < \infty \tag{154}$$

where δ_f is the finite yet unknown bound of $d(t)$.

6.1.2. Super-Twisting Sliding Mode Guidance Law Design

Here, the STWSM control method, which is one of the high order sliding mode methods, is preferred instead of the first order SMC method as the design method of the guidance law. STWSMC, like the first order SMC method, offers the advantage of robustness [170]. Moreover, it presents an additional advantage of chattering attenuation or even sometimes removal.

For super-twisting SM guidance law, the sliding manifolds are described as follows, using the system dynamics provided by (86).

$$s_1 := x_2 + k_1 \left|x_1\right|^{\rho} \operatorname{sgn}(x_1) \tag{155}$$

$$s_2 := x_4 + k_2 \left|x_3\right|^{\rho} \operatorname{sgn}(x_3) \tag{156}$$

where k_1, k_2 are positive constants, ρ is a positive constant satisfying $0.5 < \rho < 1$, and the vector of sliding manifolds is $s := [s_1 \; s_2]^T$.

The design procedure for the overall control signal $u := [a_{M\phi}; a_{M\theta}]^T$ is carried out in two terms: the equivalent control (u_{eq}) and the super-twisting control (u_{stw}).

$$u = u_{eq} + u_{stw} \tag{157}$$

At first, the equivalent control is obtained by setting $\dot{s} = 0$ and solving for the control term. The super-twisting control term in (157) is given as in (158).

$$\begin{aligned} u_{stw} &:= -\alpha \left|s\right|^{\frac{1}{2}} \operatorname{sgn}(s) + \upsilon \\ \dot{\upsilon} &= -\frac{\beta}{2} \operatorname{sgn}(s) \end{aligned} \tag{158}$$

where $\alpha > 0$ and $\beta > 0$ are the controller gains.

6.1.3. Design of the Adaptive Super-Twisting Sliding Mode Guidance Law

This subsection proposes an ASTWSM guidance law for the system in (86). The adaptive law is used to provide approximately of the super-twisting controller's unknown control gains. Thanks to the adaptive law, the chattering phenomenon is suppressed without the need for an upper bound information of the disturbance. Moreover, the control gains of the super-twisting SMC are able to adapt to uncertainties online.

The control gains given in (158) can be calculated by using the following adaptive law.

$$\begin{aligned} \dot{\alpha} &= \begin{cases} w_1 \sqrt{\gamma_1/2} \operatorname{sgn}(|s| - \zeta) & : \alpha \geq \alpha_m \\ \eta & : \alpha < \alpha_m \end{cases} \\ \beta &= 2\,\kappa\,\alpha \end{aligned} \tag{159}$$

in which w_1, γ_1, ζ, η, κ are arbitrary positive constants and α_m is a small threshold value. Using the adaptation law given in (159), the super-twisting SMG law in (158) is enhanced.

Theorem 6.1. Consider the nonlinear system in (86) and the sliding manifolds (155)-(156). There exist a range of arbitrary positive constants w_1, γ_1, ζ, η, κ and a finite time $T_1 > 0$ such that the sliding manifolds converge to the domain $|s| \leq \zeta$ in finite time if the control law is designed with the adaptive gains given by (159).

Proof. Initially, it is assumed that $x_1 \neq 0$, $x_3 \neq 0$ and also $s_1 \neq 0$, $s_2 \neq 0$. Taking Assumption 4 into account and calculating $\dot{s}$, we have

$$\begin{aligned} \dot{s} &= -\alpha \left|s\right|^{\frac{1}{2}} \operatorname{sgn}(s) + \upsilon + d(t) \\ \dot{\upsilon} &= -\frac{\beta}{2} \operatorname{sgn}(s) \end{aligned} \tag{160}$$

in which $d(t)$ is the total disturbance of the system [73].

Before choosing the Lyapunov function, it is necessary to make some definitions to make the stability analysis. At the outset, a new state vector z is defined as follows [22].

$$z = \begin{bmatrix} z_1 & z_2 \end{bmatrix}^T = \begin{bmatrix} \left|s\right|^{\frac{1}{2}} \operatorname{sgn}(s) & \upsilon \end{bmatrix}^T \tag{161}$$

Equation (161) can be rewritten as below.

$$\begin{aligned} \dot{z}_1 &= \frac{1}{2\left|z_1\right|} \left(-\alpha z_1 + z_2 + d(t)\right) \\ \dot{z}_2 &= -\frac{\beta}{\left|z_1\right|} z_1 \end{aligned} \tag{162}$$

Using (154) and Assumption 4 as a reference, the following inequality can be written:

$$\left|d(t)\right| \leq \varsigma_0 \sqrt{\left|s\right|} \tag{163}$$

where ς_0 is a positive and unknown constant. It can now be derived that

$$\left|d(t)\right| = \varsigma(x,t) \sqrt{\left|s\right|} \operatorname{sgn}(s) = \varsigma(x,t)\, z_1 \tag{164}$$

where $\varsigma\left(x,t\right)$ is a bounded function and $0<\varsigma\left(x,t\right)\leq\varsigma_0$.

The system given in (162) is rewritten as below.

$$\begin{bmatrix}\dot{z}_1\\ \dot{z}_2\end{bmatrix}=A\begin{bmatrix}z_1\\ z_2\end{bmatrix} \tag{165}$$

where

$$A:=\frac{1}{2\left|z_1\right|}\begin{bmatrix}-\alpha+d(t) & 1\\ -\beta & 0\end{bmatrix} \tag{166}$$

According to this discussion, two cases can be observed. In the first case, $|z_1|=|s|^{\frac{1}{2}}$ and $\mathrm{sgn}(z_1)=\mathrm{sgn}(s)$. In the second case, if $z_1,z_2\to 0$, then $s,\dot{s}\to 0$ in finite time [22].

A Lyapunov function candidate V is selected as below.

$$V=V_0+\frac{1}{2\gamma_1}(\alpha-\alpha^*)^2+\frac{1}{2\gamma_2}(\beta-\beta^*)^2 \tag{167}$$

where $\gamma_1>0$ and $\gamma_2>0$. Besides, the adaptive gains are bounded and the unknown bounds of the adaptive gains are expressed as $\alpha^*>0$ and $\beta^*>0$. In (167), V_0 is described as follows.

$$V_0:=(\lambda+4\varepsilon^2)z_1^2+z_2^2-4\varepsilon z_1z_2=z^TPz \tag{168}$$

with

$$P:=\begin{bmatrix}\lambda+4\varepsilon^2 & -2\varepsilon\\ -2\varepsilon & 1\end{bmatrix}$$

in which λ is positive constant and ε is a real number.

Time derivative of the Lyapunov function in (167) is given below.

$$\dot{V}=\dot{V}_0+\frac{1}{\gamma_1}(\alpha-\alpha^*)\dot{\alpha}+\frac{1}{\gamma_2}(\beta-\beta^*)\dot{\beta} \tag{169}$$

Considering (165)-(166), we have

$$\dot{V}_0 = \dot{z}^T P z + z^T P \dot{z} \leq -\frac{1}{2\left|z_1\right|} z^T Q z \tag{170}$$

The symmetric matrix, Q, is computed as follows.

$$Q = \begin{bmatrix} Q_{11} & Q_{12} \\ Q_{21} & 4\varepsilon \end{bmatrix} \tag{171}$$

where

$$\begin{aligned} Q_{11} &= 2\lambda\alpha + 4\varepsilon(2\varepsilon\alpha - \beta) + 4\varepsilon\rho\left(x,t\right) \\ Q_{12} &= Q_{21} = \beta - 2\varepsilon\alpha - \lambda - 4\varepsilon^2 - \rho\left(x,t\right) \end{aligned}$$

We enforce $\beta = 2\varepsilon\alpha$ to guarantee the positive definiteness of the matrix Q and then Q will be positive definite with minimum eigenvalue $\lambda_{\min}(Q) \geq 2\varepsilon$ if the following condition holds true.

$$\alpha > -\frac{\varepsilon(4\delta+1)}{\lambda} + \frac{(2\delta+\lambda+4\varepsilon^2)^2}{12\varepsilon\lambda} \tag{172}$$

As a result, the following inequality is obtained:

$$\dot{V}_0 \leq -\frac{\varepsilon\lambda_{\min}^{1/2}(P)}{\lambda_{\max}(P)} V_0^{1/2} \tag{173}$$

Taking (173) into account, we can rewrite (169) and (170) as follows:

$$\begin{aligned}\dot{V} &= \dot{z}^T P z + z^T P \dot{z} + \frac{1}{\gamma_1}(\alpha - \alpha^*)\dot{\alpha} + \frac{1}{\gamma_2}(\beta - \beta^*)\dot{\beta} \\ &\leq -\frac{1}{|z_1|} z^T Q z + \frac{1}{\gamma_1}(\alpha - \alpha^*)\dot{\alpha} + \frac{1}{\gamma_2}(\beta - \beta^*)\dot{\beta} \\ &\leq -\frac{\varepsilon \lambda_{\min}^{1/2}(P)}{\lambda_{\max}(P)} V_0^{1/2} - \frac{\omega_1}{\sqrt{2\gamma_1}} |\alpha - \alpha^*| \\ &- \frac{\omega_2}{\sqrt{2\gamma_2}} |\beta - \beta^*| - |\alpha - \alpha^*| \left(\frac{1}{\gamma_1}\dot{\alpha} - \frac{\omega_1}{\sqrt{2\gamma_1}} \right) \\ &- |\beta - \beta^*| \left(\frac{1}{\gamma_2}\dot{\beta} - \frac{\omega_2}{\sqrt{2\gamma_2}} \right) \end{aligned} \tag{174}$$

Taking Lemma 6 into account, the following inequality is obtained:

$$-\frac{\varepsilon \lambda_{\min}^{1/2}(P)}{\lambda_{\max}(P)} V_0^{1/2} - \frac{\omega_1}{\sqrt{2\gamma_1}} |\alpha - \alpha^*| - \frac{\omega_2}{\sqrt{2\gamma_2}} |\beta - \beta^*| \leq -\eta_0 \sqrt{V} \tag{175}$$

where $\eta_0 = \min(\frac{\varepsilon \lambda_{\min}^{1/2}(P)}{\lambda_{\max}(P)} V_0^{1/2}, \omega_1, \omega_2)$. Then (174) can be rewritten as

$$\begin{aligned}\dot{V} \leq &- \eta_0 \sqrt{V} - |\alpha - \alpha^*| \left(\frac{1}{\gamma_1}\dot{\alpha} - \frac{\omega_1}{\sqrt{2\gamma_1}} \right) \\ &- |\beta - \beta^*| \left(\frac{1}{\gamma_2}\dot{\beta} - \frac{\omega_2}{\sqrt{2\gamma_2}} \right) \end{aligned} \tag{176}$$

Equation (176) can be written as in (177).

$$\dot{V} \leq -\eta_0 \sqrt{V} + \xi \tag{177}$$

where

$$\xi := - |\alpha - \alpha^*| \left(\frac{1}{\gamma_1}\dot{\alpha} - \frac{\omega_1}{\sqrt{2\gamma_1}} \right) - |\beta - \beta^*| \left(\frac{1}{\gamma_2}\dot{\beta} - \frac{\omega_2}{\sqrt{2\gamma_2}} \right) \tag{178}$$

To show the finite time convergence, ξ can be vanished by using the following adaptation laws for α and β.

$$\begin{aligned} \dot{\alpha} &= \omega_1 \sqrt{\frac{\gamma_1}{2}} \\ \dot{\beta} &= \omega_2 \sqrt{\frac{\gamma_2}{2}} \end{aligned} \tag{179}$$

With these selections, we have $\xi = 0$ and

$$\dot{V} \leq -\eta_0 \sqrt{V} \tag{180}$$

According to Lemma 7, there exists a finite time $T_1 > 0$, for $t \geq T_1$ and the sliding variable s enters the domain $|s| \leq \zeta$.

$$T_1 \leq T_0 + \frac{2V^{1/2}(T_0)}{\eta_0} \tag{181}$$

in which $\eta_0 = \min(r, \omega_1, \omega_2)$ and T_0 denotes the initial time.

Theorem 6.2. The switching variable s enters the domain $|s| \leq \zeta$ in finite time and it may violate this inequality for finite time intervals. However, there always exists a larger domain called W to which $|s|$ belongs.

$$W := \left\{ s, \dot{s} : |s| \leq \eta_1, |\dot{s}| \leq \eta_2, \eta_1 > \zeta \right\} \tag{182}$$

where $\eta_1 > 0$ and $\eta_2 > 0$ are some boundary parameters.

Proof. Suppose that $|s| \leq \zeta$ for α given by (108). This leads to the following:

$$\dot{\alpha} = \begin{cases} -w_1 \sqrt{\gamma/2} & : \alpha \geq \alpha_m \\ \eta & : \alpha < \alpha_m \end{cases} \tag{183}$$

If α is less than α_m, its value immediately starts to increase such that $\alpha = \alpha_m + \eta t$. When the system states satisfy $|s| \leq \zeta$, the control gains α and β will decline gradually. Afterwards,

the system states may deviate from the domain $|s| \leq \zeta$ because of the decrease of the gains α and β. In this case, α and β will gradually increase thanks to the effect of the adaptive law and the sliding variable s enters the domain, which is $|s| \leq \zeta$, in finite time [171, 172]. Accordingly, it can be assured that $|s| \leq \eta_1, \eta_1 > \zeta$, [73]. Moreover, when $|s| \leq \zeta$, the first derivative of the sliding variable value $|\dot{s}|$ satisfies the inequality given below:

$$|\dot{s}| \leq \alpha \zeta^{\frac{1}{2}} + (\varepsilon\alpha + \zeta)(T_2 - T_1) := \bar{\eta}_2 \tag{184}$$

where T_1 is the time instant when s enters the domain $|s| \leq \zeta$ and T_2 is the time instant when s leaves this domain, [73].

There is a final case $\zeta < |s| \leq \eta_1$, which needs to be studied.

$$\begin{aligned} |\dot{s}| &\leq \left(\eta_1^{\frac{1}{2}} + \varepsilon\right)\left(\alpha + \omega_1\sqrt{\frac{\eta_1\gamma_1}{2}}\right)(T_3 - T_2) + \zeta(T_3 - T_2) \\ &:= \tilde{\eta}_2 \end{aligned} \tag{185}$$

where T_2 is the time instant when s leaves the domain $|s| \leq \zeta$ and T_3 is the time instant when s enters this domain afterwards. When the conditions given in (184) and (185) are taken into consideration, the following inequality can be written.

$$|s| \leq \max(\bar{\eta}_2, \tilde{\eta}_2) := \eta_2 \tag{186}$$

Taking into account the above inequality, the switching variable s is guaranteed to stay always in a larger domain and the sliding regime is established for α and β given by (179). Hence, the stability in the super-twisting sliding mode method is proved.

6.2. Adaptive Super-Twisting Sliding Mode Guidance Law Design with Fuzzy Logic System

In this subsection, a novel guidance law is designed based on the aforementioned STWSM control, adaptive algorithm and a fuzzy gain scheduler. The STWSM control method and the adaptive algorithm are described in detail and designed in the previous section. Moreover, the parameters k_1, k_2 of the sliding manifold given in (155)-(156) are unknown constants and the fuzzy logic system is used for the selection of gains. Various uncertainty problems may arise in determining these gains manually as determining these gains is difficult and complicated and additionally the process requires experience. In Figure 6.1, the block diagram of the AFSTWSM guidance law is illustrated.

A fuzzy logic system consists of four fundamental units, namely, fuzzifier, inference engine, rule base and defuzzifier, respectively. Figure 6.2 shows a general fuzzy logic system structure and the details are given in the sequel.

- **Selection of the fuzzy logic system inputs and outputs**

  There are two independent fuzzy modules in the design of the proposed guidance law. The elevation LOS angle and its time derivative (θ, $\dot{\theta}$) are introduced as the input to the first fuzzy module and the azimuth LOS angle and its rate (ϕ, $\dot{\phi}$) are introduced as the input to the second module. The output of each fuzzy module provides control gains k_1 and k_2 given in (155) and (156), respectively.

- **Membership Functions**

  Initially, fuzzy sets for variables are defined, since operations are performed on fuzzy sets in fuzzy rule base and fuzzy inference mechanism. Here, Triangular Membership Functions (MFs), which are the well-known and widely used function, are preferred to determine fuzziness in a fuzzy set. In this system, the input variables are N, Z, P, denoting negative, zero and positive, respectively. In addition, S, M, B, which stand for small, medium and big, are used for the output variables. Moreover, The MFs in this study are demonstrated in Figure 6.3.

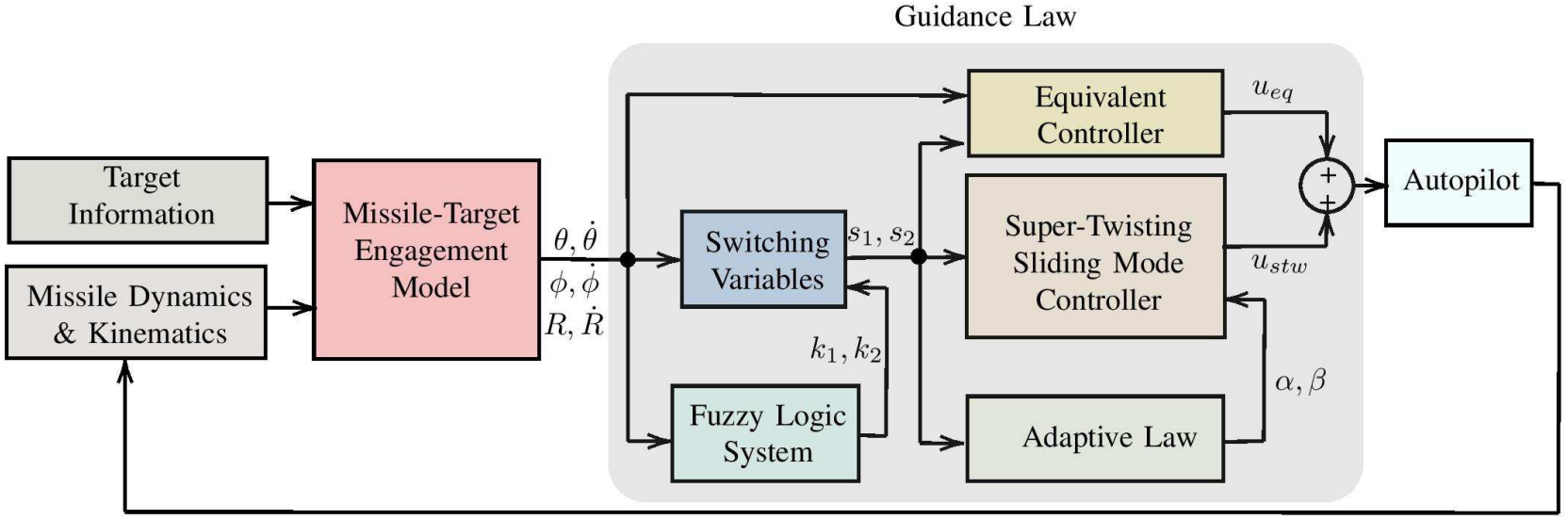

Figure 6.1 The block diagram of the ASTWSM with Fuzzy Logic System guidance law

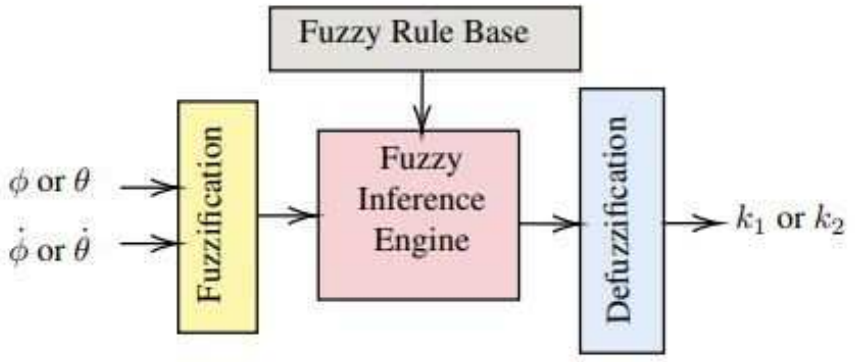

Figure 6.2 General fuzzy logic system structure with input/output quantities $(\phi, \dot{\phi}) \rightarrow k_1$ and $(\theta, \dot{\theta}) \rightarrow k_2$.

ϕ / $\dot{\phi}$	**N**	**Z**	**P**
N	S	S	M
Z	S	M	B
P	M	B	B

Table 6.1 Two Dimensional Fuzzy Rule Bases

- **Fuzzy Rule Base**

  j-th fuzzy rules for ϕ and θ subsystems are given as

  $$Rule\#j : \text{IF } \phi \text{ is } \mathrm{F}_1^{l_1} \text{ and } \dot{\phi} \text{ is } \mathrm{F}_2^{l_2} \text{ THEN } k_1 \text{ is } B^j$$

  $$Rule\#j : \text{IF } \theta \text{ is } \mathrm{F}_1^{l_1} \text{ and } \dot{\theta} \text{ is } \mathrm{F}_2^{l_2} \text{ THEN } k_2 \text{ is } B^j$$

  where $l_i = 1, 2, 3,\ i = 1, 2,\ j = 1, 2, .., 9$ and B^j is the fuzzy output of the *j*-th fuzzy rule. Table 6.1 and 6.2 present the lingustic descriptions used in the fuzzy modules.

- **Defuzzifier**

  We used centroid deffuzzifier with the output MFs shown in Figure 6.3.

θ / $\dot{\theta}$	**N**	**Z**	**P**
N	S	S	M
Z	S	M	B
P	M	B	B

Table 6.2 Two Dimensional Fuzzy Rule Bases

The fuzzy modules' main purpose is to give suitable gains, as indicated in the rule tables shown above. This avoids the use of excessively large gains in fuzzy subspaces where small values are required.

6.3. Results of the Numerical Simulations

The robust guidance law design is validated over a variety of scenarios. The conditions of the simulations, for instance, the missile, target and scenarios parameters considered, and the results are given in detail in the following parts.

6.3.1. Simulation Scenarios Setting

The initial conditions of the presented guidance system are selected as follows. The initial velocity of the missile is $V_{M0} = 800$ m/s and the initial position of the missile is $x_{M0} = 0$ m, $y_{M0} = 5000$ m, and $z_{M0} = 0$ m. The initial velocity of the target is $V_{T0} = 300$ m/s and the initial position of the target is $x_{T0} = 2500$ m, $y_{T0} = 4000$ m and $z_{T0} = 200$ m. In addition to these, the initial flight-path angle of the missile is $\phi_{M0} = 0\,^\circ$ and the heading angle of the missile is $\theta_{M0} = 8\,^\circ$. For the target, the initial flight-path angle is $\phi_{T0} = 0\,^\circ$ and the heading angle is $\theta_{T0} = 8\,^\circ$. $g = 9.81$ m/s^2 is the gravitational constant.

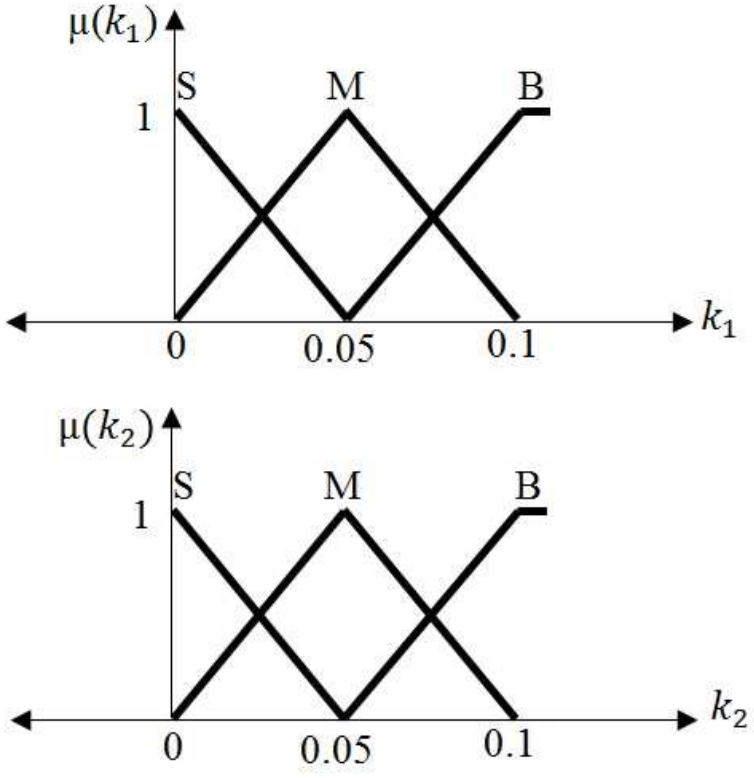

Figure 6.3 Membership function of linguistic variables for the outputs k_1, k_2

To verify the performance of the proposed guidance laws, these guidance laws are compared with the SM guidance law in [168]. Thus, the obtained results from four different guidance laws are given in this article and these are SM, STWSM, ASTWSM, and AFSTWSM guidance law.

Table 6.3 gives two different scenarios that describe target accelerations. These scenarios will be used to show the effectiveness of the presented guidance laws. Besides, the simulations are carried out in the presence of external disturbances in order to assess the performance of the guidance laws fairly.

Interception Scenarios	Azimuth acceleration	Elevation acceleration
non-maneuvering	g	0
time-varying maneuvering	$3g + \sin 2\pi t$	$3g + \sin 2\pi t$

Table 6.3 Accelerations setting of target in interception scenarios

6.3.2. Simulation Results

In this subsection, numerical simulations are studied for two different scenarios to prove the merits and effectiveness of the proposed guidance law and the results of these simulations are presented by comparing it with the aforementioned guidance laws.

Case 1: Non-maneuvering target

In Case 1, the goal of the missile is to intercept the target, which is non-maneuvering. The parameters of the sliding variables (155)-(156) are chosen as $k_1 = 0.03, k_2 = 0.0025$ for using in the STWSM guidance law. The parameters of the STWSM guidance law (158) are selected as $\alpha = 0.007$ and $\beta = 0.012$. Further to these, $\omega_1 = 2$, $\gamma = 0.02$, $\zeta = 0.06$, $\eta = 0.02$, $\kappa = 0.01$ and $\alpha_m = 0.005$ are chosen to use in the developed ASTWSM guidance law and the proposed AFSTWSM guidance law.

Scenario	Guidance law	Miss distance (m)	Interception time (s)
Case 1	SMGL	0.4043	4.501
	STWSMGL	0.4103	4.498
	ASTWSMGL	0.2471	4.499
	AFSTWSMGL	0.1551	4.498

Table 6.4 Miss distance and Interception time for Case 1

Table 6.4 tabulates the final miss distance and the time of interception for Case 1. The small miss distance and earliest interception time are the most significant criteria in the

missile-target interception system. It is noted from Table 6.4 that, according to these criteria, both ASTWSM and AFSTWSM guidance laws have the smallest miss distance compared to other guidance laws. Also, the AFSTWSM guidance law hits the target in a shorter time than the other guidance laws.

The simulation results obtained by using the proposed ASTWSM and AFSTWSM guidance laws are plotted between Figures 6.4 - 6.9. The results are presented in the figures in comparison with the classical SM and STWSM methods. The figures will be explained here in turn. It is obvious from Figure 6.4 that the relative range decreases to zero at the intercept time in all of the guidance laws. Thus, the missile with these guidance laws successfully hits the target in this case. Figure 6.5 demonstrates the response of the LOS angles. Figures 6.6 and 6.7 show the controlled phase space behavior of the switching manifold defined for the elevation angle and the azimuth angle, respectively. From Figures 6.8 and6.9, the missile's and target's trajectories guided by guidance law is given from different angles. Also, as it can be clearly seen from these figures, the missile hits the target accurately according to all guidance laws.

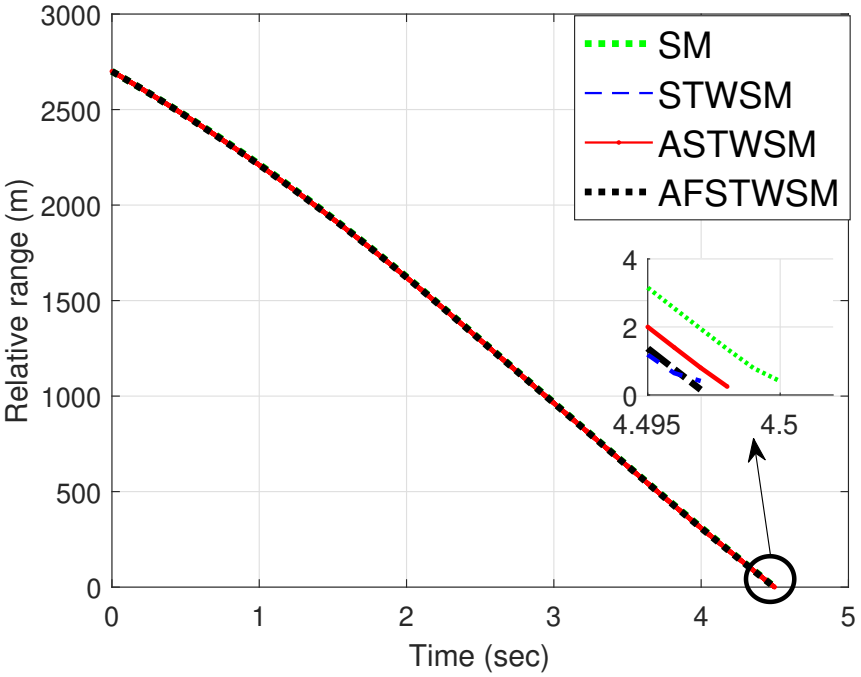

Figure 6.4 Results of Case 1: Relative range

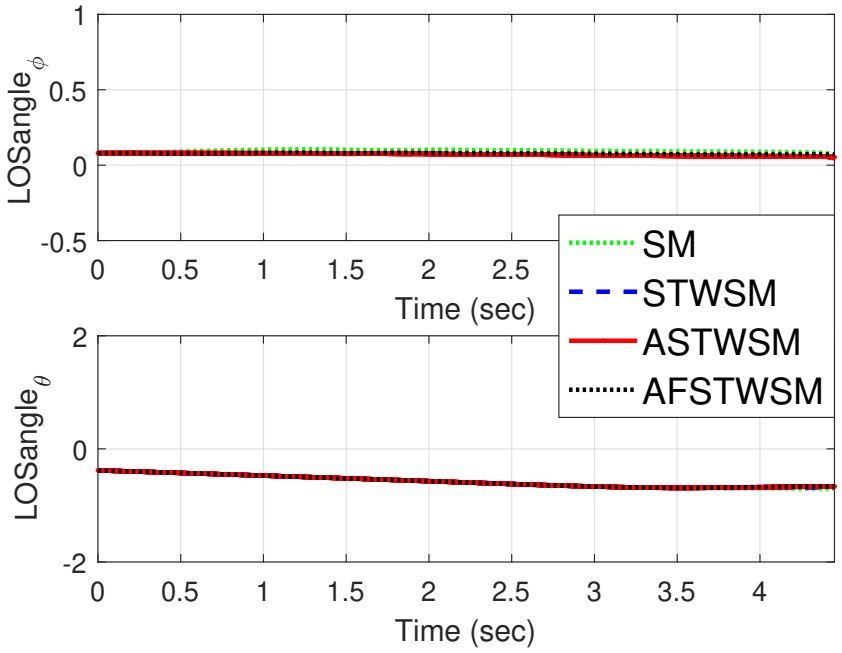

Figure 6.5 Results of Case 1: LOS angles

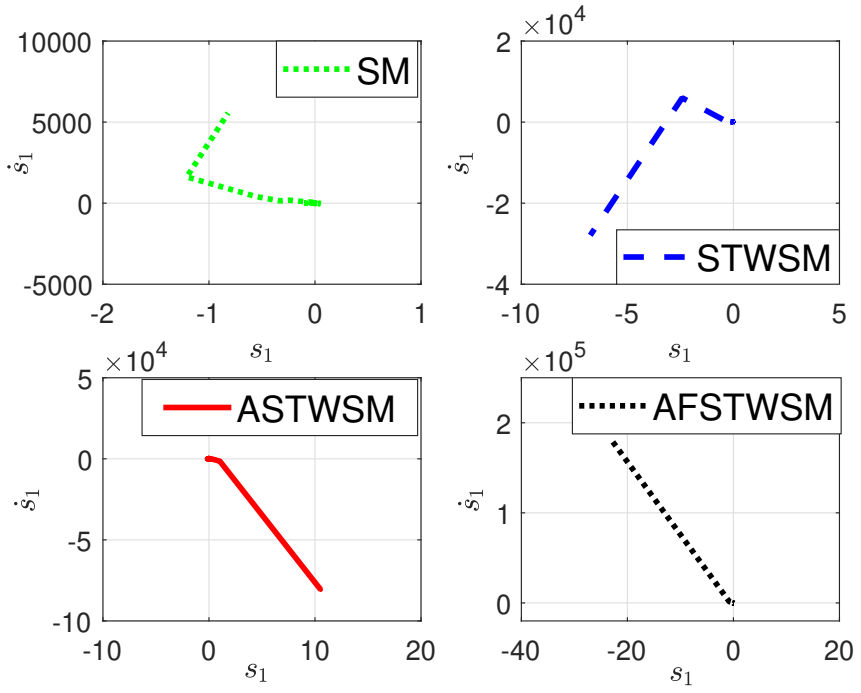

Figure 6.6 Results of Case 1: Phase space behavior of the elevation angle

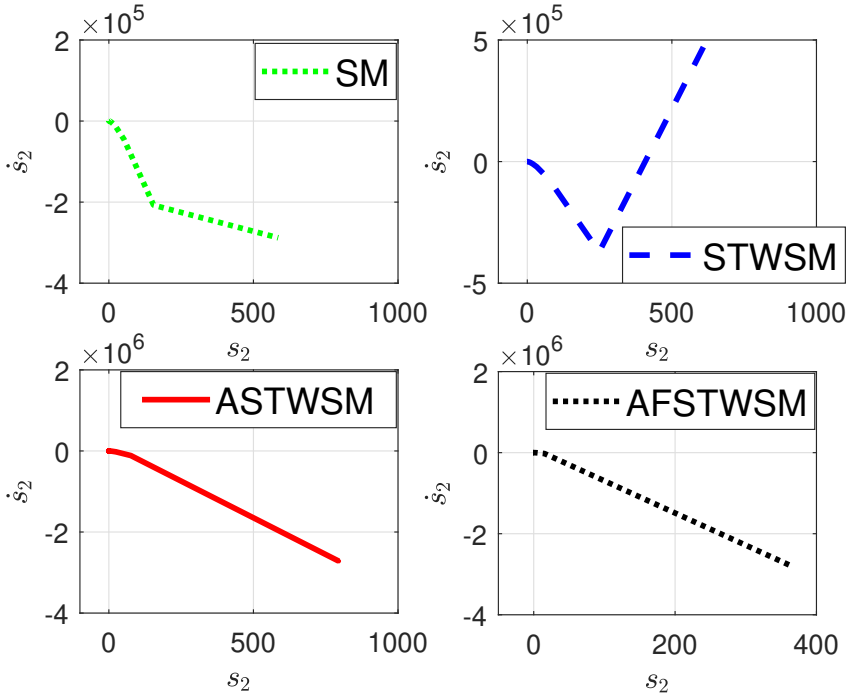

Figure 6.7 Results of Case 1: Phase space behavior of the azimuth angle

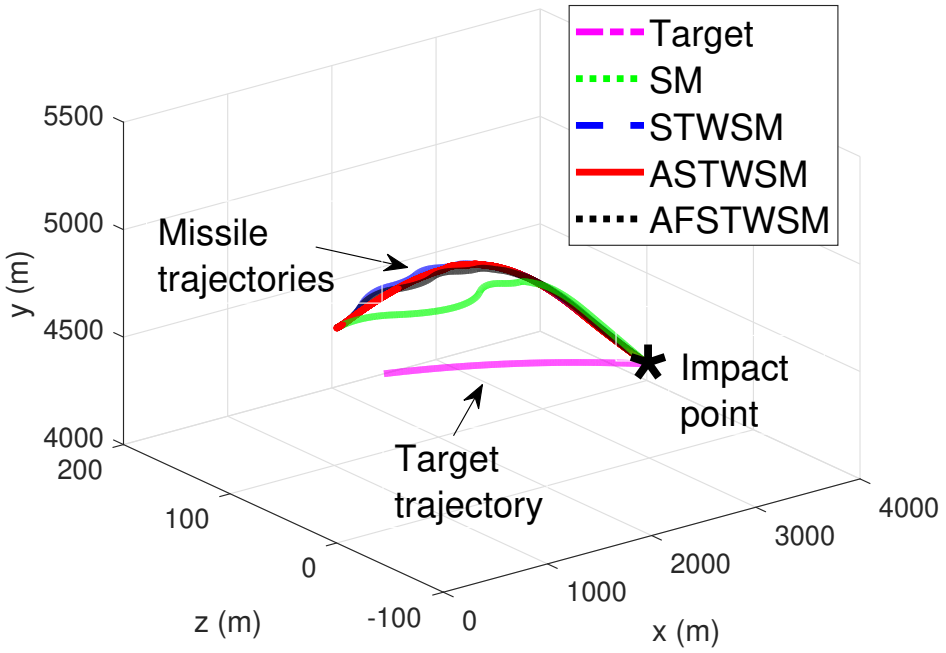

Figure 6.8 Results of Case 1: Missile and Target trajectories

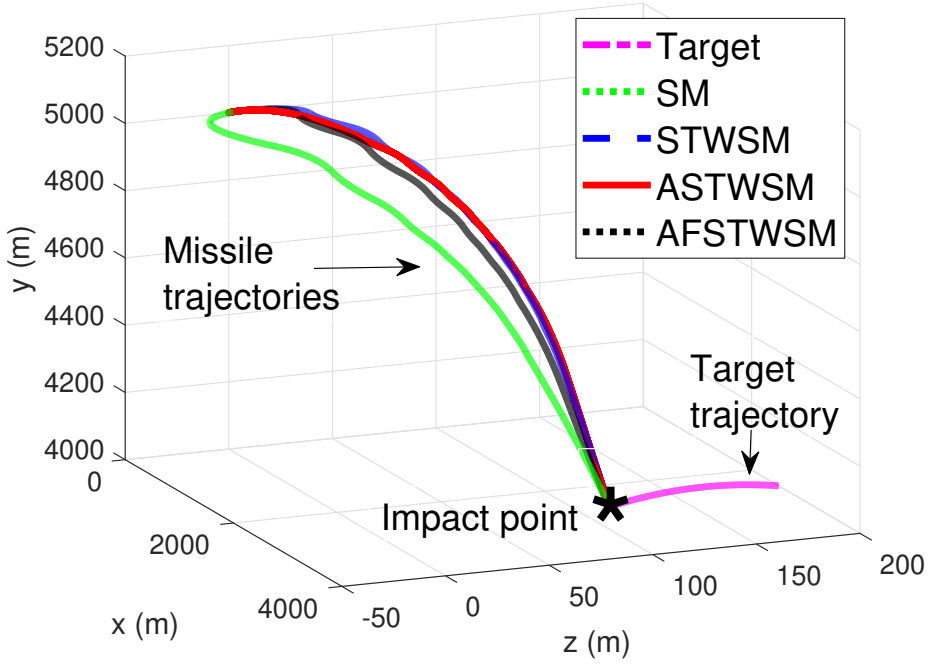

Figure 6.9 Results of Case 1: Missile and Target trajectories

Case 2: Time-varying maneuvering target

In Case 2, the target has a maneuvering trajectory and the missile aims to intercept this target. The parameters of the switching variables in (155)-(156) are set as $k_1 = 0.023, k_2 = 0.023$ for the STWSM guidance law. Moreover, the parameters of the STWSM guidance law (158) are selected as $\alpha = 0.002$ and $\beta = 0.05$. We chose $\omega_1 = 2$, $\gamma = 0.2$, $\zeta = 0.05$, $\eta = 0.02$, $\kappa = 0.01$ and $\alpha_m = 0.005$ for the ASTWSM and AFSTWSM guidance laws.

Scenario	**Guidance law**	**Miss distance (m)**	**Interception time (s)**
Case 2	SMGL	0.4072	4.237
	STWSMGL	0.1291	4.234
	ASTWSMGL	0.2508	4.232
	AFSTWSMGL	0.2434	4.229

Table 6.5 Miss distance and Interception time for Case 2

Table 6.5 tabulates the comparison of the interception performances of the four guidance laws by giving the final time and the miss distance for Case 2. According to the tabulated results, we can infer that the miss distance arising under the proposed AFSTWSM guidance law is smaller than the distances in other alternatives. Moreover, the proposed AFSTWSM guidance approach is one of the best performing approaches among the given guidance laws for the interception time.

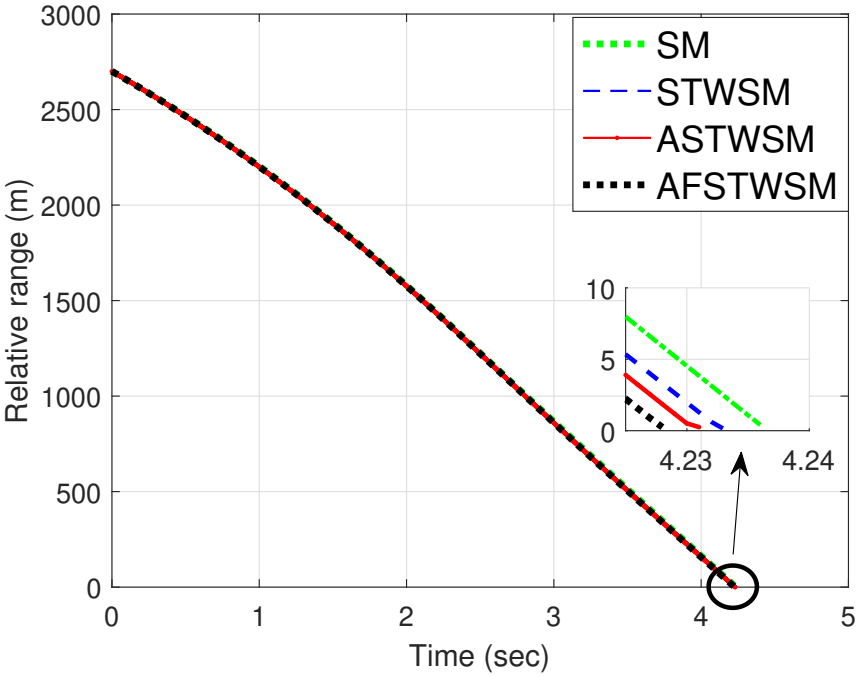

Figure 6.10 Results of Case 2: Relative range

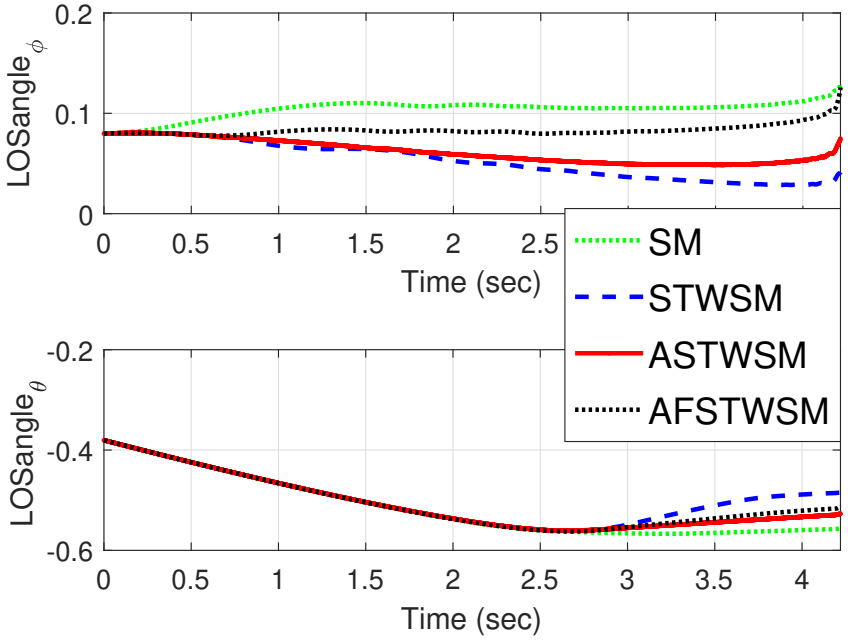

Figure 6.11 Results of Case 2: LOS angles

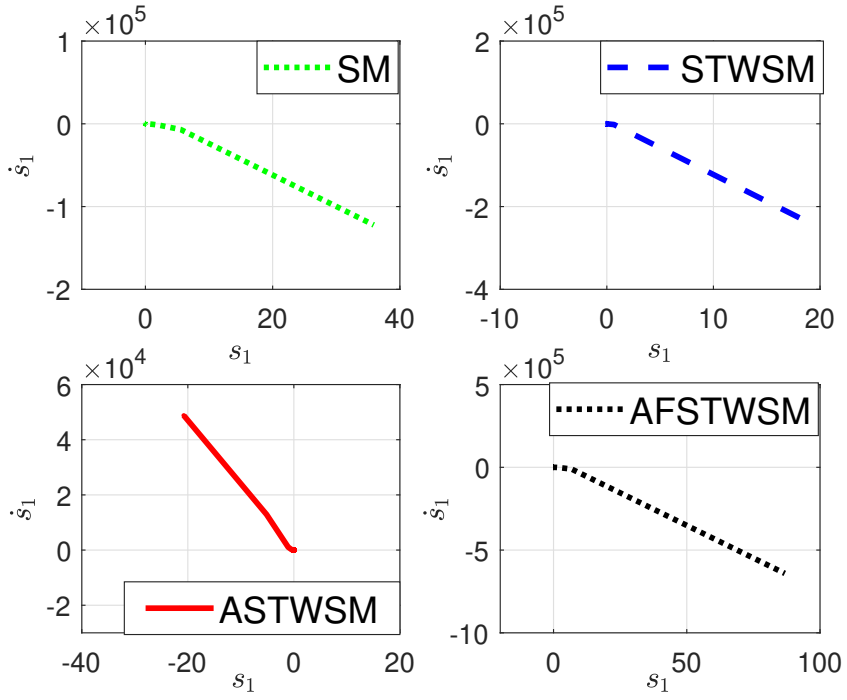

Figure 6.12 Results of Case 2: Phase space behavior of the elevation angle

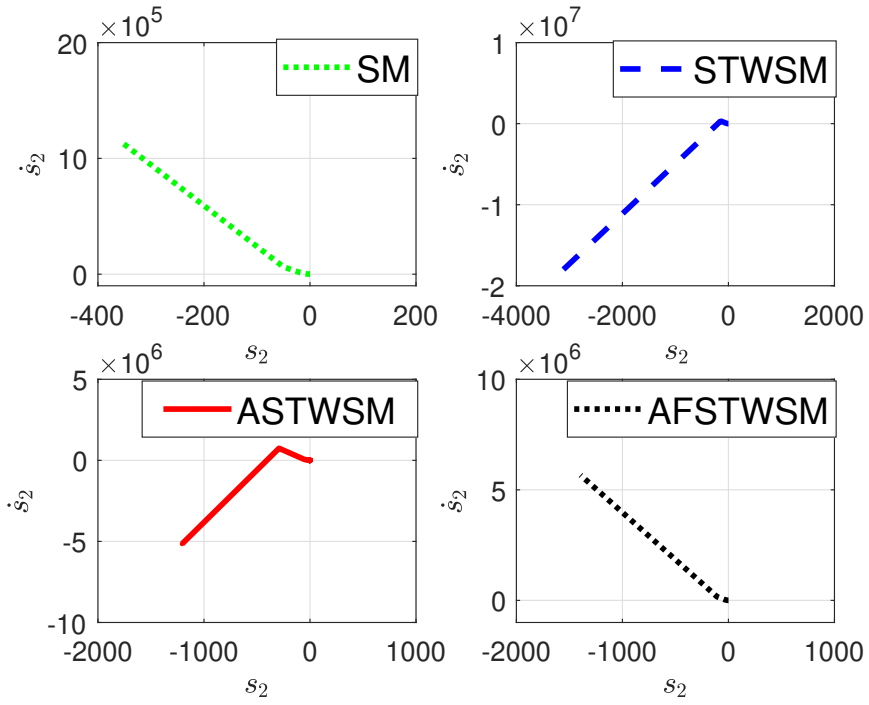

Figure 6.13 Results of Case 2: Phase space behavior of the azimuth angle

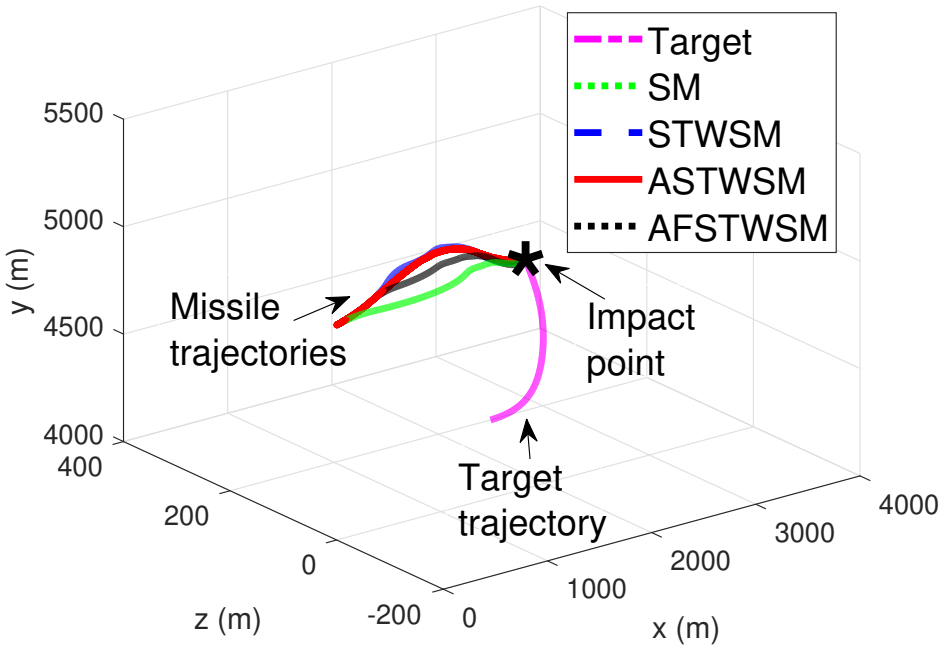

Figure 6.14 Results of Case 2: Missile and Target trajectories

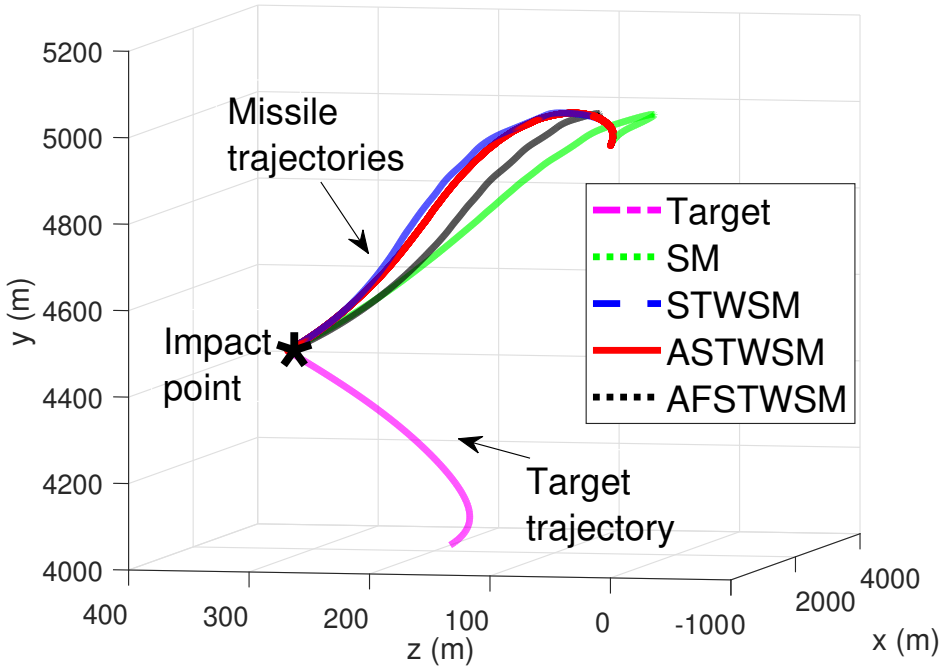

Figure 6.15 Results of Case 2: Missile and Target trajectories

The observed variables in this case are illustrated in Figures 6.10-6.15, respectively. In Figure 6.10, the relative range decreases to zero at the interception time in all of the guidance laws, i.e. the missile with the studied guidance laws successfully hits the target in this case. Figure 6.11 shows the response of the LOS angles. Figures 6.12 and 6.13 present the controlled phase space behavior of the switching manifold defined for the elevation angle and the azimuth angle. The trajectories of the missile and the target, guided by the law of guidance, are given from different angles in Figures 6.14-6.15. The observations in Figures 6.10-6.15 suggest that the missile hits the target accurately for all guidance laws yet the proposed adaptive and fuzzy-enhanced adaptive schemes display prominent features.

6.4. Summary

In this section, a new adaptive super-twisting sliding mode guidance law with a fuzzy gain scheduling is discussed for the missile-target interception. The actions used to create the novel guidance law will be outlined in sequence below.

- The STWSM guidance law is chosen to eliminate the chattering phenomenon.
- A adaptive law is used to obtain the controller gains without entailing the upper bound of the disturbance.
- The guidance system is augmented with a fuzzy inference system to prevent overestimation of the unknown parameters of the controller.

A set of simulation scenarios is studied for the four guidance laws, which are the traditional SM, the traditional STWSM, the proposed ASTWSM, the proposed AFSTWSM guidance laws. In comparison to the first three guidance methods listed, numerical simulations reveal that the proposed AFSWSMG law has significant robustness features against disturbances or parameter uncertainties. Besides all this, the obtained results demonstrate that the proposed adaptive and fuzzy-enhanced adaptive approaches have better performances in terms of the intercept time and the miss distance compared to the traditional alternatives.

7. INVESTIGATION OF THE EFFECT OF THE OBSERVER ON AUGMENTED PROPORTIONAL NAVIGATION GUIDANCE

In this section, a new 3D guidance law based on an the APN guidance law utilizing an NDOB technique is proposed. In numerical simulations, the performance of the classical APN guidance method and the new design of the APN against two different targets with non-maneuvering and maneuvering motion are described and discussed in this section.

7.1. Design the Guidance Law

7.1.1. Augmented Proportional Navigation Guidance Law

The APN guidance law is mathematically defined in the previous section. The most important advantage of the APN guidance law is that it can be used against maneuvering targets. In this method, the acceleration command is generated by multiplying a coefficient proportional to the acceleration of the target. If we restate Equations (106)-(107),

$$a_{M\phi} = N_1 V_c \dot{\phi} + 0.5 N_3 a_{T\phi}$$

$$a_{M\theta} = N_2 V_c \dot{\theta} + 0.5 N_4 a_{T\theta}$$

7.1.2. Nonlinear Disturbance Observer

For the guidance system, the NDOB definitions and equations will be given briefly again in this subsection. The mathematical expression of the guidance system given in Equations (85)

- (86) can be restated as follows.

$$\dot{x}_2 = A_1 + B_1\left(a_{M\phi} - a_{T\phi}\right) \tag{187}$$
$$\dot{x}_4 = A_2 + B_2\left(a_{M\theta} - a_{T\theta}\right)$$

in which $A = \begin{pmatrix} A_1 \\ A_2 \end{pmatrix} = \begin{pmatrix} -\frac{2\dot{R}}{R}x_2 - x_4^2 \sin x_1 \cos x_1 \\ \\ -\frac{2\dot{R}}{R}x_4 + 2x_4 x_2 \tan x_1 \end{pmatrix}$, $B = \begin{pmatrix} B_1 \\ B_2 \end{pmatrix} = \begin{pmatrix} -\frac{1}{R} \\ \\ \frac{1}{R\cos x_1} \end{pmatrix}$.

The NDOB can be mathematically redefined as given in the Equations (133)-(134).

$$\dot{z}_1 = A_1 + B_1\left(a_{M\phi} - \widehat{a}_{T\phi}\right) \tag{188}$$
$$\widehat{a}_{T\phi} = \omega_1\left(x_2 - z_1\right)$$

$$\dot{z}_2 = A_2 + B_2\left(a_{M\theta} - \widehat{a}_{T\theta}\right) \tag{189}$$
$$\widehat{a}_{T\theta} = \omega_2\left(x_4 - z_2\right)$$

where $\omega_1 > 0$ and $\omega_2 < 0$. Let $e_{T\phi}$ and $e_{T\theta}$ observer be prediction errors. Let these errors are expressed as $e_{T\phi} := a_{T\phi} - \widehat{a}_{T\phi}$ and $e_{T\theta} := a_{T\theta} - \widehat{a}_{T\theta}$. According to assumptions $\lim_{t\to\infty} e_{T\phi} = 0$ and $\lim_{t\to\infty} e_{T\theta} = 0$ given 2, the estimated accelerations, $\widehat{a}_{T\theta}$ and $\widehat{a}_{T\phi}$, converge asymptotically to the actual target accelerations.

7.1.3. Augmented Proportional Navigation Guidance Law with Nonlinear Disturbance Observer

In light of the above, the new APN guidance law designed with the observer method can be expressed as follows.

$$a_{M\phi} = N_1 V_c \dot{\phi} + 0.5 N_3 \widehat{a}_{T\phi} \tag{190}$$

$$a_{M\theta} = N_2 V_c \dot{\theta} + 0.5 N_4 \widehat{a}_{T\theta} \tag{191}$$

where $\widehat{a}_{T\phi}$ and $\widehat{a}_{T\theta}$ are the estimated target accelerations obtained using the NDOB structure.

7.2. Results of the Numerical Simulations

The newly designed guidance law has been validated over various scenarios. The conditions of the simulations and various parameters used are given, and the results are presented in detail in the following sections.

7.2.1. Simulation Scenarios Setting and Initial Conditions

In this section, numerical simulation studies are carried out on two scenarios: a target without maneuver and a target with time-varying maneuver, to evaluate the performance of the proposed guidance law. The scenario parameters are presented in the Table 7.1.

Interception Scenarios	**Azimuth acceleration**	**Elevation acceleration**
non-maneuvering	g	0
time-varying maneuvering	$3g + \sin 2\pi t$	$3g + \sin 2\pi t$

Table 7.1 Accelerations setting of target in interception scenarios

In here, the missile velocity is $V_{M0} = 800$ m/s, the initial position of the missile is $x_{M0} = 0$ m, $y_{M0} = 5000$ m and $z_{M0} = 0$ m. The target velocity is $V_{T0} = 400$ m/s and the initial position of the target $x_{T0} = 1100$ m, $y_{T0} = 5000$ m and $z_{T0} = 0$ m. The APN guidance law's parameters are $N_1 = 5$, $N_2 = 1$, $N_3 = 5$ and $N_4 = 1$. Furthermore, as shown in (133) and (134), the parameters required during the design of the disturbance observer are $\omega_1 = 3000$ and $\omega_2 = -3000$.

7.2.2. Simulation Results

The results obtained in this study are evaluated in terms of interception time and miss distance and are presented in Table 7.2 and 7.3. Considering the results obtained from both scenarios, it is clearly seen that more successful results are obtained from the new APN method, in which the target acceleration is obtained through the observer, compared to the classical APN method. In addition, it can be seen that the success achieved in Scenario 2, which was created for targets with maneuvering motion, is higher.

Scenario	**Guidance law**	**Miss distance (m)**	**Interception time (s)**
Non-maneuvering target	APN	0.1272	4.162
	APN+NDOB	0.1033	4.162

Table 7.2 Miss distance and Interception time for Case 1

The results for scenario 1 are given in Figure 7.1-7.5. It can be clearly seen in Figure 7.1 that the relative range decreases to zero at the time of interception for both guidance laws. From Figure 7.2, it can be verified that the LOS angular rates $\dot{\theta}$ and $\dot{\phi}$ fall to zero in finite time as a result of the applied guidance laws. This means that the studied guidance laws give the desired results. Figure 7.3 and 7.4 show the actual target accelerations and the estimated target accelerations obtained using the NDOB technique. It can be seen that the estimated accelerations by the NDOB converge to the accelerations of the actual target. Figure 7.5 presents the trajectories and encounter geometry of the missile and target. It is seen that the missile successfully met the target with the application of both the presented guidance laws.

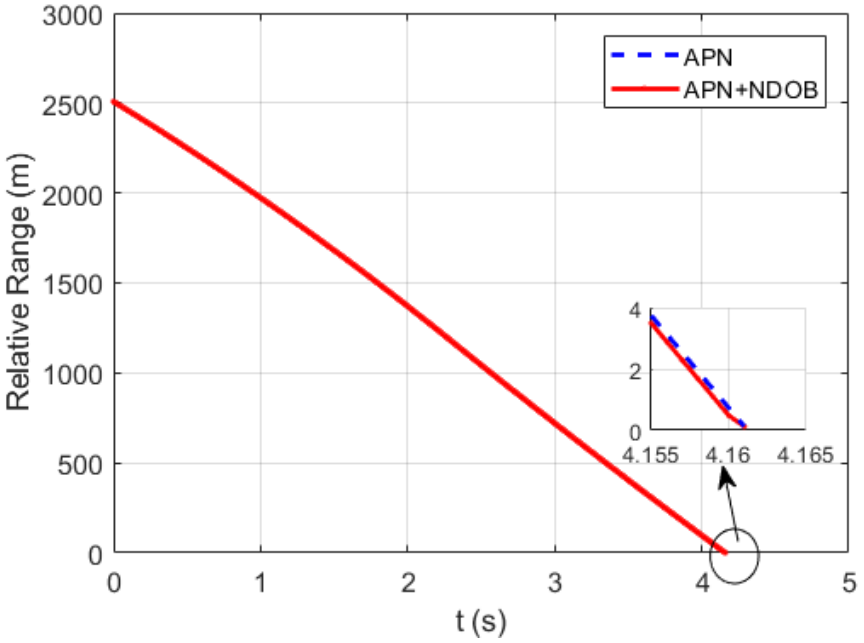

Figure 7.1 Results of Case 2: Relative range

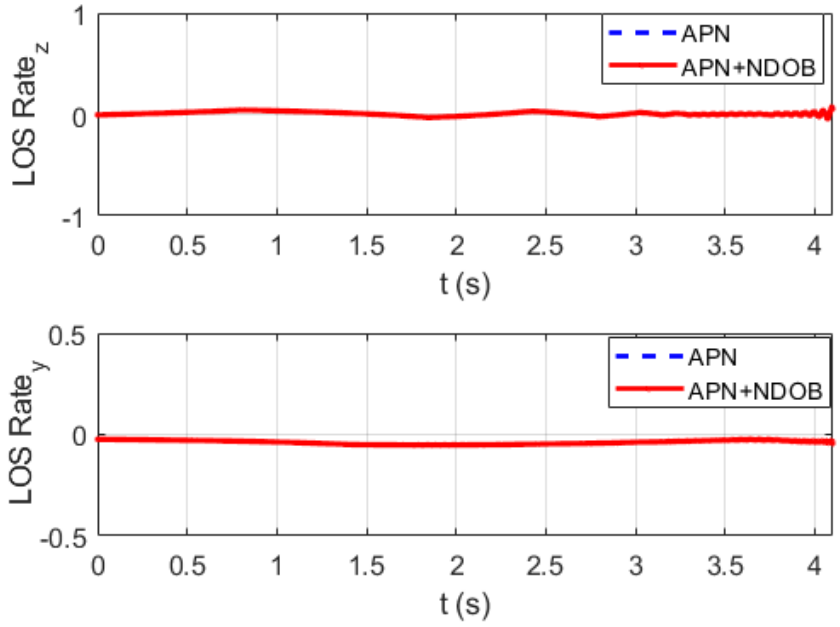

Figure 7.2 Results of Case 2: LOS angular rates

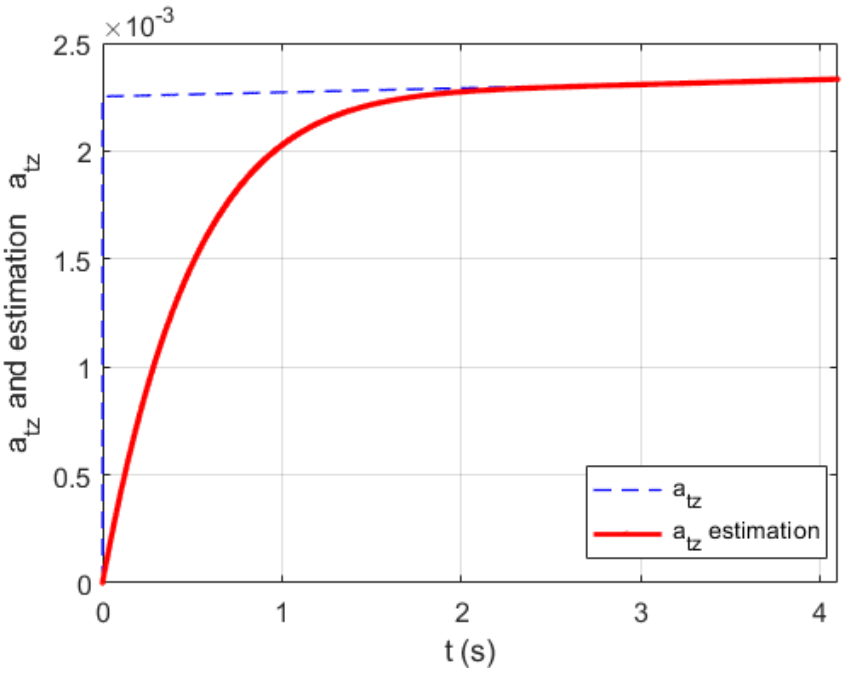

Figure 7.3 Results of Case 2: The actual and the estimated target accelerations

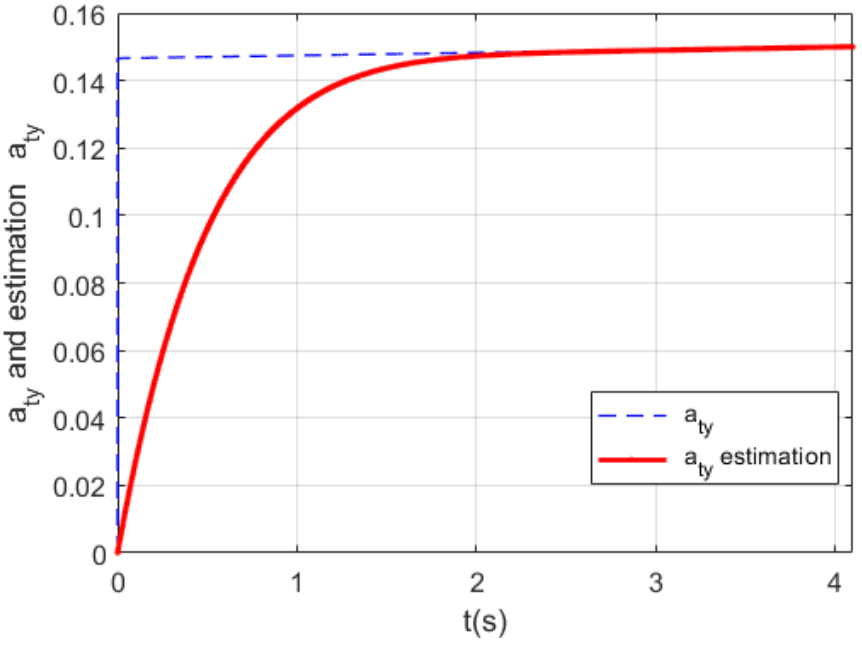

Figure 7.4 Results of Case 2: The actual and the estimated target accelerations

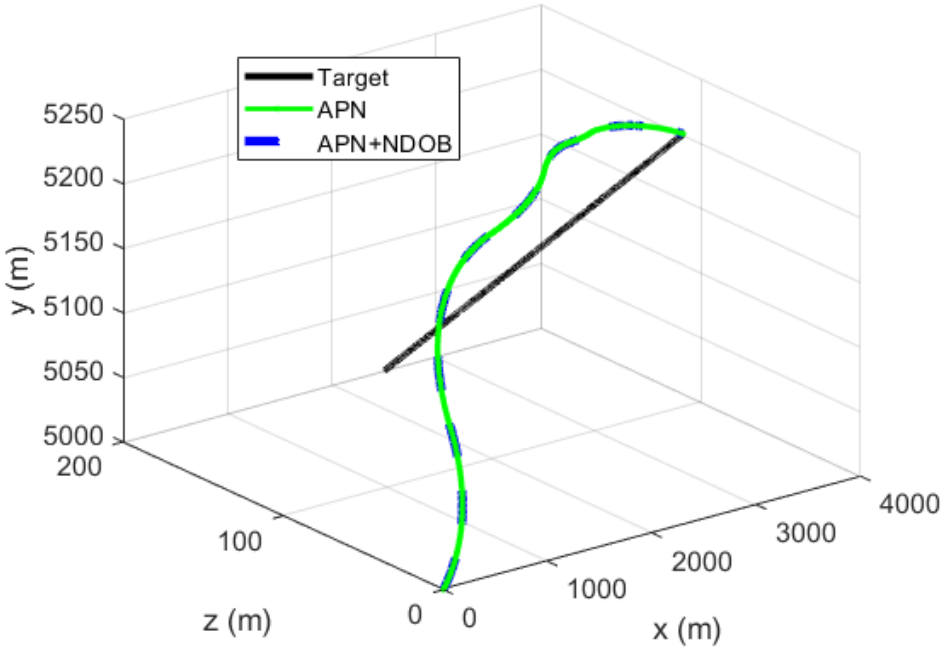

Figure 7.5 Results of Case 2: Missile and Target trajectories

Scenario	Guidance law	Miss distance (m)	Interception time (s)
Maneuvering target	APN	0.2309	4.124
	APN+NDOB	0.1200	4.124

Table 7.3 Miss distance and Interception time for Case 2

The results for Scenario 2 are given in Figure 7.6 and Figure 7.10. In Figure 7.6, it can be clearly seen that the relative range decreases to zero at the time of interception for all presented guidance laws. From Figure 7.7, it can be seen that the LOS angular rates $\dot{\theta}$ and $\dot{\phi}$ decrease to zero in finite time. This means that the studied guidance laws work as desired in this scenario. Figure 7.8 and 7.9 demonstrate the actual target accelerations and the estimated target accelerations obtained using the NDOB technique. The accelerations estimated by the NDOB appear to converge to the accelerations of the actual target. Looking at Figure 7.10, it is seen that the missile successfully hits the target by applying both guidance laws.

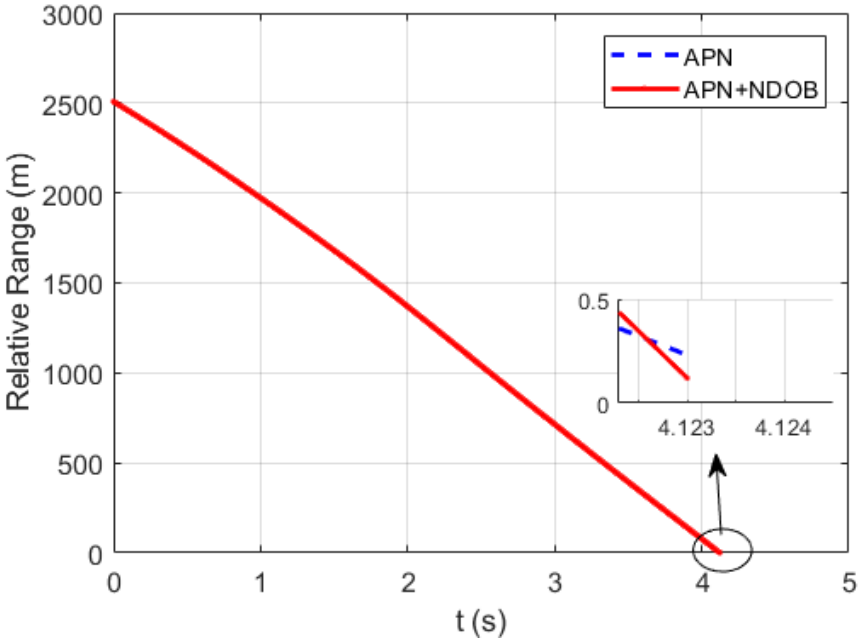

Figure 7.6 Results of Case 2: Relative range

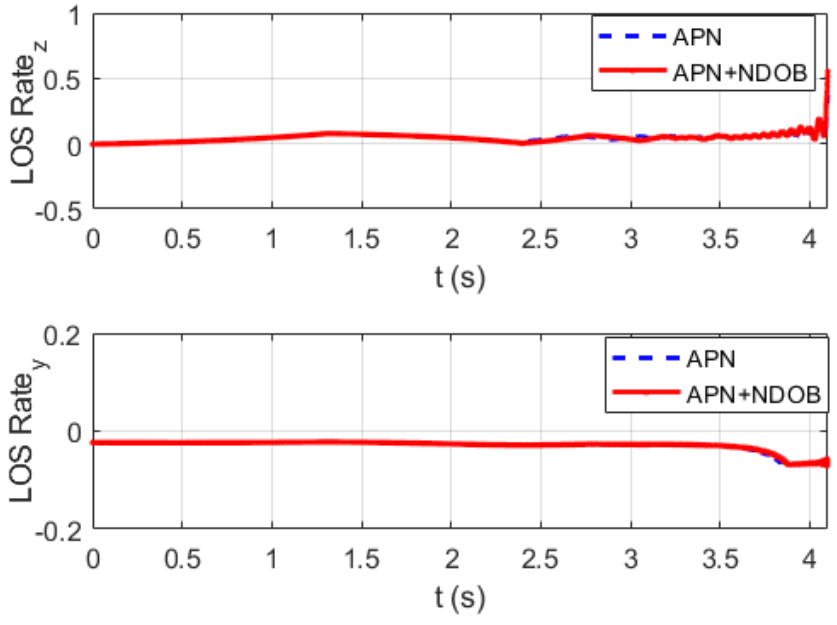

Figure 7.7 Results of Case 2: LOS angular rates

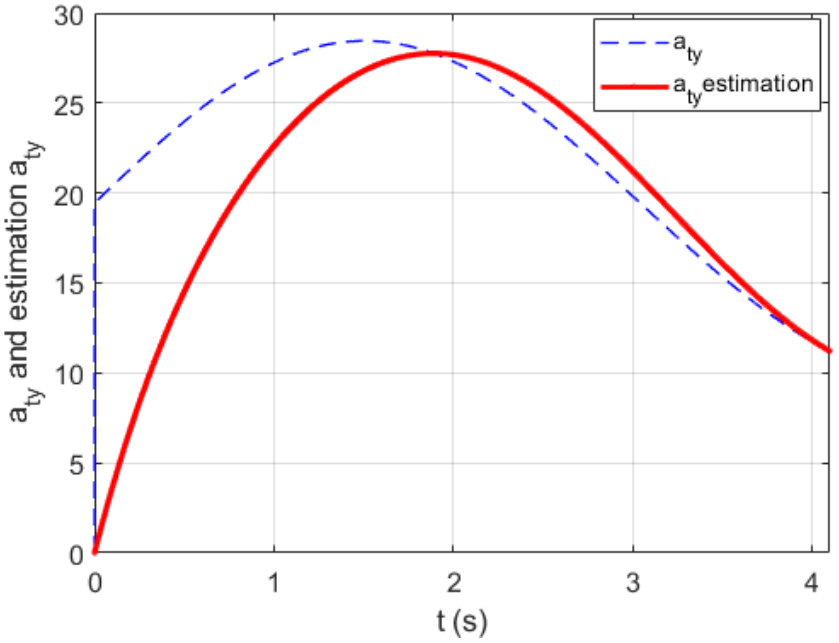

Figure 7.8 Results of Case 2: The actual and the estimated target accelerations

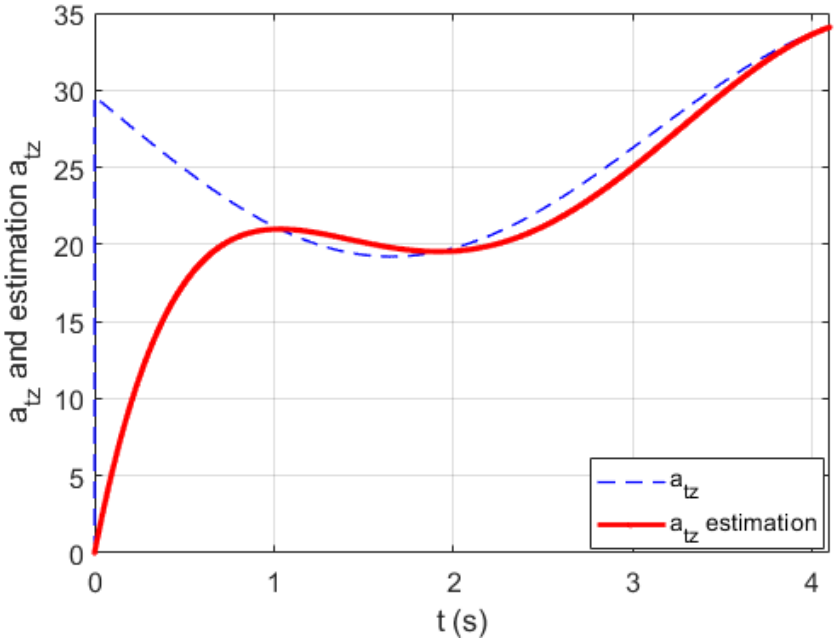

Figure 7.9 Results of Case 2: The actual and the estimated target accelerations

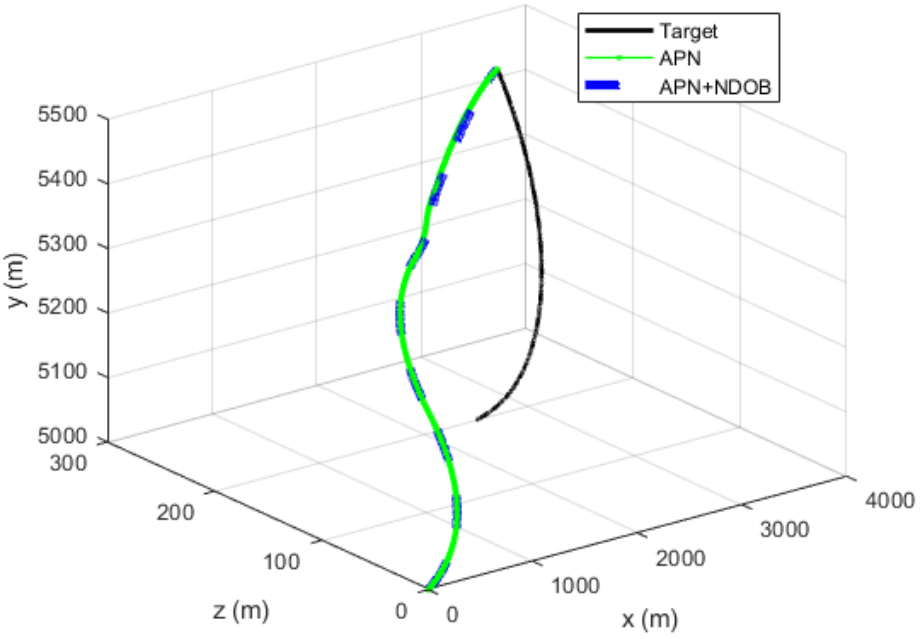

Figure 7.10 Results of Case 2: Missile and Target trajectories

7.3. Summary

In this section, a new method is presented, and simulation studies are carried out by using the APN guidance and disturbance observer on the 3D missile-target engagement geometry. The following steps have been followed for this new method:

- First, the APN guidance law, which is one of the traditional guidance laws, is designed.
- Then, the new method, which is presented as the basis of this study, is developed, and the target acceleration is obtained by the observer, considering it as a disturbance, and given to the system. Thus, the applicability of the APN guidance law without knowing the target acceleration has been made possible thanks to this newly designed method.

The comparative simulation results of the classical APN guidance law and the newly designed guidance law are presented. It has been determined that the new guidance law is more successful than the classical guidance law in terms of interception time and miss

distance. As a result, it has been understood that the APN guidance law is open to development and will continue to form the basis of different guidance systems for many years to come.

8. CONCLUSION

In the last section, the entire thesis work is summarized and various results given in the previous summary sections are synthesized. Limitations and important points are highlighted and recommendations are made for future work.

The dissertation, attempts to design robust controllers for missile systems. For this purpose, guidance laws have been focused on in order to make robust the missile's encounter with the target. The results are examined on the basic guidance laws and control methods, and novel guidance laws are designed in line with the main goal of dissertation.

For all these purposes, firstly, missile dynamic and kinematic models are constructed as 6-DOF, and the intercept geometry is generally expressed in 3D space using the engagement kinematics.

The PID and SMC methods, which are used as a basis for designing control-based guidance laws and form the basis of many studies, have been chosen as the main principle of the presented guidance law scheme, instead of the traditional guidance law. These methods are examined against the traditional guidance laws, PPN and APN. It has been observed that the laws in which control methods are utilized are more successful against both maneuvered and non-maneuvered targets. However, these methods are known to be vulnerable to system uncertainties and external disturbances, and this is observed in the results. Therefore, in this thesis, novel guidance laws have been developed by using new, robust methods to overcome the shortcomings of conventional control methods in this thesis.

The AISM guidance law with an NDOB method is the first novel proposed method as a composite guidance law. In the beginning, a new approach is handled to eliminate the reaching phase, which is one of the most important disadvantages of the SMC method, and the ISMC method is chosen as the foundation for the guidance law to be proposed. However, during the design of this law, upper bound information of the target acceleration is needed, and it is not possible for practical applications. For this reason, the design is carried out without the need for this information by adding an adaptive algorithm to the guidance law.

Thus, the proposed guidance law has become a more applicable method. In addition to all these, an NDOB is used in the proposed system. This observer considers target accelerations as disturbances and estimates them to be as close to the actual acceleration of the target as possible. The estimated acceleration values of the target obtained by the observer are given to the system as a compensation term. In this way, the chattering problem, which is the most important disadvantage of the SMC method, is eliminated or reduced. Comparison of the proposed guide law with both the traditional guide law APN and the adaptive integral sliding mode guide law is used to show the effectiveness of the proposed scheme. The numerical simulations are conducted on the different target movements and the results are demonstrated that the new composite guidance law can be a viable solution to design.

The second proposed method is the ASTWSM guidance law with a fuzzy gain schedule as a novel guidance law. The super-twisting SMC method is chosen as the first step in the development of this new approach. With the use of this method, the chattering phenomenon, which we consider a disadvantage, is alleviated. In the next step, the adaptive law is used to obtain control gains. The major advantage offered by this adaptive algorithm is that advanced knowledge about the upper bound of the target acceleration is not a necessary requirement. In addition, The guidance system is augmented with a fuzzy inference system to prevent overestimation of the unknown parameters of the controller. The results of this proposed guidance law are presented comparing with the results of three different approaches on two different target movements. These compared approaches are the traditional sliding mode guidance law, the traditional STWSM guidance law, and the proposed ASTWSM guidance law. The results of numerical simulations show that the proposed AFSTWSM guidance law has significant robustness features against disturbances or parameter uncertainties. Besides all this, the obtained results present that the proposed adaptive and fuzzy-enhanced adaptive approaches outperform the traditional alternatives in terms of the intercept time and the miss distance.

The APN guidance law with the NDOB is the final proposed guidance scheme within the scope of the thesis.Here, the main aim is to examine the effect of the observer on the APN guidance law, which is a traditional method. First of all, the APN guidance rule is designed.

However, this design requires target acceleration information. At this point, the observer will be activated and the target acceleration information will be given to the system by estimation. Thus, the APN guidance law can be applied without having the acceleration information of the target. In simulations, the classic APN guidance law and the newly developed method were compared, and the results determined that the new guidance law is more successful than the classical guidance law in terms of interception time and miss distance.

In the future, studies on this missile guidance and control system will be expected to continue to fulfill some ultimate objectives and advance the performance of the overall system. In light of the above, the suggested methods for various target maneuvers can be considered. Also, the guidance law can be developed using more advanced controller design techniques. Moreover, new studies can be done by considering the guidance law and autopilot in an integrated way and developing the proposed methods.

REFERENCES

[1] Peter H Zipfel. *Modeling and simulation of aerospace vehicle dynamics*. Aiaa, **2000**.

[2] George M Siouris. *Missile guidance and control systems*. Springer Science & Business Media, **2004**.

[3] Bülent Özkan, Mustafa Kemal Özgören, and GÖKMEN MAHMUTYAZICIOĞLU. Performance comparison of the notable acceleration-and angle-based guidance laws for a short-range air-to-surface missile. *Turkish Journal of Electrical Engineering & Computer Sciences*, 25(5):3591–3606, **2017**.

[4] Y Kaya and S Yamamura. A self-adaptive system with a variable-parameter pid controller. *Transactions of the American Institute of Electrical Engineers, Part II: Applications and Industry*, 80(6):378–386, **1962**.

[5] KC Sio and CK Lee. Stability of fuzzy pid controllers. *IEEE Transactions on Systems, Man, and Cybernetics-Part A: Systems and Humans*, 28(4):490–495, **1998**.

[6] AN Gundes and AB Ozguler. Pid stabilization of mimo plants. *IEEE Transactions on Automatic Control*, 52(8):1502–1508, **2007**.

[7] Chen-Huei Hsieh and Jyh-Horng Chou. Design of optimal pid controllers for pwm feedback systems with bilinear plants. *IEEE transactions on control systems technology*, 15(6):1075–1079, **2007**.

[8] Handan Gürsoy and Mehmet Önder Efe. Control system implementation on an fpga platform. *IFAC-PapersOnLine*, 49(25):425–430, **2016**.

[9] Rakesh P Borase, DK Maghade, SY Sondkar, and SN Pawar. A review of pid control, tuning methods and applications. *International Journal of Dynamics and Control*, 9(2):818–827, **2021**.

[10] Vadim Utkin. Variable structure systems with sliding modes. *IEEE Trans. Autom. Control*, 22(2):212–222, **1977**.

[11] Huaiyuan Jia, Weiwei Shang, Fei Xie, Bin Zhang, and Shuang Cong. Second-order sliding-mode-based synchronization control of cable-driven parallel robots. *IEEE/ASME Trans. Mechatronics*, 25(1):383–394, **2019**.

[12] Vadim Utkin, Jürgen Guldner, and Jingxin Shi. *Sliding mode control in electro-mechanical systems*. CRC press, **2009**.

[13] Shubo Wang, Liang Tao, Qiang Chen, Jing Na, and Xuemei Ren. Usde-based sliding mode control for servo mechanisms with unknown system dynamics. *IEEE/ASME Trans. Mechatronics*, 25(2):1056–1066, **2020**.

[14] Bei Chen, Tinggang Jia, and Yugang Niu. Robust fuzzy control for stochastic markovian jumping systems via sliding mode method. *Int J Gen Syst*, 45(5):604–618, **2016**.

[15] Mehmet Önder Efe. Integral sliding mode control of a quadrotor with fractional order reaching dynamics. *Trans. Inst. Meas. Control*, 33(8):985–1003, **2011**.

[16] Syuan-Yi Chen, Hsin-Han Chiang, Tung-Sheng Liu, and Chih-Hung Chang. Precision motion control of permanent magnet linear synchronous motors using adaptive fuzzy fractional-order sliding-mode control. *IEEE/ASME Trans. Mechatronics*, 24(2):741–752, **2019**.

[17] Zhiwei Hou, Lei Liu, Yongji Wang, Jian Huang, and Huijin Fan. Terminal impact angle constraint guidance with dual sliding surfaces and model-free target acceleration estimator. *IEEE Trans. Control Syst. Technol.*, 25(1):85–100, **2016**.

[18] Hoon Lee and Vadim I Utkin. Chattering suppression methods in sliding mode control systems. *Annual reviews in control*, 31(2):179–188, **2007**.

[19] Leonid M Fridman. An averaging approach to chattering. *IEEE Transactions on Automatic Control*, 46(8):1260–1265, **2001**.

[20] Hongyu Zhao, Mingang Wang, Ximing Zhang, and Tao Zhang. A high-order sliding mode variable structure guidance law with finite time convergence. In *2016 IEEE Advanced Information Management, Communicates, Electronic and Automation Control Conference (IMCEC)*, pages 641–647. IEEE, **2016**.

[21] Zheng Wang. Adaptive smooth second-order sliding mode control method with application to missile guidance. *Transactions of the Institute of Measurement and Control*, 39(6):848–860, **2017**.

[22] Yuri B Shtessel, Jaime A Moreno, Franck Plestan, Leonid M Fridman, and Alexander S Poznyak. Super-twisting adaptive sliding mode control: A lyapunov design. In *49th IEEE conference on decision and control (CDC)*, pages 5109–5113. IEEE, **2010**.

[23] Yakun Zhao, Panfeng Huang, and Fan Zhang. Dynamic modeling and super-twisting sliding mode control for tethered space robot. *Acta Astronautica*, 143:310–321, **2018**.

[24] HJ Jayakrishnan. Position and attitude control of a quadrotor uav using super twisting sliding mode. *IFAC-PapersOnLine*, 49(1):284–289, **2016**.

[25] Zhilin Feng and Juntao Fei. Design and analysis of adaptive super-twisting sliding mode control for a microgyroscope. *PloS one*, 13(1):e0189457, **2018**.

[26] Emre Sariyildiz, Roberto Oboe, and Kouhei Ohnishi. Disturbance observer-based robust control and its applications: 35th anniversary overview. *IEEE Trans. Ind. Electron.*, 67(3):2042–2053, **2019**.

[27] Kiyoshi Ohishi. Torque-speed regulation of dc motor based on load torque estimation. In *Proc. IEEJ IPEC*, volume 2, pages 1209–1216. **1983**.

[28] Vadim Utkin and Jingxin Shi. Integral sliding mode in systems operating under uncertainty conditions. In *Proc. 35th IEEE Conf. Decis. Control*, volume 4, pages 4591–4596. IEEE, **1996**.

[29] Ranjith Ravindranathan Nair, Laxmidhar Behera, and Swagat Kumar. Event-triggered finite-time integral sliding mode controller for consensus-based formation of multirobot systems with disturbances. *IEEE Trans. Control Syst. Technol.*, 27(1):39–47, **2017**.

[30] Jianmei Wang, Xiaoyuan Luo, Li Wang, Zhiqiang Zuo, and Xinping Guan. Integral sliding mode control using a disturbance observer for vehicle platoons. *IEEE Trans. Ind. Electron.*, **2019**.

[31] XB Li, GR Zhao, S Liu, and X Han. Adaptive integral sliding mode guidance law with impact angle constraint considering autopilot lag. In *Journal of Physics: Conference Series*, page 012081. IOP Publishing, **2019**.

[32] Junhong Song and Shenmin Song. Three-dimensional guidance law based on adaptive integral sliding mode control. *Chinese J. Aeronaut.*, 29(1):202–214, **2016**.

[33] Lotfi Asker Zadeh. Fuzzy sets as a basis for a theory of possibility. *Fuzzy sets and systems*, 1(1):3–28, **1978**.

[34] Nikhil R Pal and James C Bezdek. Measuring fuzzy uncertainty. *IEEE Transactions on Fuzzy Systems*, 2:107–118, **1994**.

[35] Ali Saghafinia, Hew Wooi Ping, and M Nasir Uddin. Fuzzy sliding mode control based on boundary layer theory for chattering-free and robust induction motor drive. *The International Journal of Advanced Manufacturing Technology*, 71(1):57–68, **2014**.

[36] Sibsankar Dasmahapatra, Bikash Kumar Sarkar, Rana Saha, Amitava Chatterjee, Saikat Mookherjee, and Dipankar Sanyal. Design of an

adaptive fuzzy-bias smc and validation for a rugged electrohydraulic system. *IEEE/ASME Transactions on Mechatronics*, 20(6):2708–2715, **2015**.

[37] Asit Mohanty, Sandipan Patra, and Prakash K Ray. Robust fuzzy-sliding mode based upfc controller for transient stability analysis in autonomous wind-diesel-pv hybrid system. *IET Generation, Transmission & Distribution*, 10(5):1248–1257, **2016**.

[38] Fardila Mohd Zaihidee, Saad Mekhilef, and Marizan Mubin. Robust speed control of pmsm using sliding mode control (smc)—a review. *Energies*, 12(9):1669, **2019**.

[39] Yueneng Yang and Ye Yan. Attitude regulation for unmanned quadrotors using adaptive fuzzy gain-scheduling sliding mode control. *Aerospace Science and Technology*, 54:208–217, **2016**.

[40] Ankur Goel and Akhilesh Swarup. Adaptive fuzzy high-order super-twisting sliding mode controller for uncertain robotic manipulator. *Journal of Intelligent Systems*, 26(4):697–715, **2017**.

[41] Erjiang Liu, Yueneng Yang, and Ye Yan. Spacecraft attitude tracking for space debris removal using adaptive fuzzy sliding mode control. *Aerospace Science and Technology*, 107:106310, **2020**.

[42] Mehdi Golestani and Iman Mohammadzaman. Pid guidance law design using short time stability approach. *Aerospace Science and Technology*, 43:71–76, **2015**.

[43] Yuhao Xie and Zihan Su. Fuzzy adaptive pid control for missile guidance. In *IOP Conference Series: Materials Science and Engineering*, volume 466, page 012054. IOP Publishing, **2018**.

[44] C-Y Li and W-X Jing. Fuzzy pid controller for 2d differential geometric guidance and control problem. *IET Control Theory & Applications*, 1(3):564–571, **2007**.

[45] Paul G Gonsalves and Alper K Caglayan. Fuzzy logic pid controller for missile terminal guidance. In *Proceedings of Tenth International Symposium on Intelligent Control*, pages 377–382. IEEE, **1995**.

[46] Chaoyong Li and Wuxing Jing. Application of pid controller to 2d differential geometric guidance problem. *Journal of Control Theory and Applications*, 5(3):285–290, **2007**.

[47] Chih-Min Lin, Chun-Fei Hsu, Shing-Kuo Chang, and Rong-Jong Wai. Guidance law evaluation for missile guidance systems. *Asian Journal of Control*, 2(4):243–250, **2000**.

[48] Binfeng Pan, Usman Fareed, Wenjie Qing, and Shaohua Tian. A novel fractional order pid navigation guidance law by finite time stability approach. *ISA transactions*, 94:80–92, **2019**.

[49] Murad Yaghi and Mehmet Önder Efe. Adaptive neural fopid controller applied for missile guidance system. In *IECON 2017-43rd Annual Conference of the IEEE Industrial Electronics Society*, pages 2955–2960. IEEE, **2017**.

[50] Hadi Nobahari and Said H Pourtakdoust. An optimal-fuzzy two-phase clos guidance law design using ant colony optimisation. *The Aeronautical Journal*, 111(1124):621–636, **2007**.

[51] Çagdas Evcimen and Kemal Leblebicioglu. An adaptive, optimal proportional-integral guidance for missiles. In *AIAA Guidance, Navigation, and Control (GNC) Conference*, page 4784. **2013**.

[52] Lei Zhang. Adaptive fuzzy-pid controllers based on optimal fuzzy reasoning for missile terminal guidance. In *47th AIAA Aerospace Sciences Meeting including The New Horizons Forum and Aerospace Exposition*, page 427. **2009**.

[53] Jongki Moon, Kiseok Kim, and Youdan Kim. Design of missile guidance law via variable structure control. *Journal of Guidance, Control, and Dynamics*, 24(4):659–664, **2001**.

[54] Yuri B Shtessel, Ilya A Shkolnikov, and Arie Levant. Smooth second-order sliding modes: Missile guidance application. *Automatica*, 43(8):1470–1476, **2007**.

[55] Chang-Hun Lee, Tae-Hun Kim, Min-Jea Tahk, and Kyung-Soo Kim. Design of guidance law for passive homing missile using sliding mode control. In *ICCAS 2010*, pages 2380–2385. IEEE, **2010**.

[56] Huibo Zhou, Shenmin Song, Junhong Song, and Jing Niu. Design of second-order sliding mode guidance law based on the nonhomogeneous disturbance observer. *Journal of Control Science and Engineering*, 2014, **2014**.

[57] Yongwoo Lee and Youdan Kim. Three-dimensional impact angle control guidance law for missiles using dual sliding surfaces. *IFAC Proceedings Volumes*, 46(19):137–142, **2013**.

[58] Lianghua Sun, Weihong Wang, Ran Yi, and Shaofeng Xiong. A novel guidance law using fast terminal sliding mode control with impact angle constraints. *ISA transactions*, 64:12–23, **2016**.

[59] Jiang Wang and Shaoming He. Optimal integral sliding mode guidance law based on generalized model predictive control. *Proc. Inst. Mech. Eng., I, J. Syst. Control Eng.*, 230(7):610–621, **2016**.

[60] Yunxi Zhang, Mingwei Sun, and Zengqiang Chen. Finite-time convergent guidance law with impact angle constraint based on sliding-mode control. *Nonlinear Dynamics*, 70(1):619–625, **2012**.

[61] Hyo-Sang Shin, Antonios Tsourdos, and Ke-Bo Li. A new three-dimensional sliding mode guidance law variation with finite time convergence. *IEEE Transactions on Aerospace and Electronic Systems*, 53(5):2221–2232, **2017**.

[62] SB Phadke and Sanjay E Talole. Sliding mode and inertial delay control based missile guidance. *IEEE Transactions on Aerospace and Electronic Systems*, 48(4):3331–3346, **2012**.

[63] Zheng Zhu, Dong Xu, Jingmeng Liu, and Yuanqing Xia. Missile guidance law based on extended state observer. *IEEE Transactions on Industrial Electronics*, 60(12):5882–5891, **2012**.

[64] Hui-bo Zhou, Hong-liang Liu, and Ping Li. Adaptive sliding mode guidance law with impact angle constraint. In *Advances in Guidance, Navigation and Control*, pages 539–554. Springer, **2022**.

[65] Jianguo Guo, Yifei Li, and Jun Zhou. An observer-based continuous adaptive sliding mode guidance against chattering for homing missiles. *Transactions of the Institute of Measurement and Control*, 41(12):3309–3320, **2019**.

[66] Mehdi Golestani, Iman Mohammadzaman, Mohammad Javad Yazdanpanah, and Ahmad Reza Vali. Application of finite-time integral sliding mode to guidance law design. *ASME J. Dyn. Syst. Meas. Control*, 137(11):114501, **2015**.

[67] Xiaojian Zhang, Mingyong Liu, Yang Li, and Feihu Zhang. Impact angle control based on integral sliding mode manifold and extended state observer. *Proc. Inst. Mech. Eng., G, J. Aerosp. Eng.*, 233(6):2131–2140, **2019**.

[68] Zhenxing Zhang, Shihua Li, and Sheng Luo. Composite guidance laws based on sliding mode control with impact angle constraint and autopilot lag. *Transactions of the Institute of Measurement and Control*, 35(6):764–776, **2013**.

[69] Yew-Wen Liang, Chih-Chiang Chen, Der-Cherng Liaw, Yang-Ching Feng, Chiz-Chung Cheng, and Chun-Hone Chen. Robust guidance law via integral-sliding-mode scheme. *J. Guid. Control Dynam.*, 37(3):1038–1042, **2014**.

[70] Kezi Meng and Di Zhou. Super-twisting integral-sliding-mode guidance law considering autopilot dynamics. *Proc. Inst. Mech. Eng., G, J. Aerosp. Eng.*, 232(9):1787–1799, **2018**.

[71] Zhenxing Zhang, Shihua Li, and Sheng Luo. Terminal guidance laws of missile based on ismc and ndob with impact angle constraint. *Aerosp. Sci. Technol.*, 31(1):30–41, **2013**.

[72] Zhang Wenjie, FU Shengnan, LI Wei, and XIA Qunli. An impact angle constraint integral sliding mode guidance law for maneuvering targets interception. *Journal of Systems Engineering and Electronics*, 31(1):168–184, **2020**.

[73] Guofei Li and Yunjie Wu. Nonsingular adaptive-gain super-twisting guidance with an impact angle constraint. *Proceedings of the Institution of Mechanical Engineers, Part G: Journal of Aerospace Engineering*, 233(5):1705–1714, **2019**.

[74] Fang Yang, Kuanqiao Zhang, and Lei Yu. Adaptive super-twisting algorithm-based nonsingular terminal sliding mode guidance law. *Journal of Control Science and Engineering*, 2020, **2020**.

[75] Yi Ji, Defu Lin, Wei Wang, Shaoyong Hu, and Pei Pei. Three-dimensional terminal angle constrained robust guidance law with autopilot lag consideration. *Aerospace Science and Technology*, 86:160–176, **2019**.

[76] Shuai Xu, Min Gao, Dan Fang, Yi Wang, and Baochen Li. A novel adaptive second-order nonsingular terminal sliding mode guidance law design. *Proceedings of the Institution of Mechanical Engineers, Part G: Journal of Aerospace Engineering*, 234(16):2263–2273, **2020**.

[77] Qingchun Li, Wensheng Zhang, Gang Han, and Yuan Xie. Fuzzy sliding mode control guidance law with terminal impact angle and acceleration constraints. *Journal of Systems Engineering and Electronics*, 27(3):664–679, **2016**.

[78] YZ Elhalwagy and M Tarbouchi. Fuzzy logic sliding mode control for command guidance law design. *ISA Transactions*, 43(2):231–242, **2004**.

[79] Jinlong Zhao and Jun Zhou. Fixed-time second order sliding mode guidance law for interceptors with impact angle constraints. In *2019 IEEE 3rd Advanced Information Management, Communicates, Electronic and Automation Control Conference (IMCEC)*, pages 1010–1014. IEEE, **2019**.

[80] Ting-Kuo Wang, Li-Chen Fu, and Jong-Hann Jean. Second-order sliding mode control for passive ranging system in missile interception. In *2012 IEEE 51st IEEE Conference on Decision and Control (CDC)*, pages 6466–6471. IEEE, **2012**.

[81] Dan-xu Zhang, Yang-wang Fang, Peng-fei Yang, and Yang Xu. Stochastic fast smooth second-order sliding modes terminal guidance law design. *Optik*, 127(13):5359–5364, **2016**.

[82] Yongjie Xu, Zhijun Wang, and Benbing Gao. Six-degree-of-freedom digital simulations for missile guidance and control. *Mathematical Problems in Engineering*, 2015, **2015**.

[83] Seung-Hwan Kim, Yong-In Lee, and Min-Jea Tahk. New structure for an aerodynamic fin control system for tail fin-controlled stt missiles. *Journal of Aerospace Engineering*, 24(4):505–510, **2011**.

[84] Antonios Tsourdos and Brian A White. Modern missile flight control design: an overview. *IFAC Proceedings Volumes*, 34(15):425–430, **2001**.

[85] SN Balakrishnan, Antonios Tsourdos, and Brian A White. *Advances in missile guidance, control, and estimation*, volume 47. Crc Press, **2016**.

[86] Rafael T Yanushevsky. *Modern missile guidance*. CRC Press, **2018**.

[87] Mauricio Guelman. A qualitative study of proportional navigation. *IEEE Transactions on Aerospace and Electronic Systems*, AES-7(4):637–643, **1971**.

[88] Di Zhou, Sheng Sun, and Kok Lay Teo. Guidance laws with finite time convergence. *Journal of guidance, control, and dynamics*, 32(6):1838–1846, **2009**.

[89] Neil F Palumbo, Ross A Blauwkamp, and Justin M Lloyd. Modern homing missile guidance theory and techniques. *Johns Hopkins APL technical digest*, 29(1):42–59, **2010**.

[90] Neryahu A Shneydor. *Missile guidance and pursuit: kinematics, dynamics and control*. Elsevier, **1998**.

[91] Paul Zarchan. *Tactical and strategic missile guidance*. American Institute of Aeronautics and Astronautics, Inc., **2012**.

[92] Uday S Shukla and Pravas R Mahapatra. The proportional navigation dilemma-pure or true? *IEEE Transactions on Aerospace and Electronic Systems*, 26(2):382–392, **1990**.

[93] Pin-Jar Yuan and Jeng-Shing Chern. Ideal proportional navigation. *Journal of Guidance, Control, and Dynamics*, 15(5):1161–1165, **1992**.

[94] Ciann-Dong Yang and Chi-Ching Yang. Analytical solution of 3d true proportional navigation. *IEEE Transactions on Aerospace and Electronic Systems*, 32(4):1509–1522, **1996**.

[95] Mauricio Guelman. The closed-form solution of true proportional navigation. *IEEE Transactions on Aerospace and Electronic Systems*, AES-12(4):472–482, **1976**.

[96] Debasish Ghose. True proportional navigation with maneuvering target. *IEEE Transactions on Aerospace and Electronic Systems*, 30(1):229–237, **1994**.

[97] Ke-Bo Li, Wen-Shan Su, and Lei Chen. Performance analysis of realistic true proportional navigation against maneuvering targets using lyapunov-like approach. *Aerospace science and technology*, 69:333–341, **2017**.

[98] Mingu Kim and Youdan Kim. Lyapunov-based pursuit guidance law with impact angle constraint. *IFAC Proceedings Volumes*, 47(3):2509–2514, **2014**.

[99] QI Naiming, SUN Qilong, and ZHAO Jun. Evasion and pursuit guidance law against defended target. *Chinese Journal of Aeronautics*, 30(6):1958–1973, **2017**.

[100] Behzad Ahi and Mohammad Haeri. Novel command to line of sight guidance with practical limitations. *Asian Journal of Control*, **2021**.

[101] Qi Guodong, Yu Jianqiao, Ai Xiaolin, and Jiang Jun. Multi-missile coordination high precision guidance and control method for beam-riding guidance. In *Journal of Physics: Conference Series*, volume 1215, page 012013. IOP Publishing, **2019**.

[102] Qian Peng, Jianguo Guo, and Jun Zhou. Integrated guidance and control system design for laser beam riding missiles with relative position constraints. *Aerospace Science and Technology*, 98:105693, **2020**.

[103] Iman Mohammad Zaman and Hamid Reza Momeni. Pi guidance law design using circle criterio. *Journal of Control*, 4(2):11–19, **2010**.

[104] Kemin Zhou and John Comstock Doyle. *Essentials of robust control*, volume 104. Prentice hall Upper Saddle River, NJ, **1998**.

[105] Khaled Halbaoui, Djamel Boukhetala, and Fares Boudjema. Introduction to robust control techniques. *K. Halbaoui, B. Boukhetala, & F. Boudjema, Robust Control, Theory and Applications*, pages 1–24, **2011**.

[106] Pieter Van den Braembussche, Jan Swevers, and H Van Brüssel. Application of $h\infty$ synthesis, sliding mode control and a disturbance observer for robust control of machine axes with linear motors. In *1997 European Control Conference (ECC)*, pages 2137–2142. IEEE, **1997**.

[107] Mihai Lungu, Romulus Lungu, and Dragoş Tutunea. Control of aircraft landing using the dynamic inversion and the h-inf control. In *2016 17th International Carpathian Control Conference (ICCC)*, pages 461–466. IEEE, **2016**.

[108] Ahmed A Zaki Diab, Abou-Hashema M El-Sayed, Hossam Hefnawy Abbas, and Montaser Abd El Sattar. Robust speed controller design using h_infinity theory for high-performance sensorless induction motor drives. *Energies*, 12(5):961, **2019**.

[109] Bülent Özkan. Mekatronik sistemlerde uygulanan belli başlı kontrol yöntemleri. *Tübav Bilim Dergisi*, 2(3):302–316, **2009**.

[110] Andrey V Savkin, PUBUDU N Pathirana, and FARHAN A Faruqi. Problem of precision missile guidance: Lqr and $h\infty$ control frameworks. *IEEE Transactions on Aerospace and Electronic Systems*, 39(3):901–910, **2003**.

[111] Hsin-Yuan Chen and Ciann-Dong Yang. Nonlinear h-infinity robust guidance law for homing missiles. In *Guidance, Navigation, and Control Conference and Exhibit*, page 4212. **1998**.

[112] Christopher Edwards and Sarah Spurgeon. *Sliding mode control: theory and applications*. Crc Press, **1998**.

[113] Di Zhou, Chundi Mu, and Wenli Xu. Adaptive sliding-mode guidance of a homing missile. *Journal of guidance, control, and dynamics*, 22(4):589–594, **1999**.

[114] Mehmet Ali Guvenc, Hasan Huseyin Bilgic, and Selcuk Mistikoglu. Identification of chatter vibrations and active vibration control by using the sliding mode controller on dry turning of titanium alloy (ti6al4v). *Facta Universitatis, Series: Mechanical Engineering*, **2021**.

[115] SG Khan and J Jalani. Realisation of model reference compliance control of a humanoid robot arm via integral sliding mode control. *Mechanical Sciences*, 7(1):1–8, **2016**.

[116] SD Brierley and R Longchamp. Application of sliding-mode control to air-air interception problem. *IEEE transactions on aerospace and electronic systems*, 26(2):306–325, **1990**.

[117] Wenxing Fu, Binbin Yan, Xiaofei Chang, and Jie Yan. Guidance law and neural control for hypersonic missile to track targets. *Discrete Dynamics in Nature and Society*, 2016, **2016**.

[118] Yuri B Shtessel, Ilya A Shkolnikov, and Arie Levant. Guidance and control of missile interceptor using second-order sliding modes. *IEEE Trans. Aerosp. Electron. Syst.*, 45(1):110–124, **2009**.

[119] Chris M Bishop. Neural networks and their applications. *Review of scientific instruments*, 65(6):1803–1832, **1994**.

[120] SK Mishra, IG Sarma, and KN Swamy. Performance evaluation of two fuzzy-logic-based homing guidance schemes. *Journal of Guidance, Control, and Dynamics*, 17(6):1389–1391, **1994**.

[121] Ch Lin. Intelligent control theory in guidance and control system design: An overview. *Proceedings of the National Science Council, ROC, 2000*, 24:15–30, **2000**.

[122] Chun-Liang Lin. On the design of a fuzzy-pd based missile guidance law. In *2003 4th International Conference on Control and Automation Proceedings*, pages 7–11. IEEE, **2003**.

[123] A Özgür Vural. *Fuzzy logic guidance system design for guided missiles*. Master's thesis, Citeseer, **2003**.

[124] Aline Ingabire and Andrey A Sklyarov. Control of longitudinal flight dynamics of a fixedwing uav using lqr, lqg and nonlinear control. In *E3S Web of Conferences*, volume 104, page 02001. EDP Sciences, **2019**.

[125] Syed Asad Hussain, Gongsheng Huang, Richard Kwok Kit Yuen, and Wei Wang. Adaptive regression model-based real-time optimal control of central air-conditioning systems. *Applied Energy*, 276:115427, **2020**.

[126] Tao Sun and Xi-Ming Sun. An adaptive dynamic programming scheme for nonlinear optimal control with unknown dynamics and its application to turbofan engines. *IEEE transactions on industrial informatics*, 17(1):367–376, **2020**.

[127] Hussain Syed Asad, Richard Kwok Kit Yuen, Jinfeng Liu, and Junqi Wang. Adaptive modeling for reliability in optimal control of complex hvac systems. In *Building Simulation*, volume 12, pages 1095–1106. Springer, **2019**.

[128] Dominic Otoo, Isaac Odoi Abeasi, Shaibu Osman, and Elvis Kobina Donkoh. Mathematical modeling and analysis of the dynamics of hepatitis b with optimal control. *Commun. Math. Biol. Neurosci.*, 2021:Article–ID, **2021**.

[129] Fumiaki Imado and Takeshi Kuroda. Optimal missile guidance system against a hypersonic target. In *Astrodynamics Conference*, page 4531. **1992**.

[130] Lu-Ping Tsao and Ching-Show Lin. New optimal guidance law for short-range homing missiles. In *PROC NATL SCI COUNC REPUB CHINA PART A PHYS SCI ENG*, volume 24, pages 422–426. **2000**.

[131] Emmanuel Devaud, Jean-Philippe Harcaut, and Houria Siguerdidjane. Three-axes missile autopilot design: From linear to nonlinear control strategies. *Journal of guidance, control, and dynamics*, 24(1):64–71, **2001**.

[132] Ahmed Awad and Haoping Wang. Roll-pitch-yaw autopilot design for nonlinear time-varying missile using partial state observer based global fast terminal sliding mode control. *Chinese Journal of Aeronautics*, 29(5):1302–1312, **2016**.

[133] Vincent Fromion, Gerard Scorletti, and Gilles Ferreres. Nonlinear performance of a pi controlled missile: an explanation. *International Journal of Robust and Nonlinear Control: IFAC-Affiliated Journal*, 9(8):485–518, **1999**.

[134] Seung-Hwan Kim and Min-Jea Tahk. Missile acceleration controller design using proportional–integral and non-linear dynamic control design method. *Proceedings of the Institution of Mechanical Engineers, Part G: Journal of Aerospace Engineering*, 226(8):882–897, **2012**.

[135] Mohd Ariffanan Mohd Basri, Kumeresan A Danapalasingam, and Abdul Rashid Husain. Design and optimization of backstepping controller for an underactuated autonomous quadrotor unmanned aerial vehicle. *Transactions of FAMENA*, 38(3):27–44, **2014**.

[136] Nitai Pal, Roshan Kumar, and Milan Kumar. Design of missile autopilot using backstepping controller. In *International Conference on Electronics, Communication and Instrumentation (ICECI)*, pages 1–4. IEEE, **2014**.

[137] De-fu Lin and Jun-fang Fan. Missile autopilot design using backstepping approach. In *2009 Second International Conference on Computer and Electrical Engineering*, volume 1, pages 238–241. IEEE, **2009**.

[138] Jun-fang Fan, Zhong Su, and Zhen-xuan Cheng. Missile autopilot design and analysis based on backstepping. In *2010 3rd International Symposium on Systems and Control in Aeronautics and Astronautics*, pages 1042–1046. IEEE, **2010**.

[139] Metin U Salamci and Beyza Gökbilen. Sdre missile autopilot design using sliding mode control with moving sliding surfaces. *IFAC Proceedings Volumes*, 40(7):768–773, **2007**.

[140] Metin U Salamci, M Kemal Ozgoren, and Stephen P Banks. Sliding mode control with optimal sliding surfaces for missile autopilot design. *Journal of Guidance, Control, and Dynamics*, 23(4):719–727, **2000**.

[141] Michael B McFarland and Anthony J Calise. Adaptive nonlinear control of agile antiair missiles using neural networks. *IEEE Transactions on Control Systems Technology*, 8(5):749–756, **2000**.

[142] Wayne K Schroeder and Kai Liu. An appropriate application of fuzzy logic: a missile autopilot for dual control implementation. In *Proceedings of 1994 9th IEEE International Symposium on Intelligent Control*, pages 93–98. IEEE, **1994**.

[143] Anna L Blumel, Evan J Hughes, and Brian A White. Fuzzy autopilot design using a multiobjective evolutionary algorithm. In *Proceedings of the 2000 Congress on Evolutionary Computation. CEC00 (Cat. No. 00TH8512)*, volume 1, pages 54–61. IEEE, **2000**.

[144] Seyyed Sajjad Moosapour, Ghasem Alizadeh, Sohrab Khanmohammadi, and Hamzeh Moosapour. A novel robust proportional navigation guidance law design for missile considering autopilot dynamic. *Transactions of the Institute of Measurement and Control*, 35(5):703–710, **2013**.

[145] Bhaskar Biswas, Shashi Ranjan Kumar, and Arnab Maity. Three-dimensional nonlinear impact angle guidance for maneuvering targets. *IFAC-PapersOnLine*, 51(1):47–52, **2018**.

[146] Ciann-Dong Yang and Chi-Ching Yang. Analytical solution of generalized 3d proportional navigation. In *Proceedings of 1995 34th IEEE Conference on Decision and Control*, volume 4, pages 3974–3979. IEEE, **1995**.

[147] Inanc Moran and Turgay Altilar. Three plane approach for 3d true proportional navigation. In *AIAA Guidance, Navigation, and Control Conference and Exhibit*, page 6457. **2005**.

[148] Shashi Ranjan Kumar and Debasish Ghose. Three dimensional impact angle constrained guidance law using sliding mode control. In *2014 American Control Conference*, pages 2474–2479. IEEE, **2014**.

[149] Lijing Wang, WZ Jin, and GY Li. Three-dimensional adaptive dynamic surface guidance law against maneuvering targets with input constraints

and second-order dynamics autopilot. *International Journal of Innovative Computing, Information and Control*, 14(5):1725–1739, **2018**.

[150] Jianguo Guo, Yifei Li, and Jun Zhou. A new continuous adaptive finite time guidance law against highly maneuvering targets. *Aerosp. Sci. Technol.*, 85:40–47, **2019**.

[151] Han Yan and Hai-Bo Ji. Guidance laws based on input-to-state stability and high-gain observers. *IEEE Transactions on Aerospace and Electronic Systems*, 48(3):2518–2529, **2012**. doi:10.1109/TAES.2012.6237606.

[152] Aminurrashid Noordin, Mohd Ariffanan Mohd Basri, Zaharuddin Mohamed, and Izzuddin Mat Lazim. Adaptive pid controller using sliding mode control approaches for quadrotor uav attitude and position stabilization. *Arabian Journal for Science and Engineering*, 46(2):963–981, **2021**.

[153] Wangpeng An, Haoqian Wang, Qingyun Sun, Jun Xu, Qionghai Dai, and Lei Zhang. A pid controller approach for stochastic optimization of deep networks. In *Proceedings of the IEEE Conference on Computer Vision and Pattern Recognition*, pages 8522–8531. **2018**.

[154] JM Vazquez-Nicolas, Erik Zamora, Iván González-Hernández, Rogelio Lozano, and Humberto Sossa. Pd+ smc quadrotor control for altitude and crack recognition using deep learning. *International Journal of Control, Automation and Systems*, 18(4):834–844, **2020**.

[155] Zhongwen Li, Zhiping Cheng, Shuhui Li, Jikai Si, Jinfeng Gao, Weizhen Dong, and Himadry Shekhar Das. Virtual synchronous generator and smc based cascaded control for voltage-source grid-supporting inverters. *IEEE Journal of Emerging and Selected Topics in Power Electronics*, **2021**.

[156] Abdurrahman Bayrak, Handan Gürsoy, and Mehmet Önder Efe. A novel robust fuzzy control of an uncertain system. *Transactions of the Institute of Measurement and Control*, 39(3):324–333, **2017**.

[157] Giorgio Bartolini, Antonella Ferrara, and Elio Usai. Chattering avoidance by second-order sliding mode control. *IEEE Transactions on automatic control*, 43(2):241–246, **1998**.

[158] Ismail Bendaas and Farid Naceri. A new method to minimize the chattering phenomenon in sliding mode control based on intelligent control for induction motor drives. *SJEE*, 10(2):231–246, **2013**.

[159] Godfrey Harold Hardy, John Edensor Littlewood, and George Pólya. *Inequalities*. Cambridge university press, **1952**.

[160] Shuanghe Yu, Xinghuo Yu, Bijan Shirinzadeh, and Zhihong Man. Continuous finite-time control for robotic manipulators with terminal sliding mode. *Automatica*, 41(11):1957–1964, **2005**.

[161] Sanjay P Bhat and Dennis S Bernstein. Geometric homogeneity with applications to finite-time stability. *Math. Control, Signals, Syst.*, 17(2):101–127, **2005**.

[162] Hassan K Khalil. Nonlinear systems. *Upper Saddle River*, **2002**.

[163] Chaoyuan Man, Zhenxing Zhang, and Shihua Li. Two composite guidance laws based on the backstepping control and disturbance observers with autopilot lag. *Transactions of the Institute of Measurement and Control*, 41(10):2957–2969, **2019**.

[164] Zhenxing Zhang, Chaoyuan Man, Shihua Li, and Shi Jin. Finite-time guidance laws for three-dimensional missile-target interception. *Proc. Inst. Mech. Eng., G, J. Aerosp. Eng.*, 230(2):392–403, **2016**.

[165] Chaoyuan Man, Rongjie Liu, and Shihua Li. Three-dimensional suboptimal guidance law based on θ–d technique and nonlinear disturbance observer. *Proc. Inst. Mech. Eng., G, J. Aerosp. Eng.*, 233(14):5122–5133, **2019**.

[166] Junhong Song, Shenmin Song, and Huibo Zhou. Adaptive nonsingular fast terminal sliding mode guidance law with impact angle constraints. *Int. J. Control Autom. Syst.*, 14(1):99–114, **2016**.

[167] Yu-Jie Si and Shen-Min Song. Continuous reaching law based three-dimensional finite-time guidance law against maneuvering targets. *Trans. Inst. Meas. Control*, 41(2):321–339, **2019**.

[168] Handan Gürsoy-Demir and Mehmet Önder Efe. Comparison of three-dimensional guidance laws for missile guidance system. In *10th Ankara International Aerospace Conference, METU, Ankara, Turkey*. **2019**.

[169] Xiaodong Liu and Guofei Li. Adaptive sliding mode guidance with impact time and angle constraints. *IEEE Access*, 8:26926–26932, **2020**.

[170] Arie Levant. Robust exact differentiation via sliding mode technique. *automatica*, 34(3):379–384, **1998**.

[171] Sang-Do Lee, Bui Duc Hong Phuc, Xiao Xu, and Sam-Sang You. Roll suppression of marine vessels using adaptive super-twisting sliding mode control synthesis. *Ocean Engineering*, 195:106724, **2020**.

[172] Qi Dong, Qun Zong, Bailing Tian, and Fang Wang. Adaptive-gain multivariable super-twisting sliding mode control for reentry rlv with torque perturbation. *International Journal of Robust and Nonlinear Control*, 27(4):620–638, **2017**.